Fluorescent Nanomaterials for Biological Applications

By

Amit Jaiswal

A Thesis

Submitted in Partial Fulfillment of the
Requirements for the Degree of

DOCTOR OF PHILOSOPHY

at the

INDIAN INSTITUTE OF TECHNOLOGY GUWAHATI

Centre for Nanotechnology
Indian Institute of Technology Guwahati
Assam, India

April 2013

Fluorescent Nanomaterials for Biological Applications

A Thesis by Amit Jaiswal

Thesis Supervisors,
Siddhartha Sankar Ghosh & Arun Chattopadhyay

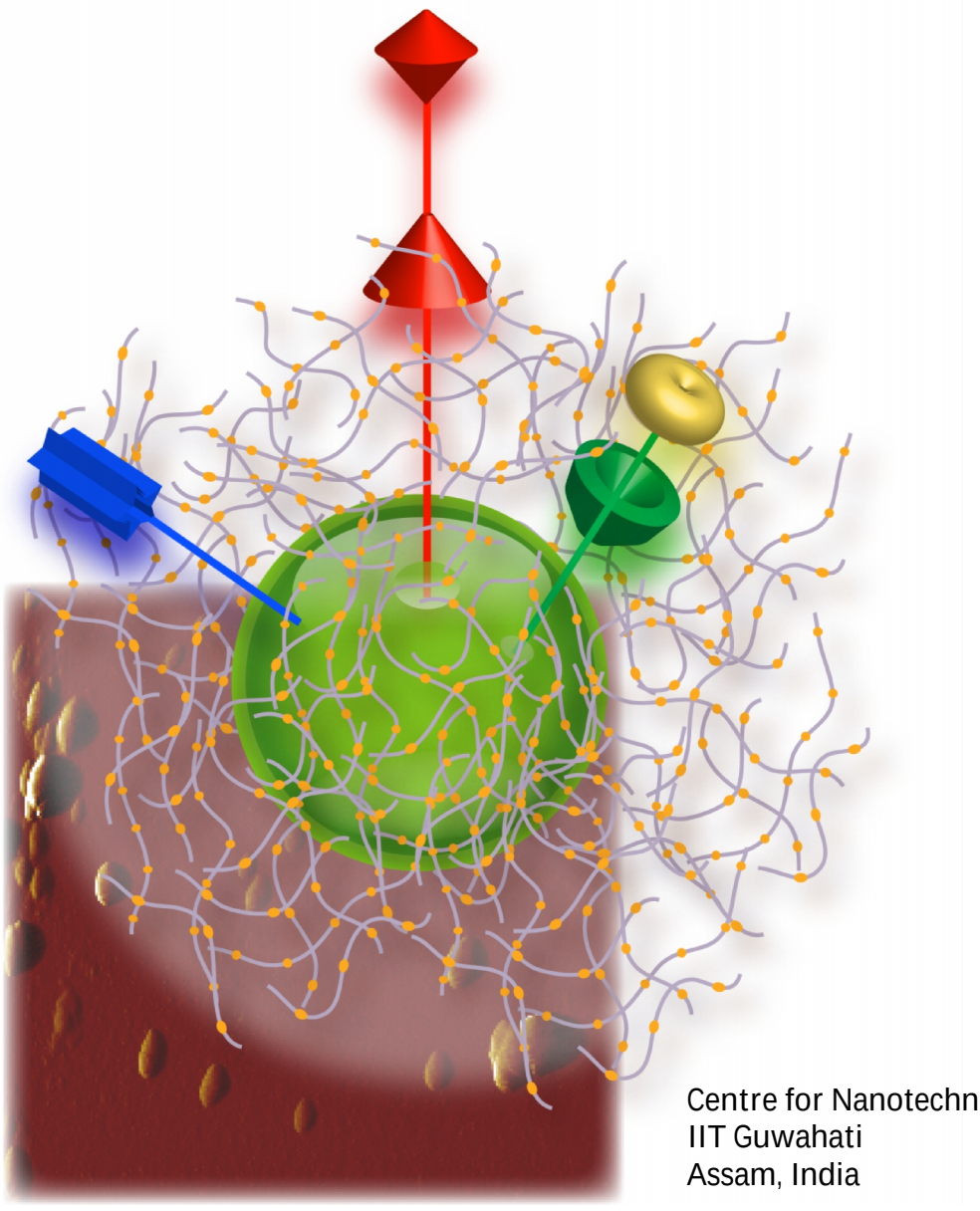

Centre for Nanotechnology
IIT Guwahati
Assam, India

Declaration

I hereby declare that the matter embodied in this thesis entitled "**Fluorescent Nanomaterials for Biological Applications**" is the result of investigations carried out by me under the supervision of Prof. Siddhartha Sankar Ghosh, Department of Biotechnology and Prof. Arun Chattopadhyay, Department of Chemistry, Indian Institute of Technology Guwahati, Assam, India, for the award of the degree of Doctor of Philosophy. This work has not been submitted elsewhere for any degree, diploma, associateship or membership etc. of any Institute or University to the best of my knowledge and belief.

Date:

Place: Guwahati

Amit Jaiswal
(Reg. No. 10615303)
Centre for Nanotechnology
IIT Guwahati,
Guwahati-781039, Assam
India

भारतीय प्रौद्योगिकी संस्थान गुवाहाटी
Indian Institute of Technology Guwahati
Guwahati 781039, Assam, India

CERTIFICATE

It is certified that the thesis entitled "**Fluorescent Nanomaterials for Biological Applications**" being submitted to the **Indian Institute of Technology Guwahati** by **Amit Jaiswal** (Roll No. 10615303) for the award of the degree of **Doctor of Philosophy** in ***Nanotechnology***, is a bonafide record of research work carried out by him. The information and data reported by him are solely the results of his original findings. He has meticulously carried out the investigations and followed the guidelines of the laboratory. This work has not been submitted elsewhere for any degree or diploma.

Dr. Siddhartha Sankar Ghosh
Professor, Department of Biotechnology,
Indian Institute of Technology Guwahati,
Guwahati-781039, Assam, India.
Thesis Supervisor

Dr. Arun Chattopadhyay
Professor, Department of Chemistry,
Indian Institute of Technology Guwahati,
Guwahati-781039, Assam, India.
Thesis Supervisor

ABSTRACT

Fluorescent Nanomaterials for Biological Applications

By

Amit Jaiswal

Submitted to the Indian Institute of Technology Guwahati in April, 2013 in Partial Fulfillment of the Requirements for the Degree of Doctor of Philosophy in Nanotechnology

Abstract:

Nanoparticles are always accompanied with the appearance of novel properties irrespective of the metallic or semiconductor origin. Evolution of the unique physical, chemical and electronic properties at the nanoscale forms the essence of the various applications of nanoscience and nanotechnology. The interplay between the nanomaterials and biological systems is of special significance, especially for the fluorescent nanomaterials, such as quantum dots (Q-dots), which have diverse imaging and sensing applications. However toxicity issues remain a lingering concern and propel research to prepare nontoxic Q-dots.

The thesis illustrates the synthesis of non-cadmium (cd) based Q-dots and its biolabeling and sensing applications. In chapter 1, the properties and implications of fluorescent nanomaterials for biological applications are discussed. In chapter 2, the synthesis of biocompatible zinc sulfide (ZnS) Q-dots and its interaction with silver nanoparticles (Ag NPs) leading to the fluorescence quenching of the Q-dots is demonstrated. The detailed mechanism involved was investigated which showed the applicability of the Q-dots–NP pair for possible Förster resonance energy transfer (FRET)/ nanometal surface energy transfer (NSET) applications. The synthesized ZnS Q-dots were employed as a fluorescent label, embedded within chitosan nanocarriers having folic acid (FA) as a targeting agent, for theranostic applications and is illustrated in chapter 3. The film forming ability of chitosan and the ability of ZnS Q-dots to undergo cation exchange transformation reaction was exploited for sensing and removal of heavy metal ions from water. The detailed procedure and mechanism of detection and removal is presented in chapter 4. Chapter 5 demonstrates a simple microwave mediated synthesis of fluorescent C-dots using a biocompatible polymer, poly(ethylene glycol) (PEG), for the first time as precursor and pasivating agent. The detailed characterization of the C-dots in addition to its biolabeling application is also elucidated in the chapter. Taking a step further, in chapter 6, a simple room temperature based synthesis of gold nanoparticles (Au NPs) utilizing the synthesized C-dots as catalyst is demonstrated. The comprehensive characteristics of the Au NPs, its stability, and the influence of the varying amounts of precursor and catalyst on the synthesis of Au NPs are also unveiled in the chapter.

Thesis Supervisors:	Siddhartha Sankar Ghosh, Ph.D	Arun Chattopadhyay, Ph.D
Title:	Professor of Biotechnology	Professor of Chemistry

Acknowledgement

Time flies like an arrow, I have been at IIT Guwahati for almost five years and I find those years as one of the most enriching times of my life. I feel that I have grown a great deal as an individual, and I couldn't have done it without the support of so many wonderful people around me. It's difficult, to put in words, how grateful I am to these people, but here, is my modest attempt.

Firstly, I would like to thank my supervisors, Prof. Siddhartha Sankar Ghosh and Prof. Arun Chattopadhyay, for giving me the opportunity to work in their group. I am highly grateful for their support, knowledgeable advice, constructive criticism and the academic freedom they allowed, for me to pursue things of my interest. In addition to the excellent lab facilities, they also provided us with sufficient funds to carry out research to our heart's content. The day in lab always started with the motivating enquiry of Prof. Chattopadhyay, "Anything New?" and with his extraordinary ideas, which drove us for an out-of-the-box thinking. The evening discussion with Prof. Ghosh always made us feel homely and his suggestions helped a lot in polishing of the research work. I feel fortunate to have them as my supervisors.

I extend my thanks, to my doctoral committee members, Prof. Lingaraj Sahoo, Dr. Biplab Bose and Dr. Debasis Manna, for continuously evaluating my work and for giving ideas and suggestion for its improvement. I also thank Dr. Anil Mukund Limaye for giving his valuable time for discussions, both on the professional and personal fronts. I owe him, for teaching the various fundamentals required to carry out research and for allowing me to attend his invaluable classes.

I would like to thank the staff members of Centre for Nanotechnology, Mr. Kaustubh Acharyya, Mr. Paran Dutta, Mrs. Pranjoli Das and Mr. Indrajit Talukdar, for treating me more like a friend than a mere student of the Centre. Special thanks to Indrajit sir, for patiently finding the nanodots in TEM. I also thank the CIF staffs, Mr. Chandan Borgohain, Dr. Kulakamal Senapati, Mr. Madhurjya Borah and Mr. Kesho Singh for their timely help.

Next, I would like to extend my thanks to Shivendra for introducing me to the world of quantum dots and most importantly to Pallab da, who has played an instrumental role in my life. I sincerely thank Pallab da for his support, suggestions and guidance throughout my research. I learnt a lot from him, starting from the kind of articles to read, to design and perform experiments; to prepare manuscripts. He has always been a friend, philosopher and guide to me. He played the role of '*Keshav*' for me, guiding me through the ups and downs of my life, and for this, I will remain indebted to him forever. I extend my thanks to Aditi di for being supportive and for encouraging me to deal with the problems of my life. I cannot forget her hand cooked food, which I had chance to have several times.

I thank Chocks and Kohila for their selfless help in patiently teaching me the biological experiments. It was enjoyable doing experiments with Koi, where I had chance to listen to songs in her beautiful voice and to learn few *Tamil* words. Koi, thanks for making those boring assays into fun by citing funny *Tamil* comments. I remember how I went '*kirka*' by planning to prepare a cocktail of suicide enzymes and you reminded me of adding the

prodrug and then serving it to the unwanted people. It was really fun and pleasure to work with stupendous and meticulous Koi.

I sincerely thank my group members, Madhuchanda Mam, Amaresh, Shilpa, Upashi, Bandhan, Subhamoy, Nidhi di, Archita, Sharmila, Asif, Deepshikha, Mitun, Sadhu da, Subhojit da, Raihana, Palash, Rumi, Satya, Rama, Sunil, Anushree and Shilaj, for providing a healthy and cheerful work environment. I thank Shilpa for giving sympathetic ear to my problems and Upashi for decorating the lab with her beautiful smile. I owe my gratitude to Agile bhaiya for helping me understand quantum mechanics and to Francis, Ravi, Santo, Devendra and Sushant for assisting me in some of my research work.

Moving ahead of research, I would like to thank the two invaluable person of my life, whom I consider to be the best gift I could ever get from IIT. Shashank and Sahil; life would have been absolutely different if I had not met you people on my first day in the campus. I will always cherish the moments spent with you buddies. I cannot forget the love, care and affection I got from you, which never let me be homesick. '*Babu*', the name given by you made me forget my real name and I miss all these, since you left the campus.

Next, I thank Zia bhai for not only being my conference partner, but, for the discussions, care, and help and for the special recipe of *Biriyani*. It was fun and adventurous time spent with him. I appreciate the care of Tedu, when I was not well and can't forget the *Khichdi* and special *Maggie* prepared by him. I thank Manab da and Ritesh for their love and care throughout. I thank Arijit for his love and for the wonderful scooty ride at the banks of Brahmaputra and at the crowded lanes of the Guwahati city.

I treasure my friendship with Arka, Queeny, Ankit, Shubaash, Sarabjeet, Chaap, Reddy, Shiva, Uma, Abhay, Rishi, Shraddha, Sumi, Sanhita, Raju, Chaku, Bodhi, Silky, Leena, Abhishek, Himanshu bhaiya, Pandey ji, Jitu, Ashish, Paramartha, Saroj, Ramesh, Prateek, Amit, Nitesh, Kausik da and many more...

Festivals in campus couldn't be complete without Amrita di, Jiju and Tiya. Thanks to all of you for being my family within the campus and giving me your love and warmth. I thank Ganesh da and Bhabhi for proving me homely food and serving me few special recipes secretly.

Next, I would like to pay tribute to my teachers, Taposh Masterjee, Miss, (Lt.) Dipen bhaiya, Mr. S. P. Singh, Mrs. Mita Dutta, Mrs. Nabonita Roy, Mrs. Swati Biswas, Prof. D. N Jha, Dr. Soma Banerjee, Dr. Srabonti Basu and Mrs. Sudipta De for teaching me the best things in life.

I would like to express my gratitude to my family members for their constant encouragement and support. I thank my younger brothers and sisters and Simran bhabhi for performing my responsibilities while I was away from home.

Last but not the least, I thank my parents for their support, encouragement, endless love and for the compromises they made, to give me the best possible education. I owe all my achievements to them and I thank The Almighty for blessing me with such wonderful parents and friends.

Amit Jaiswal

Table of Contents

For My Parents

Mrs. Simla Jaiswal & Mr. Arun Jaiswal

&

My Naani

Glossary of Acronyms

a.u.	Arbitrary Units
AAS	Atomic Absorption Spectroscopy
Ag NP	Silver Nanoparticle
AO	Acridine Orange
Apt	Aptamer
ATP	Adenosine triphosphate
Au NP	Gold Nanoparticle
C-dots	Carbon dots
CD-UPRT	Cytosine deaminase-uracil phosphoribosyl transferase
Con-A	Concanavalin A
Cy5	Cyanine dye 5
dex	Dextran
Dox	Doxorubicin
EACs	Ehrlich's Ascites Carcinoma
EB	Ethidium Bromide
EDC	N-(3-dimethyaminopropyl)-N'-ethyl carbodiimide hydrochloride
EDS	Energy Dispersive X-ray Spectroscopy
EM	Electron Microscopy
ESR	Electron Spin Resonance
FA	Folic Acid
FRET	Förster Resonance Energy Transfer
FTIR	Fourier Transformed Infra-Red
HT 29	Human colon Adenocarcinoma
IFFT	Inverse Fast Fourier Transform
LED	Light Emitting Diode
LM	Light Microscopy
MCF 7	Human breast cancer cell line
MWCNT	Multiwalled Carbon Nanotube
NC(s)	Nanocrystal(s)
NHS	N-hydroxy succinimide
NIR	Near Infra-Red
NP(s)	Nanoparticle(s)
NSET	Nanometal Surface Energy Transfer
PAGE	Polyacrylamide Gel Electrophoresis
PBS	Phosphate Buffered Saline
PEG	Poly(ethylene glycol)
Q-dot(s)	Quantum dot(s)
QY	Quantum Yield
ROS	Reactive Oxygen Species
SAED	Selected Area Electron Diffraction
SDS	Sodium dodecyl sulfate
SEM	Scanning Electron Microscopy
SWCNT	Single Walled Carbon Nanotube
TBE	Tris Borate EDTA
TCSPC	Time Correlated Single Photon Counting
TEM	Transmission Electron Microscopy
TOPO	Trioctyl phosphine oxide
TPP	Sodium Tri-Polyphosphate
U87 MG	Human glioblastoma astrocytoma
XRD	X-ray Diffraction
XTT	2,3-Bis(2-methoxy-4-nitro-5-sulfophenyl)-2H-tetrazolium-5-carboxanilide
pDNA	Plasmid DNA

List of Figures

List of Tables

Chapter 1

Introduction and Literature Review

This chapter briefly describes the importance of nanotechnology in the field of biological sciences. It concisely illustrates the properties and applications of fluorescent nanomaterials in the field of theranostics. The synthesis methodology and potential of Q-dots as imaging agent for biodiagnostics have also been elucidated along with the challenges posed by these nanomaterials for theranostic applications.

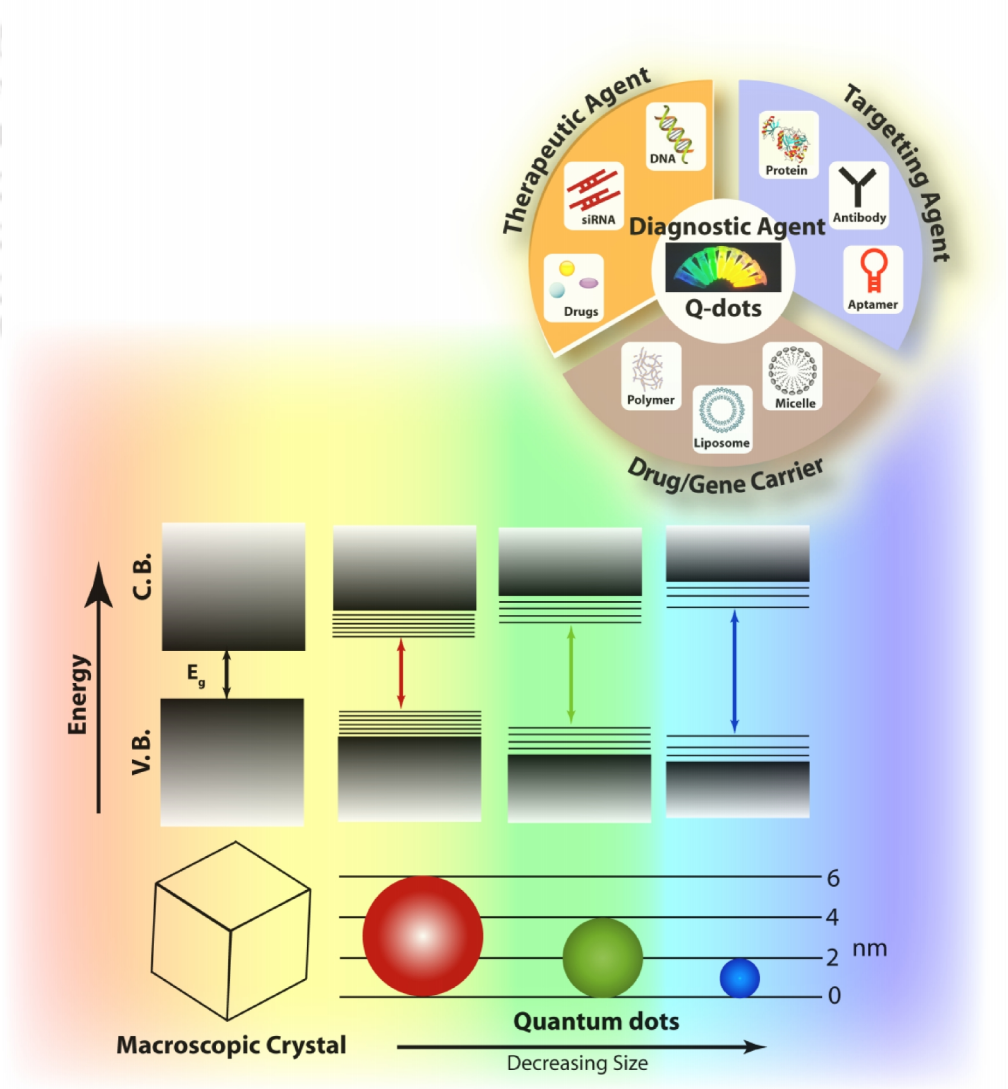

Chapter 1

Introduction and Literature Review

1.1. Introduction

The advancement in the field of science and engineering has led to the development of many new devices and revolutionized existing technologies spanning a wide range of scales, from towering skyscrapers to microfabricated electronic circuits.[1] A prominent gap, however exist between micro-scale engineering and molecular scale chemistry. This gap is in the range of few nanometers and is presently the focus of all the major disciplines of science. Physicists investigating the link between the classical and quantum physics, chemists trying to understand the interactions of colloidal macromolecules and electronic engineers aspiring to fabricate nanoscale chips for circuitry are few examples.[2] Nature has also beautifully exploited this scale range by creating proteins and nucleic acids which are the elementary functional units of biological systems and are responsible for the sustainability of life on earth.[3] Therefore, the field of life sciences will be the first to benefit or affected by the advent of nanotechnology.

In 1974, Norio Taniguchi coined the term “nanotechnology” in reference to precision machining.[4] However, the public awakening to this word occurred only when Prof. K. Eric Drexler hypothesized a future era where molecular machines will be employed to heal, compute, build and destroy efficiently.[5-6] It was during a presentation on the molecular engineering of complex biomolecular probes, inspired from the biostructural equivalences of existing macrotechnology, where Prof. Drexler conceptualized the idea of molecular machines.[5] Family of enzymes associated with adenosine triphosphate (ATP), which harness the chemical free energy released by the hydrolysis of ATP in order to perform mechanical work are

the best examples of naturally found molecular motors.[7-9] Along these lines, he proposed the creation of molecular machines by mimicking those available in nature.[5, 10-12] These ideas have found their way to science fiction like the Borg nanoprobes in Star Trek and in The Outer Limits episode 'The New Breed'.[13] Many scientists believe the idea of Prof. Dexler to be exactly that science fiction[14] and it might be a long time before humans are capable of creating these nano machines performing robotic tasks, but the recent development of DNA based nanomotors,[15-17] and several nanocarriers[18-22] is showing promise, especially in the field of medical therapy and diagnostics.

It was in the year 1959, when a friend and collaborator of Prof. Richard P. Feynman, Albert Hibbs suggested the idea of using Feynman's theoretical micromachines for medical use. This idea was included into the Feynman's 1959 lecture 'There's Plenty of Room at the Bottom', where he put his words as "it would be interesting in surgery if you could swallow the surgeon".[23] Though, nanoscience and nanotechnology are relatively novel concepts, but the inspiration actually originated from his talk and his proposal of printing the entire volumes of the Britannica Encyclopedia onto a pins head.[23] Much of the revolution in nanotechnology in the last two decades has been built upon nanometer sized materials and composites like fullerene,[24-26] carbon nanotube,[27-29] quantum dots,[30-33] polymeric and nucleic acid based nanomachines[34-37] and nanocarriers;[18-22] however, the use of gold nanocluster sols were first reported in 1857 by Prof. Michael Faraday.[38]

The most promising application of nanotechnology is in the field of medicine, with its potential of improved therapy and diagnostics i.e. theranostics.[39-40] Advances in both diagnostic tools such as imaging agents and the development and administration of therapeutics (nanocarriers) may soon come together for the creation of nanoscale devices known as nanorobots or more simply, nanobots.[41-43] These nanobots have the prospective to serve as vehicles for delivery of therapeutic agents, detectors or guardians against early disease and perhaps repair of metabolic or genetic defects.[43] In this respect, fluorescent nanomaterials have emerged as excellent labeling, imaging and sensing agents due to its superior properties over conventional organic fluorophore.[44-45] The fluorescent

nanomaterials which have revolutionized the field of biosensing and biolabeling include quantum dots,[30-33, 40] metallic nanoclusters,[46-47] and silicon[48-49] and carbon based quantum dots.[50]

1.2. Quantum dots: Physics & Chemistry

Quantum dots (Q-dots) are semiconductor nanomaterials having a nearly spherical shape and size in the range of 1 to 10 nm with bright and tunable fluorescence.[30-33] Q-dots possess certain unique physical properties by virtue of its nanoscale size, comparable to electron delocalization length, which are not available in either individual atoms or molecules or bulk semiconductor solids.[51] The bright emission of the Q-dots have made them a key fluorescent nanomaterial for bioimaging and sensing applications.[33]

1.2.1. Photophysical properties of Q-dots

Due to the small size of the Q-dots, quantum confinement of the electronic motion takes place in the crystal and they display discrete energy levels. These energy levels can absorb and emit at different wavelength regions depending on the size of the Q-dots. The reason, 'quantum' prefixes the name is because the dots exhibit quantum confinement properties in all three dimensions.[51] First of all, they exhibit quantized energy levels like an atom. For a given input energy, for instance, a Q-dot will only emit specific spectrum of light. Quantum theory predicts that with decreasing diameters of quantum dots, there will be a corresponding increase in energy of emitted light; as a result, it is possible to systematically control the emission profile of the Q-dots, by adjusting the size of the semiconductor.[51-53] This is the underlying principle behind the unique photophysical properties of Q-dots. A schematic representation of the band structure in solids quantum confinement effect on changing Q-dot size is shown in **Figure 1.1**. Due to their bright and narrow emission spectra, Q-dots are emerging as an ideal fluorescent probe for biological imaging and medical diagnostics.

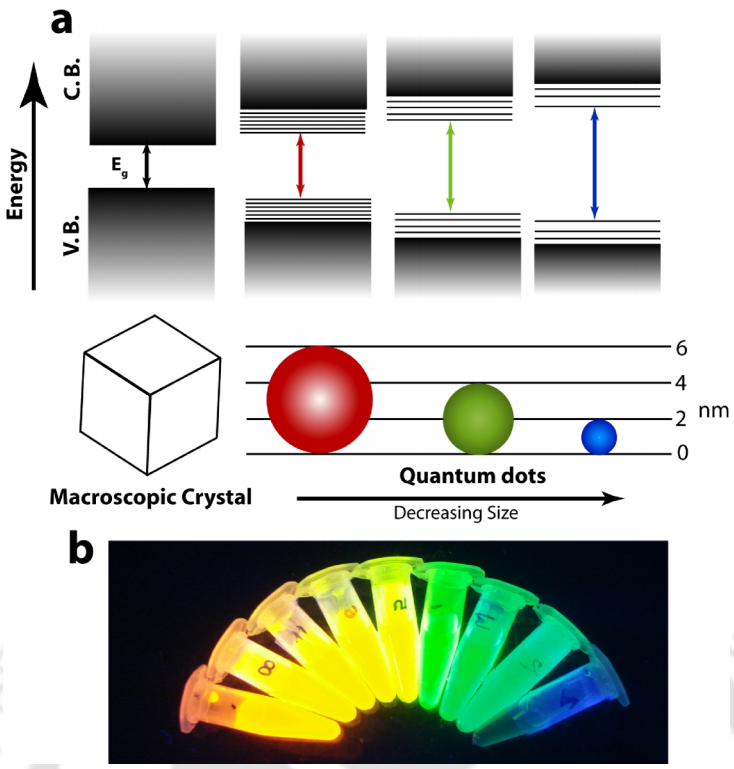

Figure 1.1. (**a**) Electronic energy states of a semiconductor in transition from macroscopic bulk crystal to nanosized quantum dots. The figure also depicts the size dependent variation in the band gap of the Q-dots. (**b**) CdTe Q-dots showing the size tunable emission when observed under UV illumination (λ_{ex} = 302 nm).

Q-dots have several appealing optical features that outdate the use of organic dyes for sensitive bioimaging applications. Firstly, the molar extinction coefficients of the Q-dots are in the order of 0.5–5.0 × 10^6 M^{-1} cm^{-1} which is several folds higher than those of conventional organic dyes.[54-55] Due to this higher absorption rate of the Q-dots, it shows about 10–20 fold brighter emission than the organic dyes, enabling its use for highly efficient fluorescence labeling of cells and tissues.[56-58] Secondly, the excellent photostability of the Q-dots allows it to be used for real time monitoring of biological processes over longer time periods, without much photobleaching, as observed in case of organic dyes.[59] Further, the Q-dots have a longer excited state life time than the organic dyes, allowing the effective separation of the Q-dots fluorescence from background noise. In addition, the large stoke shift of the Q-dots emission band from their broad absorption spectra, improves the detection sensitivity in imaging tissue biopsies and living organisms.[60] Lastly and most importantly, the size tunable emission spectra of the

Q-dots is unique and allows it to be used for multiplexing, using a single excitation source.[40] In stark contrast, the relatively broad emission profile of the organic dyes and fluorescent proteins with narrow absorption band and small stoke shift, renders the detection of separated signals from distinct fluorophore more challenging.

1.2.2. Quantum dot chemistry

The making of Q-dots to be used as a fluorescent probe for biological applications involves a multistep process which includes synthesis, surface passivation, solubilization, and bioconjugation. A single Q-dot crystal consists of hundreds to thousands of atoms that typically belongs to Group II and Group VI elements (e.g. CdSe, CdTe, ZnS) or Group III and Group V (e.g. InP and InAs) elements in the Periodic Table.[51] The Q-dots synthesis approach can broadly be divided either into aqueous phase synthesis or organic phase reaction. Aqueous phase synthesis are generally the benign methodology involving less toxic reagents and yielding water soluble Q-dots which can directly be used for biological applications, but the Q-dots produced are usually of low quality.[61] Superior quality Q-dots having high crystallinity and homogeneity are produced using the hot injection based organic phase reaction involving elevated temperatures. The most commonly used non polar solvent is generally a mixture of trioctylphosphine, trioctylphosphine oxide (TOPO) and hexadecylamine serving as a robust reaction medium, where their basic moieties coordinate with the unsaturated metal atoms on the Q-dots surface inhibiting the growth of the Q-dots into bulk semiconductors.[62-64] However, the requisite of the use of highly toxic reagents and extreme temperatures is the drawback of the organic phase synthesis of Q-dots.

Once the Q-dot nanocrystal core is synthesized, it is often coated with a shell of wider band gap semiconductor material and the process is called surface passivation.[65-66] The importance of surface passivation is multifold; it protects the core from oxidation, prevents the leaching of highly toxic Cd^{2+} ions and improves the quantum yield by reducing surface defects and averts nonradiative decay. Q-dots prepared using the hot injection methods are water insoluble due to the presence of the hydrophobic capping agent. In order to exploit these nanocrystals

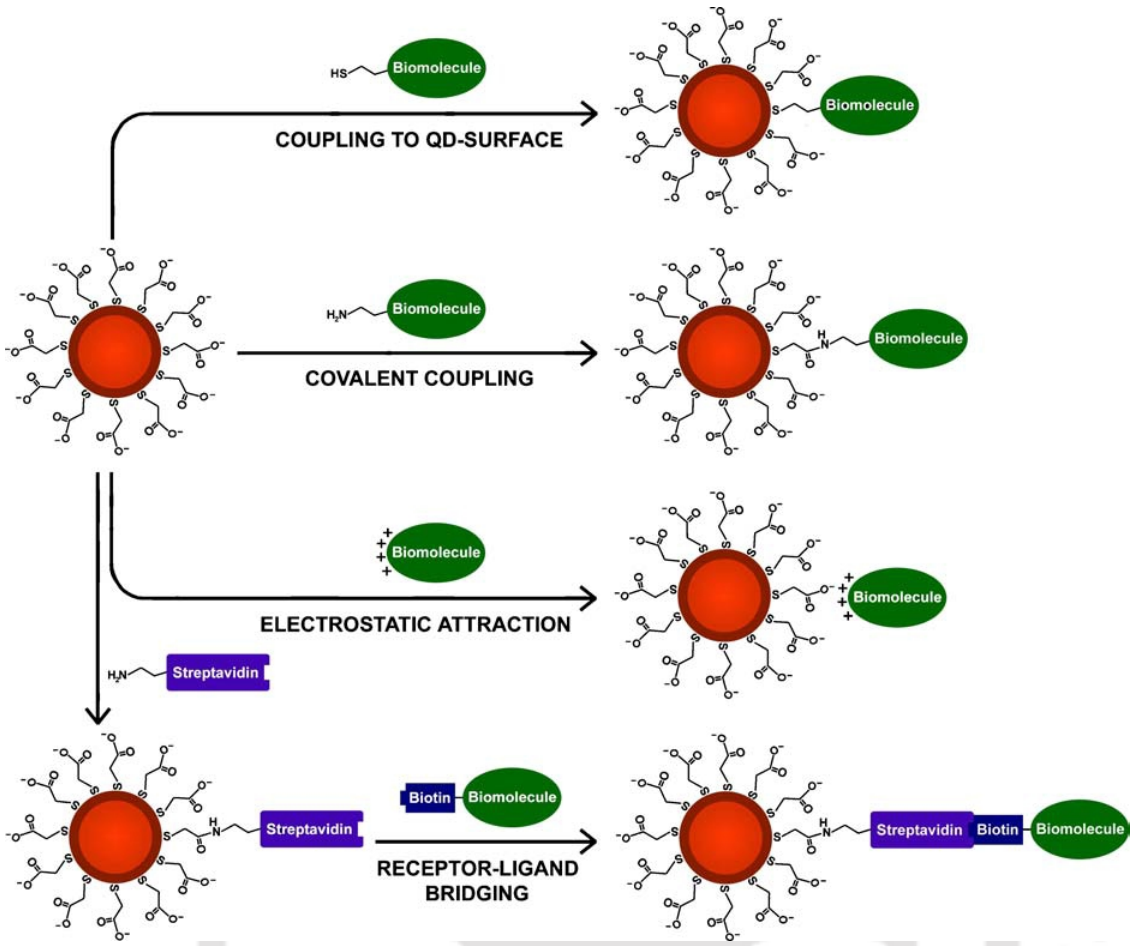

Figure 1.2. Schematic illustration showing the most common methods to conjugate Q-dots to biological molecules, such as proteins, peptides, nucleic acids, or small organic molecules. Reproduced with permission from Reference [1]. Copyright © 2006, Springer Science and Business Media Inc. [Document enclosed in the Permissions section]

for biological application, these hydrophobic molecules must first be rendered hydrophilicity, so that it can be dispersed in aqueous solvents or buffers. The strategies generally used for the surface modification of these dots are either cap exchange or the native surface modifications employing suitable amphiphilic polymer coatings.[67] The ligand or cap exchange is usually carried out using bifunctional ligands like mercaptoacetic acid or mercaptosilane, whereas, amphihilic polymers like polyethylene glycol (PEG)-derivatized phospholipids, polyanhidrides, block copolymers, and octylamine modified polyacrylic acid are reported to be used as coating to impart water solubility to the Q-dots.[60, 68-70] Further, for biological applications like specific cellular labeling, targeting, imaging and multiplexing, the Q-dots must be conjugated to biomolecules like proteins,

antibodies, peptides, DNA, or other targeting moieties. The several methodologies used for bioconjugation includes biotin streptavidin complexation, covalent conjugation using EDC/NHS chemistry for amide, thioether bond formation and electrostatic interaction between oppositely charged molecules.[1] The schematic of different examples of bioconjugation of Q-dots is shown in **Figure 1.2**.

1.3. Applications of Quantum dots

In accordance with the properties, the applications of the Q-dots are multidimensional. Q-dots find application in all the major areas of science and technology. They can be used in photovoltaic devices,[71] in light emitting diodes (LED)[20, 72] and lasers,[73] as photodetector devices,[74] as qubits in quantum computing,[75] in optical sensing[76] and so on. The major applications of the Q-dots are in the field of life sciences, where it has revolutionized the cellular labeling and imaging techniques due to its extraordinary fluorescence property.[30-33, 40] The several biological applications of the Q-dots are summarized in **Figure 1.3** and those related to diagnostics and therapeutics are discussed in details below.

1.3.1. Multiplexed Biosensing and FRET

Due to the unique optoelectronic properties of the Q-dots, it has become popular fluorescent cellular probes for light microscopy (LM), whereas, because of their electron-dense semiconductor cores, it can be directly imaged by electron microscopy (EM) even without any contrasting treatment.[77] Q-dot-mediated Förster Resonance Energy Transfer (FRET) and Nanometal Surface Energy Transfer (NSET) is widely implemented mechanisms in Q-dot-based fluorescence biosensing. Respectable progress has been made in the past few years on the use of Q-dot-FRET based biosensors, particularly on bioanalysis (nucleic acids, proteins, and immunoassays) and intracellular sensing. [78-79] The advantage of the Q-dots in terms of unique optical properties such as broad absorption, size-dependent narrow and tunable emission and strong resistance to photobleaching enables superior FRET configurations over organic fluorophores.

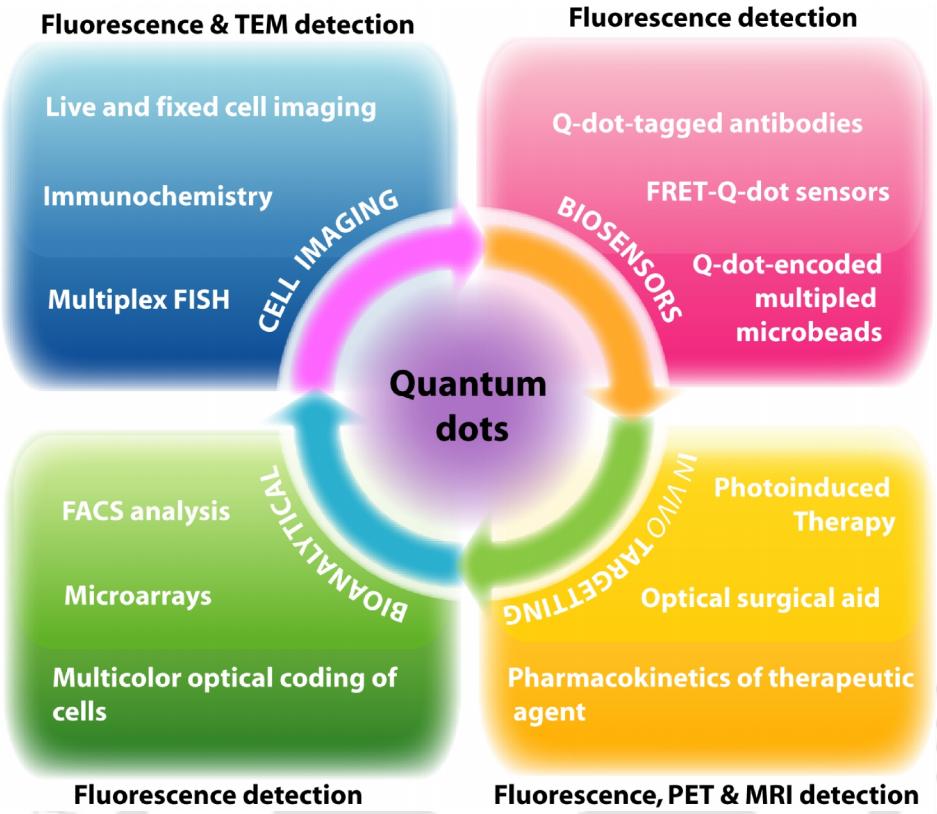

Figure 1.3. Schematic illustrating the various biological applications of quantum dots along with the detection methodology.

While using the Q-dots in conjunction with an organic fluorophore, the spectrum overlap between the donor and acceptor emissions can be effectively minimized. Meanwhile, the large Stokes shift in Q-dots emission and broad excitation spectra enables the use of UV-range excitation and thereby diminishes the possibility of direct-acceptor excitation, which is a requisite for FRET based sensors. Most importantly, a single wavelength can be used to excite multiple Q-dots to emit in non-overlapping, narrow spectral ranges that can still be distinguished. This renders Q-dots, its use towards multicolor applications[80-81] particularly valuable for cellular interactions involving multiple entities or events and even in multiplexed FRET. In addition to the organic fluorophore as an acceptor in the FRET based sensing process, metal NPs can also be used as effective acceptors. Due to the high extinction coefficient of the metal NPs, efficiency of the energy transfer increases and this results in the increase in the Förster distance, which decays with the fourth power of the separation distance 'R', instead of the sixth power in case of conventional Förster mechanism. This phenomenon of NSET

could enable the study of the kinetics involved in biological macromolecules. Oh *et al.* reported an approach for the rapid and simple detection of protein glycosylation based on the energy transfer between lectin-conjugated Au NPs and carbohydrate-conjugated Q-dots.[82] The PL intensity of the dex–Q-dots was quenched by about 70% in the presence of conA–AuNPs and was completely recovered after the addition of free conA which inhibited the binding of conA–Au NPs to dex–Q-dots. The system exploited NP-based energy transfer mechanism and showed its potential to be used in a high-throughput analytical method for the development of glycoprotein and carbohydrate therapeutics.[82]

1.3.2. Cell-specific targeting and subsequent uptake

With the substantial progress in *in vitro* diagnostics,[83] bioconjugated Q-dots have emerged as imaging probes for detection of specific cell types, tissues and organelles [30-33, 59, 84-85] that are exploited in clinical translation,[86] especially for cancer research and therapy. In 2003, Wu *et al.* first demonstrated the use of Q-dots for the static immunostaining of cellular targets and shown to be both brighter and more photostable than conventional organic fluorophores without non-specific labeling.[68] Subsequently, specific targeting of the tumor tissues in live cells using the Q-dot–peptide conjugate was reported by Akerman *et al.*[87] Inspired by the *in vitro* success, Gao *et al.* designed an ABC triblock copolymer-coated Q-dot probe to target and image prostate cancer *in vivo*.[60] The tumor site could be actively probed by the antibody-conjugated Q-dots and imaged in living animals, after proper signal post-processing. It is worth mentioning that the surface of the Q-dots can be conjugated with multiple biomarkers, imparting Q-dots, the advantage of improved binding affinities for the receptors on the cells due to the polyvalency effect.[60, 88-89]

The uptake of exogenous material generally occurs through cellular internalization mechanisms, which includes phagocytosis, macropinocytosis, receptor-mediated endocytosis, and clathrin and caveolin-independent endocytosis.[90-91] The detailed schematic demonstrating the uptake of nanoparticles by cells is shown in **Figure 1.4**.

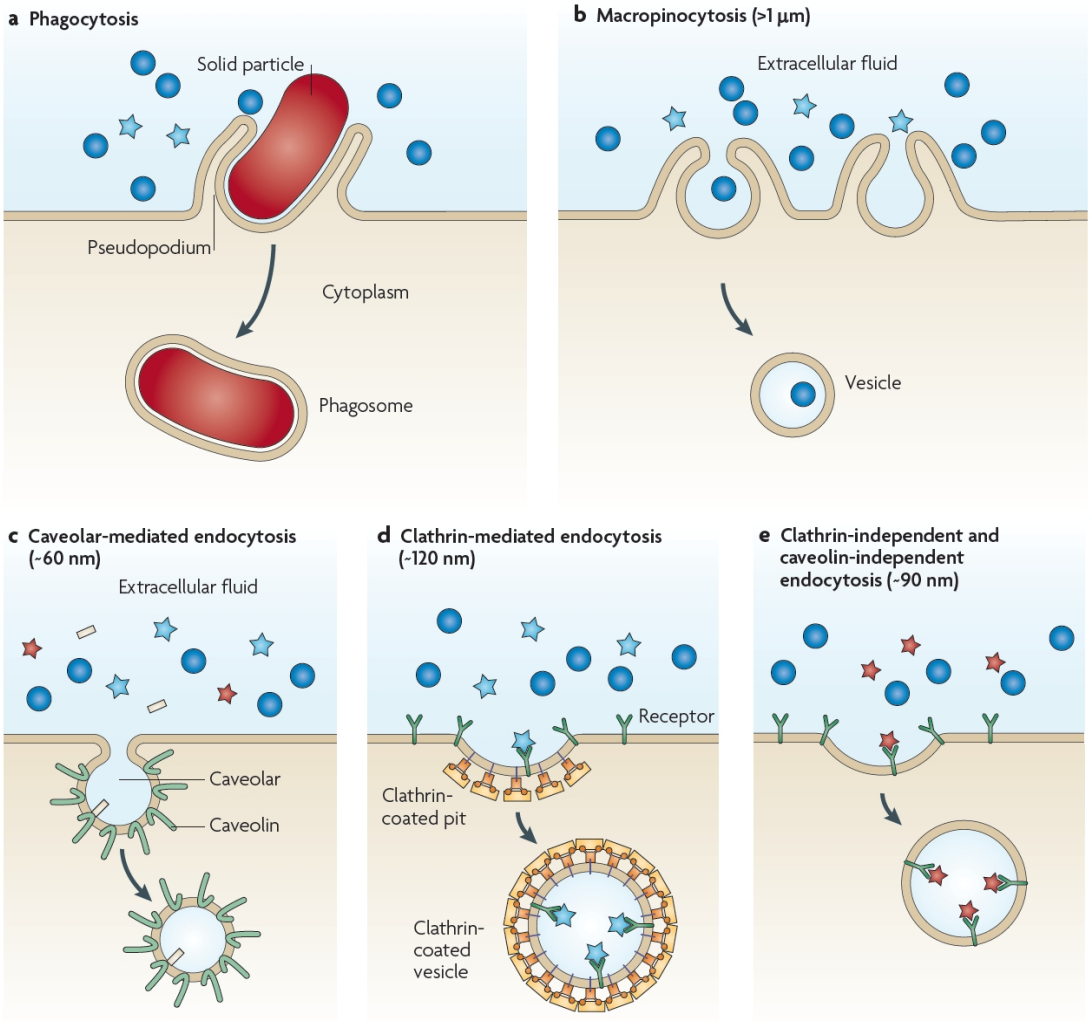

Figure 1.4. Modes of cellular internalization of nanoparticles and respective size limitations. Internalization of large particles is facilitated by phagocytosis (**a**). Nonspecific internalization of smaller particles (>1 µm) can occur through macropinocytosis (**b**). Smaller nanoparticles can be internalized through several pathways, including caveolar-mediated endocytosis (**c**), clathrin-mediated endocytosis (**d**) and clathrin-independent and caveolin-independent endocytosis (**e**), with each being subject to slightly different size constraints. Nanoparticles are represented by blue circles (> 1 µm), blue stars (about 120 nm), red stars (about 90 nm) and yellow rods (about 60 nm). Reproduced with permission from Reference [91]. Copyright © 2010, Nature Publishing Group. [Document enclosed in the Permissions section]

Parak *et al.* studied the applicability of undecorated Q-dots as an alternative marker over gold nanoparticles for phagokinetic tracking; to monitor cell motility as a potential assay for cancer metastasis.[92] The study demonstrated the passive uptake of the Q-dots via non-specific endocytosis along the migratory pathway of human mammary epithelial tumor cells. However, the uptake of Q-dots using

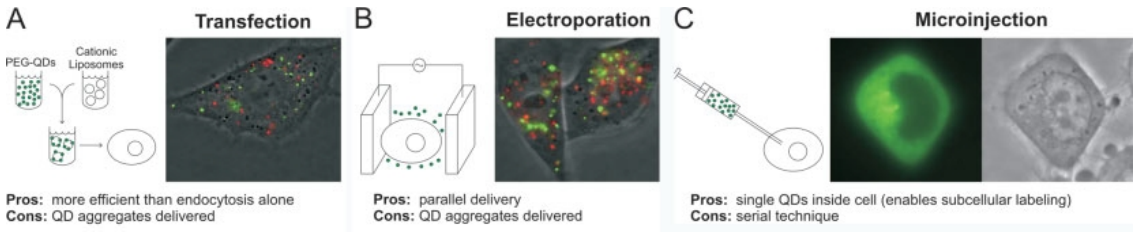

Figure 1.5. Comparison of delivery modes of Q-dots via chemical and physical methods. Fluorescence/Phase contrast micrographs of HeLa cells **A**) transfected with green Q-dots using cationic liposome and red Q-dots as endosomal label, **B**) after electroporation and **C**) after cytoplasmic injection of green Q-dots. Reproduced with permission from Reference [93]. Copyright © 2004 WILEY-VCH Verlag GmbH & Co. KGaA, Weinheim. [Document enclosed in the Permissions section]

either a transfecting agent (liposome, micelle or polymer) or ligand modification is generally more specific and efficient than non-specific endocytosis alone.[93-94] The endocytosed Q-dots are often trapped in endosomes and lysosomes, and are observed as punctate fluorescence staining as seen from **Figure 1.5A**, hence limiting their delivery to cytosol.

Microinjection,[69] and electroporation,[93, 94] are the physical approaches which have been applied to deliver Q-dots into cells. In a recent report, Yum and co-workers delivered monodispersed Q-dots into specific cells using a novel membrane-penetrating nanoneedle.[96] However, the physical mode of delivery process suffers from low efficiency and labor-intensive procedures which typically requires delicate instrumentation and optimization for different cell lines, and possibly induces irreversible damage to the cells.

A concomitant variation in the patterns of cellular labeling which can be seen from **Figure 1.5** usually results from the internalization of the Q-dot conjugates via different mechanisms (endocytosis, receptor-mediated endocytosis, electroporation or microinjection).[94] Therefore, a clearer mechanistic understanding of intracellular delivery would facilitate the rational design of ‘‘ideal’’ functionalized Q-dots, where one can optimize the density and arrangement of the different functional ligands, and their binding strength to the Q-dot nanoscaffold, for controlled theranostics.

1.3.3. Drug/gene Trafficking

Functionalized Q-dots can be employed to trace the intracellular delivery of plasmid DNA (pDNA).[97] A Q-dot–FRET based system was engineered by Ho *et al.* to investigate the structural composition and dynamic behavior of polymeric DNA nanocomplexes intracellularly.[98] The FRET system was designed between pDNA and cationic polymers; the complex coacervation brings the 605Q-dot labeled pDNA which acts as donor into the close proximity of Cy5 functionalized polymer, acting as acceptor and resulting in efficient FRET with high signal-to-noise ratio.[99] Further employment of two-step FRET, using a Q-dot paired nuclear dye on the pDNA, can serves as a novel approach to study both polyplex dissociation and DNA degradation simultaneously in a non-invasive way.[100]

To visualize the transport and release of siRNA from the carrier for optimization, Q-dots were introduced as a traceable marker to shed light on the siRNA delivery.[101] The Q-dot/siRNA was co transfected with the well-developed liposome system (Lipofectamine 2000) in this study. Tan and coworkers subsequently ameliorated the transfection system by using a non-viral vector, chitosan polyplexes doped with Q-dots for siRNA tracking system.[102] Similarly, Amphipol-mediated delivery was employed to ferry the siRNA/Q-dots into the cytoplasm, where Amphipol serves both as a gene carrier and as protecting agent to prevent siRNA from enzymatic degradation. Further, to understand the pharmacokinetic and pharmacodynamic of drug, Manabe *et al.* have suggested a Q-dot–drug tracer system,[103] where Q-dots were conjugated with an anti-hypertensive drug, catrophil.

1.4. Q-dot based Theranostics

Theranostics is a term coined from the amalgamation of diagnostics and therapeutics and it integrates real-time evaluation with delivery of a medication. Q-dots excel in imaging applications and may also serve as particulate delivery vehicles if the biocompatibility and toxicity issues are overcome. The use of such multimodal nanoparticles offers synergistic advantages over any single-modal nanoparticle alone.[104–107] The ideal properties which a theranostic system should possess include (a) accumulation in the pathological zone achieved through

targeting specific cell types, (b) efficient penetration into the cells with minimal toxicity, (c) allowing efficient intracellular trafficking by overcoming the intracellular delivery barriers, (d) responding to the local stimuli and releasing the therapeutic agent, (e) possessing a diagnostic agent (optical or magnetic) enabling real time monitoring of the treatment. In this regard, an 'all in one' multifunctional nanoplatform featuring targeting, therapeutic and imaging modalities (as shown in **Figure 1.6**) can be designed through surface immobilization of ligands and conjugation of ''drugs'' on Q-dots. Multifunctional Q-dots therefore can potentially meet the requirements of a theranostic system.

The Q-dot–aptamer(Apt)–doxorubicin(Dox) conjugate, abbreviated as Q-dot–Apt(Dox), reported by Bagalkot *et al.* is one of the most successful demonstration of Q-dot based theranostics for synchronous cancer cell imaging and traceable drug delivery.[108] In this report RNA aptamer, was functionalized onto the diagnostic modality (Q-dots) to target the prostate-specific membrane antigen, whereas, the therapeutic modality doxorubicin (Dox) was intercalated into the aptamer. This study demonstrated the enhanced therapeutic specificity *in vitro* against the targeted LNCaP cells compared to non-specific PC3 cells using the functionalized Q-dots.

Furthermore, Q-dot–liposome system may constitute another multifunctional platform for imaging and therapy. In these systems, the Q-dots can either be incorporated into the bilayer membrane or can be functionalized onto a liposome[109] forming a Q-dot–lipid vesicle. Liposomes are one of the conventional nonviral drug and gene carriers. The introduction of Q-dots in liposomes reduces the in vivo cytotoxicity of the Q-dots, without altering its labeling specificity,[110-111] which remains comparable to other approaches.[109-112] Therefore, the assistance of liposomes and other well-developed polymeric gene carriers may be exploited for multifunctional Q-dot based theranostics.

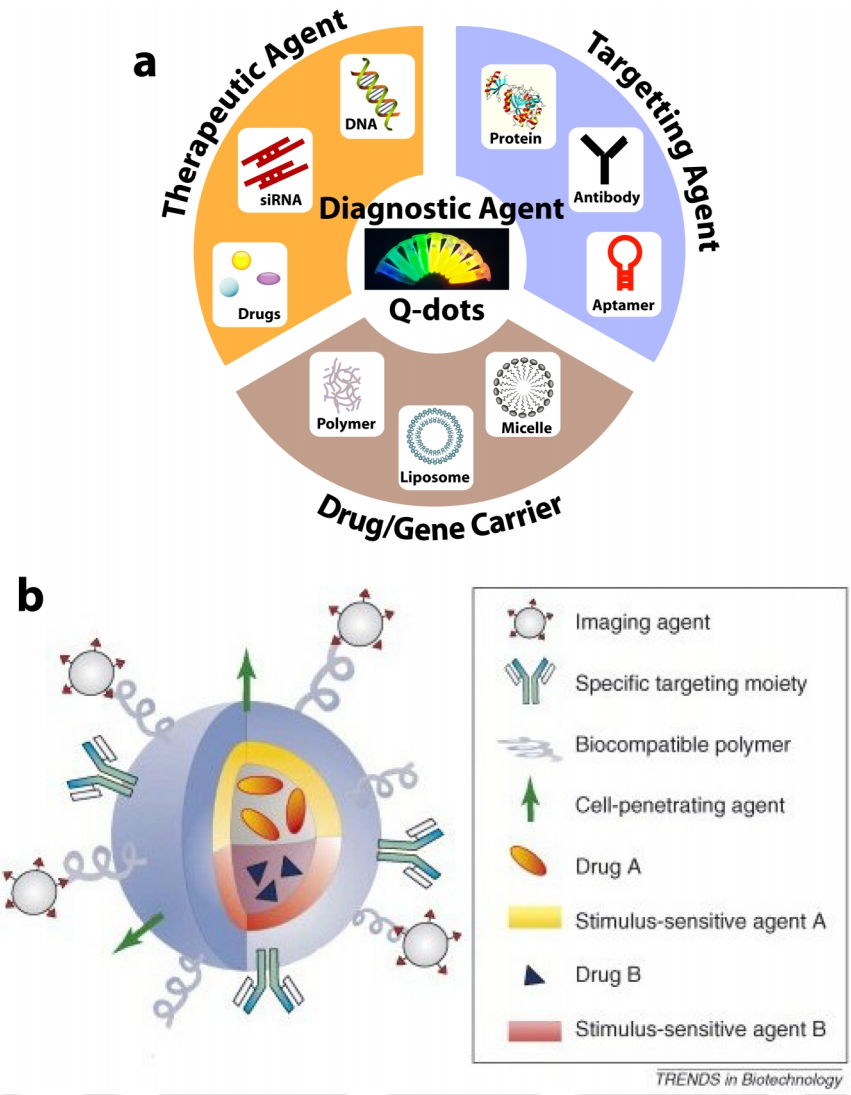

Figure 1.6. (**a**) Representation of the constituents of an idealized nanoplatform for an ideal "all in one" workstation with targeting, therapeutic and diagnostic modalities. Redrawn from Reference [40]. (**b**) Multifunctional nanoparticles for drug delivery. Multifunctional nanocarriers can combine a specific targeting agent (usually an antibody or peptide) with nanoparticles for imaging (such as quantum dots or magnetic nanoparticles), a cell-penetrating agent (e.g. the polyArg peptide TAT), a stimulus-sensitive element for drug release, a stabilising polymer to ensure biocompatibility (polyethylene glycol most frequently) and the therapeutic compound. Reproduced with permission from Reference [18]. Copyright © 2008, Elsevier. [Document enclosed in the Permissions section]

1.5. Challenges in Q-dot based Theranostics

The major and lingering concern for Q-dots based theranostics remains in the inherent cytotoxicity of the dots. Surface oxidation and leaching-out of heavy metal ions from the core remains a potential threat.[113-114] Derfus *et al.* reported that the oxidation of Cd on the Q-dot surface by oxygen or ultraviolet light and the subsequent release of the Cd^{2+} ions is a possible mechanism for the Q-dots cytotoxicity. However, when the Q-dot surface is coated with a protective shell of ZnS or hydrophilic molecules, no acute cytotoxicity or systemic toxicity in mice was detected.[114] Further, in addition to the dosage and exposure time of Q-dots, the toxicity majorly depends upon on the physicochemical properties of Q-dots, such as size, surface charge and surface coating materials.[115] The choice of an appropriate surface passivation has also been shown to be a critical parameter to address the toxicity issue, as the surface ligands itself can impair cell viability. Another source of Q-dots toxicity arises from the generation of reactive oxygen species (ROS) during the excitation of the Q-dots.[116-119] The Q-dots can transfer the absorbed energy to oxygen molecules and lead to the formation of free radicals capable of damaging DNA and other cellular components leading to apoptosis or necrosis.[120]

Q-dots are relatively new materials and their toxicity is yet to be fully understood.[121] The Q-dot mediated cellular responses must be correlated with its physicochemical properties to advance the field. Instead of paying much effort on optimization of the surface modifications of CdSe or CdTe Q-dots, alternative approaches to synthesize more biological – and environmentally – friendly Q-dots, such as silicon-based Q-dots[48-49] or carbon dots (C-dots)[50], should be pursued. Nontoxic, non Cd based Q-dots may hold the key to the future of Q-dot based theranostics. The challenge lies in the development of newer fluorescent material having photophysical properties and solubility similar to those of the group II–VI or III–V Q-dots and is nontoxic and biocompatible. Further concern remains regarding the utility of Q-dots as a tag for imaging, as the additional mass of the Q-dots conjugated to a biomolecule may alter the diffusivity of the molecule.[122] Additionally, the Q-dots can affect the functional property of the biomolecules by perturbing its native conformation. Efforts to synthesize Q-dot conjugates with a

thinner biocompatible coating, and hence reducing the overall size, would perhaps alleviate the concern. Smaller Q-dots would further benefit the FRET based sensing, by improving the energy transfer efficiency.[78, 123] The rewards of nanomedicine call for effort to synthesize well controlled, multifunctional, nontoxic Q-dot conjugates.

1.6 Carbon dots

Carbonaceous quantum dots, colloquially known as carbon nanodots or carbon dots (C-dots) has recently emerged as a fascinating class of fluorescent material that comprises discrete quasi-spherical nanoparticles with sizes less than 10 nm.[50, 124-125] Similar to its popular older cousins, the fullerene, the carbon nanotube, and graphene, C-dots have gradually become a rising star in the nanocarbon family, due to their benign and inexpensive nature.[50, 126-127] Additionally, these surface passivated C-dots have several attributes similar to those of the traditional semiconductor Q-dots, namely, size and excitation tuneable emission, photostability and ease of bioconjugation without suffering from the burden of cytotoxicity or elemental scarcity or the need of expensive and tedious synthesis steps as in case of the semiconductor Q-dots.[50, 124-127] The C-dots were discovered by Scrivens *et al.* in serendipity.[128] While purifying single walled carbon nanotubes (SWCNT) using gel electrophoresis, they were amazed to observe a fast moving luminescent band. These researchers analyzed the basic property of the then-unknown fluorescent nanomaterial, which was distinct from the SWCNT and ascertain their possibility to emerge as a promising nanomaterial in their own right. Since their discovery these materials came to be known as C-dots and immense research have been channelized in this field in order to understand its photophysical behavior and establish its possible applications.[50, 124-127]

C-dots have excellent water solubility due to the surface coverage with many carboxylic acid moieties which also helps in its functionalization with various organic, polymeric, inorganic or biological species. In contrast to nanodiamonds, which possess a sp^3 hybridized core, C-dots have greater sp^2 characteristic and are relatively close to the graphene Q-dots and contain low carbon to oxygen ratio.[50]

C-dots are also sometimes referred to as carbogenic nanodots due to its high oxygen content.[129-130] Typically, C-dots have strong optical absorption in the UV range with a tail extending to the visible spectrum. The fluorescence profiles of the C-dots are generally broad and are excitation tunable.[50, 124-127] The phenomenon responsible for the emergence of fluorescence from the C-dots is still a paradox. Whether the excitation dependent fluorescence arises from the optical selection of differently sized particle and/or due to the presence of emissive traps on the C-dots surface or some newer mechanism altogether remains unsolved.

1.6.1 Synthesis

The synthetic methods for C-dots can be broadly classified into two groups: top-down and bottom-up approaches.[50, 124-127] The various techniques demonstrated for the synthesis are summarized in **Figure 1.7**. In the top-down method, the C-dots are formed or broken off from a larger carbon material and the techniques involved include arc discharge, laser ablation and electrochemical oxidation.

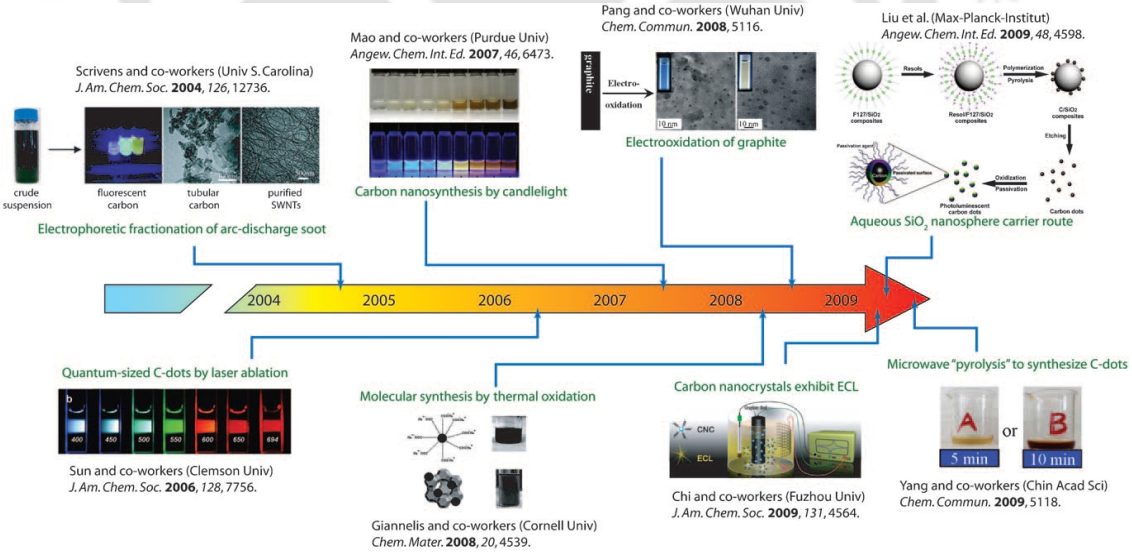

Figure 1.7. Timeline showing the development in the field of C-dots synthesis. Reproduced with permission from Reference [50]. Copyright © 2010 WILEY-VCH Verlag GmbH & Co. KGaA, Weinheim. [Document enclosed in the Permissions section]

Whereas, in case of bottom-up approach the C-dots are formed from molecular precursors via combustion/thermal, supported synthetic or microwave methods. After synthesis, their surfaces are oxidized by nitric acid or other oxidizing agents and finally purified by using centrifugation, dialysis or electrophoretic techniques.

In the year 2004, Xu *et al.* isolated fluorescent C-dots from the purification step of SWCNTs derived from arc discharge soot.[128] The synthesized C-dots resolved into 3 bands exhibiting green-blue, yellow and orange emission when excited at 366 nm. Sun and coworkers produced C-dots by laser ablation method.[131-134] They prepared a carbon target by hot pressing a mixture of graphite and cement, which was ablated by a Q-switched Nd:YAG laser and the resulting product was refluxed using 2.6 M HNO_3 to yield 3 to 10 nm sized C-dots which was finally passivated using diamine terminated poly(ethylene glycol). The electrochemical synthetic method was exploited by Zhao *et al.* to prepare C-dots.[135] They used multiwalled cabon nanotube (MWCNT) as working electrode in an electrochemical cell with degassed acetonitrile solution containing 0.1 M tetrabutylammonium perchlorate as the electrolyte. Cycling of the applied potential resulted in the development of yellow to brown coloration of the colorless solution, indicating the exfoliation of the C-dots from the MWCNT electrode into the solution.

Several researchers have used soot derived from the combustion of unscented candles, natural gas as an elegant raw material for the synthesis of C-dots following bottom-up approach.[136-138] Mao *et al.* collected soot by placing a piece of aluminium foil or glass plate on the top of a burning candle and the obtained soot were refluxed using 5 M HNO_3 to oxidize the particles.[136] Subsequently, Chen and coworkers collected soot from the combustion of natural gas and oxidized following procedures similar to those of Mao *et al.*[138] Giannelis and co-workers demonstrated a single-step thermal decomposition of low temperature melting molecular precursor to synthesize surface passivated hydrophilic or organophillic C-dots.[130] Ammonium citrate salt was used as the precursor molecule for preparing the hydrophilic C-dots, where the citrate provided the carbon source and the ammonium the stabilizer. The organophillic C-dots were synthesized by

calcining the precursor octadecylammonium citrate or 4-aminoantipyrene. Another bottom-up approach involving supported growth of C-dots was reported by Liu and coworkers.[139] In this method, a composite of silica spheres with pluronic F127 was prepared and resols acting as carbon precursor were introduced into it; subsequent polymerization and thermal heating of the composite yielded C-dot/SiO_2 composite. NaY zeolite supported growth of C-dots were later demonstrated by Giannelis *et al.*[133] Microwave mediated synthesis of C-dots were also demonstrated using different saccharides as the precursor molecules.[140-141]

1.6.2 Applications

The major applications of the C-dots are in the field of bioimaging and photocatalysis.[50, 124-125] Due to the established low toxicity and excitation tunable emission property of the C-dot, they are appearing as emergent nanolights for bioimaging applications. The first demonstration on the bioimaging capability of the C-dots was reported by Sun and coworker which was subsequently followed by many other researchers.[131-132, 142-143] In their study, they showed the potential ability of the PEI-EI passivated C-dots for visualizing the human breast cancer MCF-7 cells using a two photon luminescence microscopy.[131] On the similar lines Ray *et al.* demonstrated the use of C-dots in conventional bioimaging application in Ehrilch ascites carcinoma (EACs) cells.[137] Recently, Chen and coworkers demonstrated the light triggered theranostic application of C-dots.[144] In their study they showed the C-dots–Ce6 conjugate can act as a good candidate with excellent imaging and tumor-homing ability for NIR fluorescence imaging monitored PDT treatment.

C-dots have also been demonstrated to be used in photocatalytic applications.[125] Kang *et al.* demonstrated the design of complex photocatalytic system comprising TiO_2/C-dots and SiO_2/C-dots which was used to harness the entire solar spectrum based on the upconversion luminescence properties of C-dots.[145] Based on similar principle they further reported a series of C-dots composite photocatalytic system such as C-dots/ZnO, C-dots/Fe_2O_3, C-dots/Ag/$AgPO_4$ and etc.[146-148] Additionally, C-dots were also demonstrated to be

used for the catalytic reduction of metal salts either by the application of microwave irradiation or through exposure using Xe arc/ mercury vapor lamp. [149-150]

1.7. Key Areas and Scopes

Based on the literature review in the field of therapeutic and diagnostic applications of Q-dots, the research areas with potential scope are summarized below:

- Synthesis of nontoxic fluorescent Q-dots (semiconductor/ carbon based)
- Investigating the interaction of Q-dots with metallic NPs for possible FRET/NSET based applications
- Designing biocompatible Q-dot based traceable polymer nanocarriers for theranostics
- Exploring novel strategies for sensing and water remediation using Q-dots
- Demonstrating the applicability of C-dots in material sciences

1.8. The Present Work

1.8.1. Objectives

The main objectives of the present work are as follows:

- To study the interaction between the ZnS Q-dots and Ag NPs for predicting the applicability of the Q-dots in tracing Ag NP delivery and for FRET/NSET based applications.
- To evaluate the application potential of multimodal chitosan nanocarriers for suicide gene therapy.
- To fabricate Q-dots impregnated chitosan film for heavy metal ion sensing and removal from contaminated water.
- To design a simple novel technique for the synthesis of C-dots using biocompatible polymer and demonstrate its biolabeling property.

- To demonstrate the catalytic activity of the synthesized C-dots for a simple, room temperature based methodology for Au NP synthesis.

1.8.2. Significance and Salient Features of the Present Study

The significance and salient features of the present study are summarized below

- The effect of silver nanoparticles on the fluorescent properties of the biopolymer stabilized ZnS Q-dots was investigated in order to predict the suitability of the Q-dots as a probe for the delivery of Ag NPs.
- The mechanism involved in the fluorescence quenching of the ZnS Q-dots by Ag NPs were demonstrated and its practicability to act as donor acceptor pair in FRET/NSET process was illustrated.
- Multifunctional chitosan nanocarriers having ZnS Q-dots and folic acid as imaging and targeting moieties were demonstrated for theranostics.
- The synthesized functional nanocarriers were used for binding and cellular delivery of the bifunctional suicide gene cytosine deaminase-uracil phosphoribosyl transferase (CD-UPRT) for potential application in gene therapy.
- The chitosan stabilized ZnS Q-dots were also exploited for the fabrication of chitosan film for sensing and removal of heavy metal ions from water.
- The detailed mechanism of cation exchange reaction in Q-dots responsible for the sensing and removal of heavy metal ions from water were validated.
- Carbon dots, a newer fluorescent nanomaterial were synthesized by the microwave mediated caramelization of an FDA approved polymer, PEG, for the first time as precursor and passivating agent. The biolabeling application of the C-dots was successfully demonstrated on cancer cell lines.
- The synthesized C-dots were also demonstrated to be used as catalyst for a simple room temperature synthesis of mono-disperse Au NPs. The influence of varying concentration of the precursor and the catalyst on Au NP synthesis in the present case was also studied.

1.9. References

1. A. M. Smith, G. Ruan, M. N. Rhyner, S. Nie, *Ann. Biomed. Eng.*, **2006**, 34, 3–14.
2. V. Balzani, *Small*, **2005**, 1, 278–283.
3. R. F. Service, *Science*, **1999**, 283, 27–28.
4. N. Taniguchi, "*Nanotechnology: Materials Processing with an Atomic or Molecular Size Working Unit*," Kinzoku Hyomen Gijustu, **1978**, 29, 220-231
5. E. Drexler, *Engines of Creation: The Coming Era of Nanotechnology*, First Ed., Anchor Books, Doubleday: New York, **1986**.
6. K. Eric Drexler, "Preface," in K. Eric Drexler, Chris Peterson, Gayle Pergamit, *Unbounding the Future: The Nanotechnology Revolution* (New York: Morrow, **1991**), 10.
7. W. Junge, *Proc. Natl. Acad. Sci. U. S. A.*, **1999**, 96, 4735–4737.
8. Y. Sambongi, I. Ueda, Y. Wada, M. Futai, *J. Bioenerg. Biomembr.*, **2000**, 32, 441–448.
9. S. A. Endow, *BioEssays*, **2003**, 25, 1212–1219.
10. K. E. Drexler, *Annual Review of Biophysics and Biomolecular Structure* **1994**, 23, 377–405.
11. K. E. Drexler, *Phil. Trans. R. Soc. Lond. A,* **1995**, 353, 323–331.
12. K. E. Drexler, *Trends in Biotecnol.*, **1999**, 17, 5–7
13. The Brog are cybernetically–enhanced biological beings linked through a collective conscience. The nanoprobes integrated into their circulatory systems fulfill the purposes of constructing, maintaining and repairing as well as assimilating other humanoid "species" and technologies. The Brog seek perfection through the intake of technology. "We are the Brog. You will be assimilated. Resistance is futile."
14. S. Catellin, *J. Incl. Phenom. Macro. Chem.*, **2009**, 65, 197–204.
15. J. Bath, A. J. Turberfield, *Nat. Nanotechnol.*, **2007**, 2, 275–284.
16. J. J. Li, W. Tan, *Nano Lett.*, **2002**, 2, 315–318.
17. R. P. Goodman, M. Heilemann, S. Doose, C. M. Erben, A. N. Kapanidis, A. J. Turberfield, *Nat. Nanotechnol.*, **2008**, 3, 93–96.
18. N. Sanvicens, M. P. Marco, *Trends Biotechnol.*, **2008**, 26, 425–433.
19. D. Peer, J. M. Karp, S. Hong, O. C. Farokhzad, R. Margalit, R. Langer, *Nat. Nanotechnol.*, **2007**, 2, 751–760.
20. K. Bourzac, *Nature,* **2012**, 491, S58–S60.
21. N. Nishiyama, *Nat. Nanotechnol.*, **2007**, 2, 203–204.
22. P. Debbage, *Curr. Pharm. Design*, **2009**, 15, 153–172.
23. R. P. Feynman, *Engineering and Science,* **1960**, 22–36.

24. Kroto, J. R. Heath, S. C. O'Brien, R. F. Curl, R. E. Smalley, *Nature,* **1985**, 318, 162–163.
25. W. Krätschmer, L. D. Lamb, K. Fostiropoulos, D. R. Huffman, *Nature,* **1990**, 347, 354–358.
26. M. S. Dresselhaus, G. Dresslhaus, *Annual Review of Materials Science,* **1995**, 25, 487–523.
27. T. W. Ebbesen, P. M. Ajayan, *Nature,* **1992**, 358, 220–222.
28. M. Ganzhorn, S. Klyatskaya, M. Ruben, W. Wernsdorfer, *Nat. Nanotechnol.*, **2013**, 8, 165–169.
29. M. C. Hersam, *Nat. Nanotechnol.*, **2008**, 3, 387–394.
30. X. Michalet, F. F. Pinaud, L. A. Bentolila, J. M. Tsay, S. Doose, J. J. Li, G. Sundaresan, A. M. Wu, S. S. Gambhir, S. Weiss, *Science,* **2005**, 307, 538–544.
31. K. Bourzac, *Nature,* **2013**, 493, 283–283.
32. M. Han, X. Gao, J. Z. Su, S. Nie, *Nat. Biotechnol.*, **2001**, 19, 631–635.
33. I. L. Medintz, H. T. Uyeda, E. R. Goldman, H. Mattoussi, *Nat. Mater.*, **2005**, 4, 435–446.
34. E. M. Pridgen, R. Langer, O. C. Farokhzad, *Nanomedicine*, **2007**, 2, 669–680.
35. F. Gu, L. Zhang, B. A. Teply, N. Mann, A. Wang, A. F. Radovic-Moreno, R. Langer, O. C. Farokhzad, *Proc. Natl. Acad. Sci. U. S. A.*, **2008**, 105, 2586–2591.
36. T. Patel, J. Zhou, J. M. Piepmeier, W. M. Saltzman, *Adv. Drug Deliv. Rev.*, **2012**, 64, 701–705.
37. M. A. C. Stuart, W. T. S. Huck, J. Genzer, M. Müller, C. Ober, M. Stamm, G. B. Sukhorukov, I. Szleifer, V. V. Tsukruk, M. Urban, F. Winnik, S. Zauscher, I. Luzinov, S. Minko, *Nat. Mater.*, **2010**, 9, 101–113.
38. M. Faraday, *Philosophical Transactions of the Royal Society of London,* **1857**, 147, 145–181.
39. K. Park, *J. Control. Release*, **2007**, 120, 1–3.
40. Y.-P. Ho, K. W. Leong, *Nanoscale* **2010**, 2, 60–68.
41. H. Sajja, M. East, H. Mao, Y. Wang, S. Nie, L. Yang, *Curr. Drug Discov. Tech.*, **2009**, 6, 43–51.
42. M. Sitti, *Nature,* **2009**, 458, 1121–1122.
43. O. M. Koo, I. Rubinstein, H. Onyuksel, *Nanomed. Nanotechno. Biol. Med.*, **2005**, 1, 193–212.
44. J. L. West, N. J. Halas, *Ann. Rev. Biomed. Eng.*, **2003**, 5, 285–292.
45. W. Zhong, *Anal. Bioanal. Chem.*, **2009**, 394, 47–59.

46. G. Schmid, M. Bäumle, M. Geerkens, I. Heim, C. Osemann, T. Sawitowski, *Chem. Soc. Rev.*, **1999**, 28, 179–185.
47. L. Shang, S. Dong, G. U. Nienhaus, *Nano Today*, **2011**, 6, 401–418.
48. K. Dohnalová, A. N. Poddubny, A. A. Prokofiev, W. D. de Boer, C. P. Umesh, J. M. Paulusse, H. Zuilhof, T. Gregorkiewicz, *Light Sci. Appl.*, **2013**, 2, e47.
49. F. Erogbogbo, C.-A. Tien, C.-W. Chang, K.-T. Yong, W.-C. Law, H. Ding, I. Roy, M. T. Swihart, P. N. Prasad, *Bioconjugate Chem.*, **2011**, 22, 1081–1088.
50. S. N. Baker, G. A. Baker, *Angew. Chem. Int. Ed.*, **2010**, 49, 6726–6744.
51. A. M. Smith, S. Nie, *Acc. Chem. Res.*, **2010**, 43, 190–200.
52. G. Schmid, Ed., *Nanoparticles: From Theory to Application*, Wiley-VCH, **2010**.
53. C. S. S. R. Kumar, *Semiconductor Nanomaterials*, John Wiley & Sons, **2010**.
54. C. A. Leatherdale, W.-K. Woo, F. V. Mikulec, M. G. Bawendi, *J. Phys. Chem. B*, **2002**, 106, 7619–7622.
55. U. Resch-Genger, M. Grabolle, S. Cavaliere-Jaricot, R. Nitschke, T. Nann, *Nat. Meth.*, **2008**, 5, 763–775.
56. M. Bruchez, M. Moronne, P. Gin, S. Weiss, A. P. Alivisatos, *Science*, **1998**, 281, 2013–2016.
57. W. C. W. Chan, S. Nie, *Science*, **1998**, 281, 2016–2018.
58. B. O. Dabbousi, J. Rodriguez-Viejo, F. V. Mikulec, J. R. Heine, H. Mattoussi, R. Ober, K. F. Jensen, M. G. Bawendi, *J. Phys. Chem. B*, **1997**, 101, 9463–9475.
59. X. Gao, L. Yang, J. A. Petros, F. F. Marshall, J. W. Simons, S. Nie, *Curr. Opin. Biotechnol.*, **2005**, 16, 63–72.
60. X. Gao, Y. Cui, R. M. Levenson, L. W. K. Chung, S. Nie, *Nat. Biotechnol.*, **2004**, 22, 969–976.
61. A. R. Kortan, R. Hull, R. L. Opila, M. G. Bawendi, M. L. Steigerwald, P. J. Carroll, L. E. Brus, *J. Am. Chem. Soc.*, **1990**, 112, 1327–1332.
62. L. Qu, X. Peng, *J. Am. Chem. Soc.*, **2002**, 124, 2049–2055.
63. C. B. Murray, D. J. Norris, M. G. Bawendi, *J. Am. Chem. Soc.*, **1993**, 115, 8706–8715.
64. D. V. Talapin, A. L. Rogach, A. Kornowski, M. Haase, H. Weller, *Nano Lett.*, **2001**, 1, 207–211.
65. H. Yang, P. H. Holloway, *Adv. Funct. Mater.*, **2004**, 14, 152–156.
66. M. A. Hines, P. Guyot-Sionnest, *J. Phys. Chem.*, **1996**, 100, 468–471.
67. X. Gao, S. R. Dave, *Bio-Applications of Nanoparticles* (Ed.: W.C.W. Chan), Springer New York, **2007**, 57–73.
68. X. Wu, H. Liu, J. Liu, K. N. Haley, J. A. Treadway, J. P. Larson, N. Ge, F. Peale, M. P. Bruchez, *Nat. Biotechnol.*, **2003**, 21, 41–46.

69. B. Dubertret, P. Skourides, D. J. Norris, V. Noireaux, A. H. Brivanlou, A. Libchaber, *Science*, **2002**, 298, 1759–1762.
70. C. Kirchner, T. Liedl, S. Kudera, T. Pellegrino, A. Muñoz Javier, H. E. Gaub, S. Stölzle, N. Fertig, W. J. Parak, *Nano Lett.*, **2005**, 5, 331–338.
71. J.-W. Lee, D.-Y. Son, T. K. Ahn, H.-W. Shin, I. Y. Kim, S.-J. Hwang, M. J. Ko, S. Sul, H. Han, N.-G. Park, *Sci. Rep.*, **2013**, 3, DOI 10.1038/srep01050.
72. L. Sun, J. J. Choi, D. Stachnik, A. C. Bartnik, B.-R. Hyun, G. G. Malliaras, T. Hanrath, F. W. Wise, *Nat. Nanotechnol.*, **2012**, 7, 369–373.
73. N. Kirstaedter, N. N. Ledentsov, M. Grundmann, D. Bimberg, V. M. Ustinov, S. S. Ruvimov, M. V. Maximov, P. S. Kop'ev, Z. I. Alferov, U. Richter, P. Werner, U. Gosele, J. Heydenreich, *Electronics Lett.*, **1994**, 30, 1416–1417.
74. G. Konstantatos, E. H. Sargent, *Proceedings of the IEEE*, **2009**, 97, 1666–1683.
75. D. Loss, D. P. DiVincenzo, *Phys. Rev. A*, **1998**, 57, 120–126.
76. R. Freeman, I. Willner, *Chem. Soc. Rev.*, **2012**, 41, 4067–4085.
77. B. N. G. Giepmans, T. J. Deerinck, B. L. Smarr, Y. Z. Jones, M. H. Ellisman, *Nat. Methods*, **2005**, 2, 743–749.
78. I. L. Medintz, H. Mattoussi, *Phys. Chem. Chem. Phys.*, **2009**, 11, 17–45.
79. W. R. Algar, U. J. Krull, *Anal. Bioanal. Chem.*, **2008**, 391, 1609–1618.
80. H. X. Xu, M. Y. Sha, E. Y. Wong, J. Uphoff, Y. H. Xu, J. A. Treadway, A. Truong, E. O'Brien, S. Asquith, M. Stubbins, N. K. Spurr, E. H. Lai, W. Mahoney, *Nucleic Acids Res.*, **2003**, 31, e43.
81. Y. P. Ho, M. C. Kung, S. Yang, T. H. Wang, *Nano Lett.*, **2005**, 5, 1693–1697.
82. E. Oh, D. Lee, Y.-P. Kim, S. Y. Cha, D.-B. Oh, H. A. Kang, J. Kim, H.-S. Kim, *Angew. Chem. Int. Ed.*, **2006**, 45, 7959–7963.
83. K. E. Sapsford, T. Pons, I. L. Medintz, H. Mattoussi, *Sensors*, **2006**, 6, 925–953.
84. A. P. Alivisatos, W. Gu, C. Larabell, *Annu. Rev. Biomed. Eng.*, **2005**, 7, 55–76.
85. X. Michalet, F. Pinaud, T. D. Lacoste, M. Dahan, M. P. Bruchez, A. P. Alivisatos, S. Weiss, *Single Mol.*, **2001**, 2, 261–276.
86. I. L. Medintz, H.Mattoussi, A. R. Clapp, *Int. J. Nanomed.*, **2008**, 3, 151–167.
87. M. E. Akerman, W. C. Chan, P. Laakkonen, S. N. Bhatia, E. Ruoslahti, *Proc. Natl. Acad. Sci. U. S. A.*, **2002**, 99, 12617–12621.
88. M. Mammen, S. K. Choi, G. M. Whitesides, *Angew. Chem., Int. Ed.*, **1998**, 37, 2754–2794.
89. J. J. Storhoff, A. A. Lazarides, R. C. Mucic, C. A. Mirkin, R. L. Letsinger, G. C. Schatz, *J. Am. Chem. Soc.*, **2000**, 122, 4640–4650.
90. T. Kirchhausen, *Nat. Rev. Mol. Cell Biol.*, **2000**, 1, 187–198.

91. R. A. Petros, J. M. DeSimone, *Nat. Rev. Drug Discov.,* **2010**, 9, 615–627.
92. W. J. Parak, R. Boudreau, M. Le Gros, D. Gerion, D. Zanchet, C. M. Micheel, S. C. Williams, A. P. Alivisatos, C. Larabell, *Adv. Mater.*, **2002**, 14, 882–885.
93. A. M. Derfus, W. C. W. Chan, S. N. Bhatia, *Adv. Mater.*, **2004**, 16, 961–966.
94. J. B. Delehanty, H. Mattoussi, I. L. Medintz, *Anal. Bioanal. Chem.*, **2009**, 393, 1091–1105.
95. F. Q. Chen and D. Gerion, *Nano Lett.*, **2004**, 4, 1827–1832.
96. K. Yum, S. Na, Y. Xiang, N. Wang, M. Yu, *Nano Lett.*, **2009**, 9, 2193–2198.
97. C. Srinivasan, J. Lee, F. Papadimitrakopoulos, L. K. Silbart, M. Zhao, D. J. Burgess, *Mol. Ther.*, **2006**, 14, 192–201.
98. Y. P. Ho, H. H. Chen, K. W. Leong, T. H. Wang, *J. Control. Release*, **2006**, 116, 83–89.
99. C. Y. Zhang, H. C. Yeh, M. T. Kuroki, T. H. Wang, *Nat. Mater.*, **2005**, 4, 826–831.
100. H. H. Chen, Y. P. Ho, X. Jiang, H. Q. Mao, T. H. Wang, K. W. Leong, *Nano Today*, **2009**, 4, 125–134.
101. A. A. Chen, A. M. Derfus, S. R. Khetani,S. N. Bhatia, *Nucleic Acids Res.*, **2005**, 33, e190.
102. W. B. Tan, S. Jiang, Y. Zhang, *Biomaterials*, **2007**, 28, 1565–1571.
103. N. Manabe, A. Hoshino, Y. Liang, T. Goto, N. Kato, K. Yamamoto, *IEEE Trans. NanoBiosci.*, **2006**, 5, 263–267.
104. V. P. Torchilin, *Adv. Drug Delivery Rev.*, **2006**, 58, 1532–1555.
105. K. Park, S. Lee, E. Kang, K. Kim, K. Choi, I. C. Kwon, *Adv. Funct. Mater.*, **2009**, 19, 1553–1566.
106. A. K. Salem, P. C. Searson, K. W. Leong, *Nat. Mater.*, **2003**, 2, 668–671.
107. S. Santra, C. Kaittanis, J. Grimm, J. M. Perez, *Small*, **2009**, 5, 1862–1868.
108. V. Bagalkot, L. Zhang, E. Levy-Nissenbaum, S. Jon, P. W. Kantoff, R. Langer, O. C. Farokhzad, *Nano Lett.*, **2007**, 7, 3065–3070.
109. K. C. Weng, C. O. Noble, B. Papahadjopoulos-Sternberg, F. F. Chen, D. C. Drummond, D. B. Kirpotin, D. Wang, Y. K. Hom, B. Hann, J. W. Park, *Nano Lett.*, **2008**, 8, 2851–2857.
110. W. T. Al-Jamal, K. T. Al-Jamal, P. H. Bomans, P. M. Frederik, K. Kostarelos, *Small*, **2008**, 4, 1406–1415.
111. W. T. Al-Jamal, K. T. Al-Jamal, B. Tian, A. Cakebread, J. M. Halket, K. Kostarelos, *Mol. Pharmaceutics*, **2009**, 6, 520–530.
112. G. D. Bothun, A. E. Rabideau, M. A. Stoner, *J. Phys. Chem. B*, **2009**, 113, 7725–7728.
113. E. Chang, N. Thekkek, W. W. Yu, V. L. Colvin, R. Drezek, *Small*, **2006**, 2, 1412–1417.
114. A. M. Derfus, W. C. W. Chan, S. N. Bhatia, *Nano Lett.*, **2004**, 4, 11–18.

115. A. Hoshino, N. Manabe, K. Fujioka, K. Suzuki, M. Yasuhara, K. Yamamoto, *J. Artif. Organs*, **2007**, 10, 149–157.
116. S. J. Cho, D. Maysinger, M. Jain, B. Röder, S. Hackbarth, F. M. Winnik, *Langmuir*, **2007**, 23, 1974–1980.
117. J. Lovrić, S. J. Cho, F. M. Winnik, D. Maysinger, *Chem. Biol.*, **2005**, 12, 1227–1234.
118. B. I. Ipe, M. Lehnig, C. M. Niemeyer, *Small*, **2005**, 1, 706–709.
119. W.-H. Chan, N.-H. Shiao, P.-Z. Lu, *Toxicol. Lett.*, **2006**, 167, 191–200.
120. M. Green, E. Howman, *Chem. Commun.*, **2005**, 121–123.
121. H. Mok, K. H. Bae, C. H. Ahn, T. G. Park, *Langmuir*, **2009**, 25, 1645–1650.
122. H. Chen, I. Titushkin, M. Stroscio, M. Cho*, Biophys J.*, **2007**, 92, 1399–1408.
123. D. Zhou, L. Ying, X. Hong, E. A. Hall, C. Abell, D. Klenerman, *Langmuir*, **2008**, 24, 1659–1664.
124. Z. Liu, *Theranostics*, **2012**, 2, 235–237.
125. H. Li, Z. Kang, Y. Liu, S.-T. Lee, *J. Mater. Chem.*, **2012**, 22, 24230–24253.
126. P. G. Luo, S. Sahu, S.-T. Yang, S. K. Sonkar, J. Wang, H. Wang, G. E. LeCroy, L. Cao, Y.-P. Sun, *J. Mater. Chem. B*, **2013**, DOI 10.1039/C3TB00018D.
127. S. Zhu, Q. Meng, L. Wang, J. Zhang, Y. Song, H. Jin, K. Zhang, H. Sun, H. Wang, B. Yang, *Angew. Chem. Int. Ed.*, **2013**, DOI: 10.1002/anie.201300519
128. X. Xu, R. Ray, Y. Gu, H. J. Ploehn, L. Gearheart, K. Raker, W. A. Scrivens, *J. Am. Chem. Soc.*, **2004**, 126, 12736–12737.
129. A. B. Bourlinos, A. Stassinopoulos, D. Anglos, R. Zboril, V. Georgakilas, E. P. Giannelis, *Chem. Mater.*, **2008**, 20, 4539–4541.
130. A. B. Bourlinos, A. Stassinopoulos, D. Anglos, R. Zboril, M. Karakassides, E. P. Giannelis, *Small*, **2008**, 4, 455–458.
131. L. Cao, X. Wang, M. J. Meziani, F. Lu, H. Wang, P. G. Luo, Y. Lin, B. A. Harruff, L. M. Veca, D. Murray, S.-Y. Xie, Y.-P. Sun, *J. Am. Chem. Soc.*, **2007**, 129, 11318–11319.
132. Y.-P. Sun, B. Zhou, Y. Lin, W. Wang, K. A. S. Fernando, P. Pathak, M. J. Meziani, B. A. Harruff, X. Wang, H. Wang, P. G. Luo, H. Yang, M. E. Kose, B. Chen, L. M. Veca, S.-Y. Xie, *J. Am. Chem. Soc.*, **2006**, 128, 7756–7757.
133. A. B. Bourlinos, A. Stassinopoulos, D. Anglos, R. Zboril, V. Georgakilas, E. P. Giannelis, *Chem. Mater.*, **2008**, 20, 4539–4541.
134. S.-L. Hu, K.-Y. Niu, J. Sun, J. Yang, N.-Q. Zhao, X.-W. Du, *J. Mater. Chem.*, **2009**, 19, 484–488.
135. Q.-L. Zhao, Z.-L. Zhang, B.-H. Huang, J. Peng, M. Zhang, D.-W. Pang, *Chem. Commun.*, **2008**, 5116–5118.
136. H. Liu, T. Ye, C. Mao *Angew. Chem. Int. Ed.*, **2007**, 119, 6593–6595.

137. S. C. Ray, A. Saha, N. R. Jana, R. Sarkar, *J. Phys. Chem. C*, **2009**, 113, 18546–18551.
138. L. Tian, D. Ghosh, W. Chen, S. Pradhan, X. Chang, S. Chen, *Chem. Mater.*, **2009**, 21, 2803–2809.
139. R. Liu, D. Wu, S. Liu, K. Koynov, W. Knoll, Q. Li, *Angew. Chem. Int. Ed.*, **2009**, 121, 4668–4671.
140. H. Zhu, X. Wang, Y. Li, Z. Wang, F. Yang, X. Yang, *Chem. Commun.*, **2009**, 5118–5120.
141. X. Wang, K. Qu, B. Xu, J. Ren, X. Qu, *J. Mater. Chem.*, **2011**, 21, 2445–2450.
142. S.-T. Yang, L. Cao, P. G. Luo, F. Lu, X. Wang, H. Wang, M. J. Meziani, Y. Liu, G. Qi, Y.-P. Sun, *J. Am. Chem. Soc.*, **2009**, 131, 11308–11309.
143. S.-T. Yang, X. Wang, H. Wang, F. Lu, P. G. Luo, L. Cao, M. J. Meziani, J.-H. Liu, Y. Liu, M. Chen, Y. Huang, Y.-P. Sun, *J. Phys. Chem. C*, **2009**, 113, 18110–18114.
144. P. Huang, J. Lin, X. Wang, Z. Wang, C. Zhang, M. He, K. Wang, F. Chen, Z. Li, G. Shen, D. Cui, X. Chen, *Adv. Mater.*, **2012**, 24, 5104–5110.
145. H. T. Li, X. D. He, Z. H. Kang, H. Huang, Y. Liu, J. L. Liu, S. Y. Lian, C. H. A. Tsang, X. B. Yang, S. T. Lee, *Angew. Chem., Int. Ed.*, **2010**, 49, 4430–4434
146. H. C. Zhang, H. Ming, S. Lian, H. Huang, H. Li, L. Zhang, Y. Liu, Z. Kang, S. T. Lee, *Dalton Trans.*, **2011**, 40, 10822–10825.
147. H. C. Zhang, H. Huang, H. Ming, H. T. Li, L. L. Zhang, Y. Liu, Z. H. Kang, *J. Mater. Chem.*, **2012**, 22, 10501–10506.
148. H. Yu, H. C. Zhang, H. T. Li, H. Huang, Y. Liu, H. Ming, Z. H. Kang, *New J. Chem.*, **2012**, 36, 1031–1035.
149. X. Qin, W. Lu, G. Chang, Y. Luo, A. M. Asiri, A. O. Al-Youbi, X. Sun, *Gold Bull.*, **2012**, 45, 61–67.
150. S. Mitra, S. Chandra, P. Patra, P. Pramanik, A. Goswami, *J. Mater. Chem.*, **2011**, 21, 17638–17641.

Chapter 2

Investigating Fluorescence Quenching of ZnS Quantum dots by Silver Nanoparticles*

This chapter demonstrates the effect of silver nanoparticles on the fluorescence property of ZnS Q-dots. The quenching phenomenon was analyzed using Stern-Volmer plot and the mechanisms involved were explicated using steady state and time resolved spectroscopy.

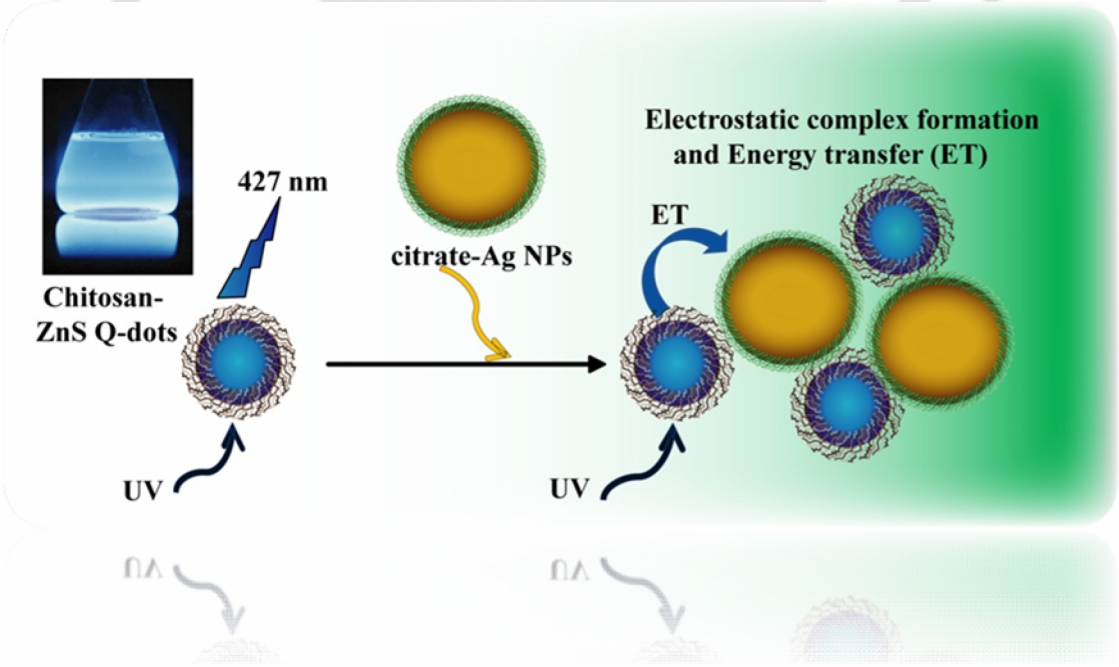

* Much of this work has appeared in print. It is reproduced with permission from *Plasmonics*, 2011, 6, 125-132. Copyright © 2010, Springer.

Chapter 2

Investigating Fluorescence Quenching of ZnS Quantum dots by Silver Nanoparticles

2.1. Introduction

Quantum dots (Q-dots) are inorganic semiconductor nanocrystals with remarkable optoelectronic properties originated from quantum confinement of the electronic motion, otherwise unavailable in either discrete atoms or bulk materials.[1-3] Q-dots have several advantages over conventional organic fluorophores because of their excellent resistance to photobleaching and optical properties tunable by size and material composition.[4] Most importantly, the broad absorption with narrow emission spectra of Q-dots makes them potential candidate for multiplex applications in bio-imaging as well as bio-tagging.[1, 3] In recent years, the extraordinary photo-physical properties Q-dots have been successfully exploited in various fields such as optoelectronic devices, imaging as well as biodiagnostics.[3, 5-7] Various sensing application has been developed based on the quenching of Q-dots fluorescence by metal nanoparticles or other molecules.[8-9] Q-dots can also act as efficient energy transfer donors or acceptors in Förster resonance energy transfer (FRET) based applications.[10-11] Several bioanalysis formats like molecular beacons, Taq man probes and immunoassays have been developed based on either quenching or FRET of Q-dots.[1, 11]

In last few years, a great deal of research – theoretical as well as experimental – has been carried out to understand the influence of metal surface on the emission properties of fluorophore.[12-14] A fluorophore near a metal film/metal NPs has been reported to show a varied degree of fluorescence depending on the distance between the metal surface and fluorophore.[15-16] However, the exact mechanism of differential fluorescence exhibited by a

fluorophore near a metal surface is still to be understood completely. In this regard, the fluorescent enhancement of conventional fluorophore or Q-dots in presence of Ag NPs has been well studied.[17-18] However, there are only few reports where Ag NPs have been used as an efficient quencher of the fluorophore.[19-20] Tay *et al.* has showed that the photoluminescence of surface functionalized Si was quenched by Ag NPs.[21] Recently, it has been reported that Ag NPs quenched the fluorescence of 1,4-dihydroxy-2,3-dimethyl-9,10-anthraquinone depending upon the particle size.[22] Ag NPs have been reported to act as enhancer of FRET efficiency, where hybridization of the donor-labeled oligonucleotide with the acceptor-labeled complimentary strand on Ag NP surface led to larger Förster distance. Zhang *et al.* showed that the FRET efficiency between cy5 and cy5.5 on the surface of Ag NPs was increased with particle size.[23] The report suggested that the conventional Förster distance can be increased to 75% by varying the particle size of the Ag NPs. However, the length scale for detecting dynamic changes in FRET – based methods is limited to a distance of < 10 nm by the nature of the dipole-dipole mechanism. On the other hand, Yun *et al.* reported that the energy transfer from a dipole to a nanometal surface (nanometal surface energy transfer, NSET) follows a $1/R^4$ distance dependence and the traditional Förster distance can be increased up to the range of 22 nm.[24] The quenching property of Ag NPs in FRET or NSET applications could stem from their plasmon resonance in the visible range which makes them strong absorbers with large extinction coefficients.[25] The development of long range FRET is therefore critical to investigate the biological multi-component systems, such as ribosomes or various nucleoprotein complexes.[24]

2.2. Outline of the Research Work

1) Water dispersible, chitosan stabilized ZnS Q-dots (~3 nm) were synthesized in an environment friendly way. The Q-dots showed bright blue emission with λ_{max} at 427 nm.
2) The fluorescence of ZnS Q-dots was significantly quenched in presence of citrate capped – Ag NPs (~37 nm) in a concentration dependent manner.

The quenching mechanism was analyzed using Stern-Volmer plot which indicated dual nature of quenching with K_{sv} value of 9×10^9 M^{-1}.

3) Static mechanism was evident from the formation of electrostatic complex between positively charged ZnS Q-dots and negatively charged Ag NPs, confirmed by absorbance study.
4) The role of energy transfer process as an additional quenching mechanism was investigated by time resolved fluorescence measurements which demonstrated decrease in the average lifetime of ZnS Q-dots fluorescence. The corresponding Förster distance for the Q-dot – NP pair was estimated to be 18.4 nm.
5) The results of the present study indicate that the ZnS Q-dot – Ag NP pair can be applied in FRET or NSET based analysis of biological multi-component systems such as ribosome, nucleoprotein complex, etc.

2.3. Experimental Section

2.3.1. Materials

Zinc acetate dihydrate [$Zn(CH_3COO)_2$, $2H_2O$], sodium sulfide [Na_2S], trisodium citrate, silver nitrate [$AgNO_3$] and acetic acid (glacial, 99–100 %) were purchased from Merck India Ltd, Mumbai, India. Chitosan (high MW, > 75 % deacetylated) was obtained from Sigma-Aldrich Chemical Pvt. Ltd., Kolkata, India. All chemicals employed were of AR grade and were used as received without further purification. Mili-Q ultrapure water (>18 MΩ cm, Millipore) was used in all experiment.

2.3.2. Synthesis of chitosan stabilized ZnS Q-dots

The synthesis of chitosan stabilized ZnS Q-dots was carried out using a modified inorganic wet-chemical synthesis method reported by Warad *et al.*[26] Briefly, 21 mg zinc acetate (0.01 M) was added to 9 mL of 0.05 % (w/v) chitosan solution under constant stirring and heated at 80 °C for 15 min. After cooling to room temperature, 1 mL of freshly prepared 16 mg mL^{-1} sodium sulfide was added dropwise to the mixture in an ice bath with continuous stirring. This resulted in

the formation of a milky white suspension without any sedimentation for more than 24 h, indicating the synthesis of ZnS nanocrystals. The as prepared colloidal solution of ZnS Q-dots was ultrasonicated to remove the dissolved gases, if any. Next, ZnS Q-dots were characterized by transmission electron microscopy (TEM) using a JEOL 2100 UHR-TEM instrument. 5 µL of ZnS Q-dots solution was drop-cast on carbon-coated copper grids and subsequently air-dried before TEM analysis. X-ray diffraction (XRD) pattern were recorded with Brucker D8 Advanced X-ray diffraction measurement system, with Cu Kα source (λ = 1.54 Å). UV-visible absorption spectra were recorded on a Varian Cary 100 spectrophotometer. Steady state fluorescence intensity was measured using Jobin-Yvon Fluoromax-3 spectrofluorimeter at an excitation wavelength of 315 nm. Quantum yield of ZnS Q-dots were calculated according to Williams' method[27] using Rhodamine 101 as a reference (Q.Y. = 100 %).[28]

2.3.3. Synthesis of citrate – capped Ag NPs

Citrate – capped Ag NPs were prepared by a modified Turkevich method.[29] Briefly, 1 mM aqueous solution of $AgNO_3$ was heated until it started to boil. As the boiling started, sodium citrate (5 mM) was added to it. The color of the solution slowly turned yellow and then grayish yellow after 30 min of boiling, indicating the formation of Ag NPs. The reaction was performed under refluxing condition to avoid loss of water by evaporation during boiling. The solution was cooled to room temperature and kept for 1 day. In order to remove excess Ag^+ ions, if any, the Ag NPs solution was centrifuged at 13000 g for 15 min and the pellet was washed for several times. Finally, the washed Ag NPs were resuspended in Milli-Q water and subsequently characterized by using UV-visible absorption spectroscopy (Varian, Cary 100 spectrophotometer) and TEM (JEOL 2100, UHR-TEM instrument).

2.3.4. Fluorescence Quenching of ZnS Q-dots by Ag NPs

The chitosan stabilized ZnS Q-dots were diluted to 1.4 µM in Milli-Q water and different concentrations of citrate – capped Ag NPs were added to it. The pH of all

the samples was 5.5. After 1 h of incubation, each sample was studied by steady state fluorescence as well as absorption spectroscopy. For all steady state fluorescence measurement excitation was set at 315 nm and the fluorescence emission spectra were recorded in the wavelength range of 360-560 nm. For quenching experiments, the integrated fluorescence intensity in the above mentioned range was used to determine F_o/F since it gave a flat baseline free from Raman scatter. Time-resolved intensity decays of the ZnS Q-dots both in absence and presence of quencher were recorded using a Life Spec II spectrofluorimeter (Edinburgh Instrument). The sample was excited by Pico-quant 308 nm LED source, and the decay was measured in a time scale of 0.0488 ns/channel. The decay curves were analyzed by FAST software, provided by Edinburgh Instrument along with the fluorescence instrument.

2.4. Results and Discussion

2.4.1. Synthesis and characterization of ZnS Q-dots

As is evident from the TEM image (**Figure 2.1a**), the chitosan stabilized ZnS Q-dots synthesized in the present study were nearly monodisperse and spherical in shape. The average particle size was found to be 2.9 nm from the corresponding particle size distribution shown in **Figure 2.1b**. The high resolution TEM (HRTEM) image shown in the inset of **Figure 2.1a**, depicts the lattice-resolved structure of ZnS Q-dots.

The UV-visible absorption spectrum (**Figure 2.1c**) of the ZnS Q-dots showed absorption edge around 300 nm, considerably blue-shifted compared to that of bulk ZnS at 340 nm.[30] This shift in band gap can be explained by the effective mass approximation model with the particle in a box approach.[31] Based on the first order approximation of Brus equation[32], the relationship between the particle radius (r) and band gap E_g in ZnS nanocrystal[33] is given by equation 2.1

$$r(E_g) = \frac{0.32 - 2.9\sqrt{(E_g - 3.49)}}{2(3.50 - E_g)} \qquad (2.1)$$

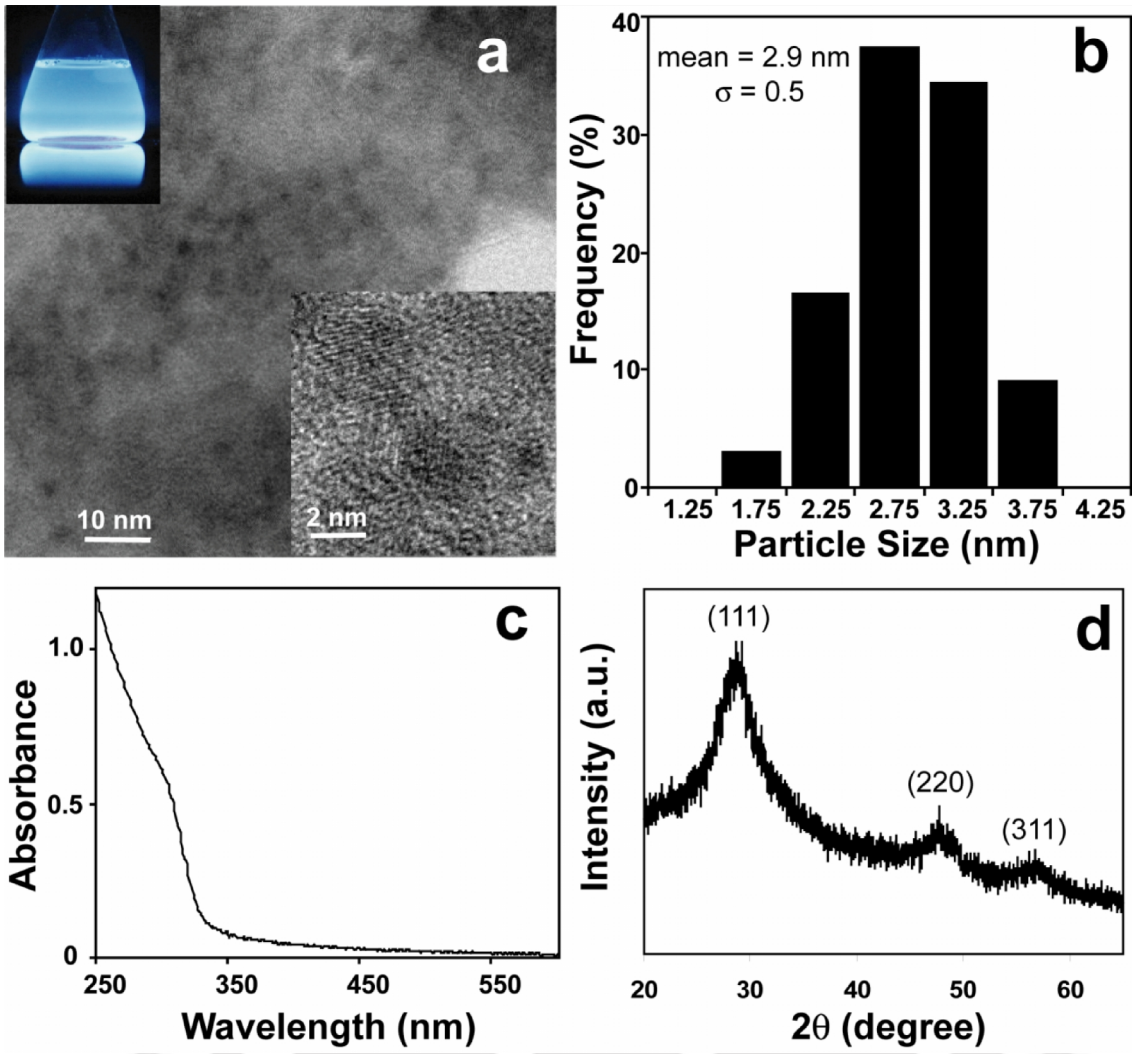

Figure 2.1. (**a**) TEM image of ZnS Q-dots with HRTEM image (inset) showing lattice fringes. (**b**) Particle size distribution, (**c**) UV-visible spectra and (**d**) XRD pattern of the corresponding ZnS Q-dots

Using equation (2.1), the diameter of the ZnS nanocrystal (considering E_g = 4.14 eV) was calculated to be 3.14 nm which is in good agreement with TEM results. The extinction coefficient of ZnS Q-dots at 315 nm was estimated to be 3.3 × 10^5 M^{-1} cm^{-1}. The crystallinity of the ZnS Q-dots was confirmed by powder XRD analysis. The XRD pattern (**Figure 2.1d**) consisted of characteristic peaks at 28.5°, 47.5° and 56.5° corresponding to principal Bragg reflections in {111}, {220} and {311} lattice planes, respectively, of bulk ZnS crystallizing in cubic zinc blende structure according to the JCPDS-ICDD database.[34] The quantum yield of ZnS Q-dots was calculated to be 9.5 %.

2.4.2. Synthesis and characterization of citrate – capped Ag NPs

Citrate-capped Ag NPs were prepared using a modified Turkevich process.[29] The TEM images revealed that the prepared Ag NPs are well-separated and mostly spheroid in shape. Selected area electron diffraction (SAED) pattern of the Ag NPs (*inset* of **Figure. 2.2**) indicated poly-crystalline nature of the NPs. The average particle size was determined to be 37 nm from the corresponding particle size distribution (*inset,* **Figure 2.2**). A strong surface plasmon resonance (SPR) band at 418 nm, characteristic of Ag NPs,[35-36] was observed in the corresponding UV-visible spectra. The extinction coefficient of citrate-capped Ag NPs at 418 nm was estimated to be 1×10^{10} M^{-1} cm^{-1}. It may be mentioned here that no significant emission was observed for the prepared Ag NPs at the excitation wavelength of 315 nm.

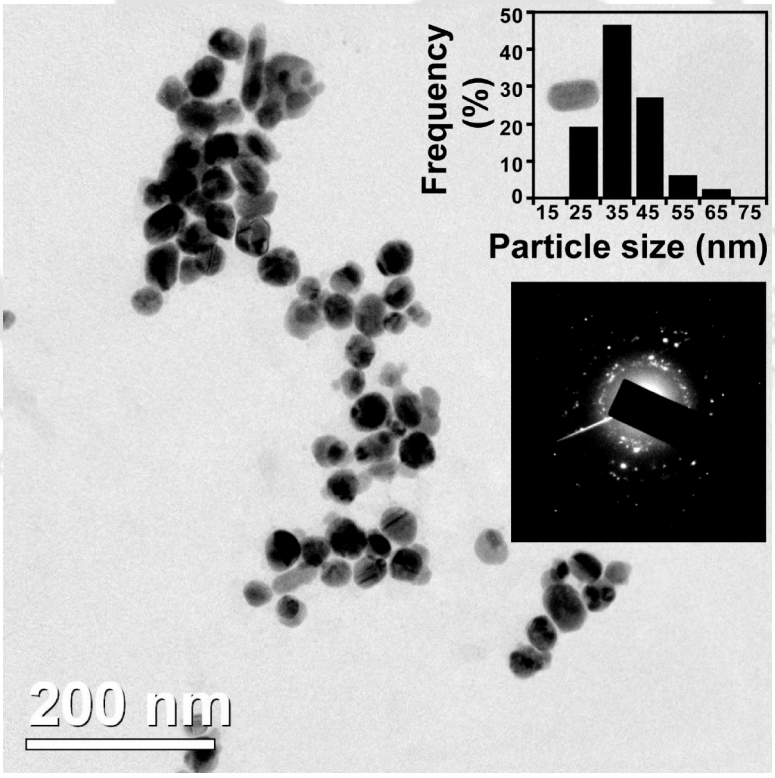

Figure 2.2. TEM image of Ag NPs with corresponding particle size distribution and SAED pattern (*inset*).

2.4.3. Fluorescence Quenching of ZnS Q-dots by Ag NPs

The effect of Ag NPs on the fluorescence properties of ZnS Q-dots was first investigated by steady state fluorescence spectroscopy. The fluorescence intensity of ZnS Q-dots in presence of different concentrations of Ag NPs was recorded and the results are shown in **Figure 2.3a**. It clearly shows that the fluorescence of ZnS Q-dots was efficiently quenched by Ag NPs in a concentration dependent way. It may be mentioned here that no quenching of ZnS Q-dots fluorescence was observed in presence of citrate, indicating the Ag NPs to be solely responsible for quenching effect.

The fluorescence quenching was further analyzed using the well-known Stern-Volmer equation[28] as given in equation 2.2

$$\frac{F_0}{F} = 1 + K_{sv}[Q] \qquad (2.2)$$

where, F_0 and F represents the integrated fluorescence intensity in absence and presence of quencher, respectively, K_{sv} is the Stern-Volmer quenching constant and [Q] is the concentration of quencher.

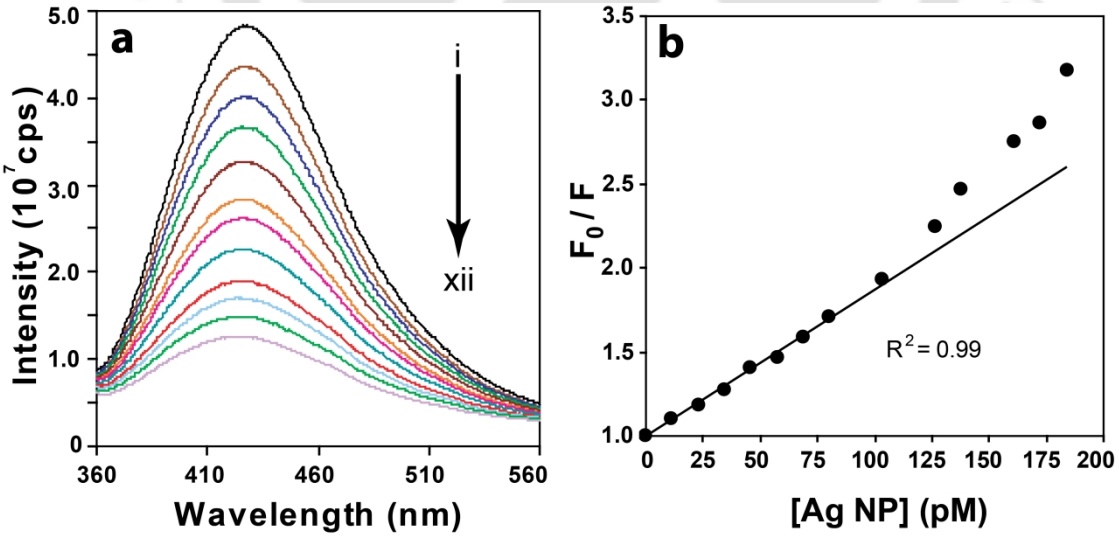

Figure 2.3. (**a**) Fluorescence of chitosan capped ZnS Q-dots (1.4 µM) in presence of (i) 0, (ii) 11.5, (iii) 2.30, (iv) 3.45, (v) 4.60, (vi) 6.90, (vii) 8.05, (viii) 10.35, (ix) 12.65, (x) 13.8, (xi) 16.1 and (xii) 18.4 pM Ag NPs. (**b**) Stern-Volmer plot of the corresponding fluorescence quenching.

The corresponding Stern-Volmer plot (**Figure 2.3b**) demonstrates the quenching in the present Q-dot-NP pair is linear in the lower quencher concentration range (0–100 pM.) with a K_{sv} value of 9×10^9 M^{-1}. The high K_{sv} value indicates the efficient quenching in the present study.[37] Additionally, positive deviation (concave toward Y-axis) in the Stern-Volmer plot was observed at higher NP concentration. This superlinear behavior indicates the presence of mixed quenching[28] in the present system.

Due to strong surface complexation with citrate, surface of the Ag NPs prepared in the present study is negatively charged.[36, 38] Chitosan stabilized ZnS Q-dots, on the other hand, are positively charged as the pK_a value of the chitosan amino group is estimated to be at ~6.3.[39] The quenching of ZnS Q-dots by Ag NPs may arise from the formation of static quenching complex via attractive electrostatic interaction. In order to investigate this electrostatic interaction, UV-visible spectra of the Ag NPs in presence and absence of ZnS Q-dots were examined (**Figure 2.4a**). **Figure 2.4a** clearly shows the simultaneous damping and broadening of the SPR band of Ag NPs in presence of ZnS Q-dots. This indicates the aggregation of Ag NPs in presence of ZnS Q-dots. The electrostatic

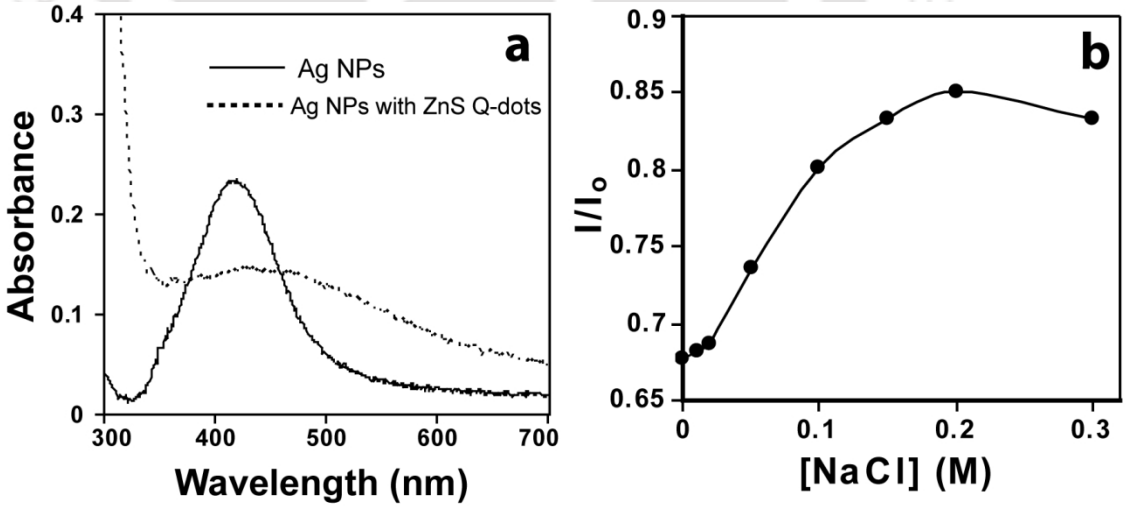

Figure 2.4: (**a**) Absorption spectra of Ag NPs (11.5 pM) in the presence and absence of ZnS Q-dots (1.4 µM). (**b**) The fluorescence recovery of ZnS Q-dots on addition of varying concentration of NaCl. Io and I are the integrated fluorescence intensity of Q-dots in absence and presence of Ag NPs respectively.

interaction between chiotsan-stabilized ZnS Q-dots and Ag NPs may lead to the formation of a Q-dot-NP ensemble where a single Ag NP can quench a large number of ZnS Q-dots. This effect in turn could result in the extraordinary quenching efficiency observed here. The formation of electrostatic complex during the quenching process was further supported by the observation that the increase in ionic strength significantly reduces the quenching efficiency.[37, 40] **Figure 2.4b** shows the regaining of fluorescence from Ag NP-quenched ZnS Q-dots upon addition of salt (NaCl). This observation was consistent with the previous reports of reduced quenching efficiency due to ionic screening.[37]

However, the positive deviation of the Stern-Volmer plot indicates that additional mechanisms, in conjunction with electrostatic complex formation, are involved[28, 37] in the quenching of ZnS Q-dot fluorescence by Ag NPs. The involvement of energy transfer and electron transfer mechanism in the interacting Q-dot – NP pair has already been reported. Electron transfer mechanism which is only predominant in smaller (< 5 nm) metal nanoparticles[41] does not seem to play significant role as the Ag NPs in the present study are much larger (~37nm). On the other hand, energy transfer may significantly influence the present quenching process due to the excellent overlap between ZnS Q-dots emission and the SPR band of Ag NPs (**Figure 2.5**).

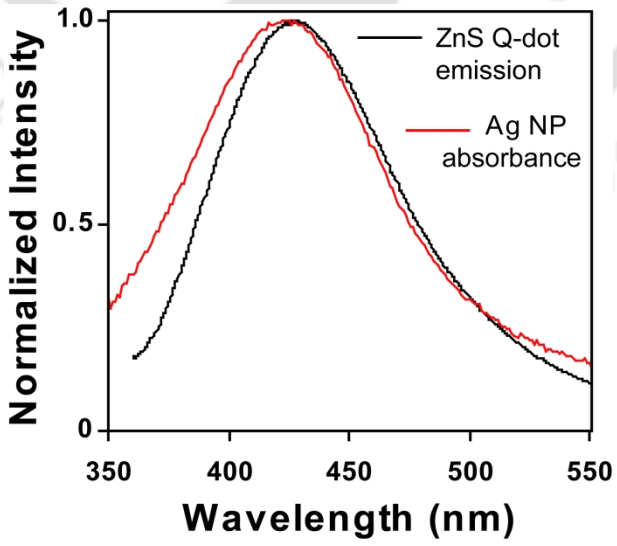

Figure 2.5. Spectral overlap between the emission spectrum of ZnS Q-dots and absorbance spectrum of Ag NPs.

FRET can be defined as a process in which the excited state energy from the initially excited 'donor' molecule is transferred to an 'acceptor' molecule. FRET occurs without the appearance of a photon and is a result of long range dipole-dipole interactions between the 'donor' and 'acceptor'.[28] In the present study, ZnS Q-dots and Ag NPs act as 'donor' and 'acceptor' respectively. The rate of energy transfer depends upon (i) the extent of spectral overlap between the donor's emission and the acceptor's absorption, (ii) the relative orientation of the transition dipole of the donor and the acceptor (iii) the distance between the donor and the acceptor, and (iv) the quantum yield of the donor.[28] The Förster distance R_o, defined as the distance at which resonance energy transfer is 50 % efficient, is given by equation 2.3

$$R_o = [8.8*10^{-25}\,\kappa^2 n^{-4}\varphi\, J]^{1/6} \quad \text{(in cm)} \qquad (2.3)$$

where κ^2 is the orientation factor between the emission dipole of the donor and the absorption dipole of the acceptor, n is the refractive index of the medium, φ is the quantum yield of the donor in absence of acceptor and $J(\lambda)$ is the overlap integral of the fluorescence emission spectra the donor and the absorption spectra of the acceptor in units of M^{-1} cm^3. $J(\lambda)$ is given by equation 2.4[28]

$$J(\lambda) = \int_0^\infty F_D(\lambda)\,\varepsilon_A(\lambda)\,\lambda^4 d\lambda \qquad (2.4)$$

where, $F_D(\lambda)$ is the corrected fluorescence intensity of the donor with total intensity normalized to unity, $\varepsilon_A(\lambda)$ is the decadic extinction coefficient of the acceptor at λ, which is in unit of M^{-1} cm^{-1}. In the present case, φ = 0.095, n = 1.33, κ^2 = 2/3. According to equation (2.3) and (2.4), values of the above parameters were found to be $J = 2.2 \times 10^{-9}$ M^{-1} cm^3 and R_o = 18.4 nm. The value of R_o is higher than the conventional Förster distance which could be due to large size and higher molar extinction coefficient of Ag NPs. This also indicates the involvement of NSET process.[42]

Were the energy transfer between the excited ZnS Q-dots and Ag NPs responsible for emission quenching, characteristic signature can be found in the

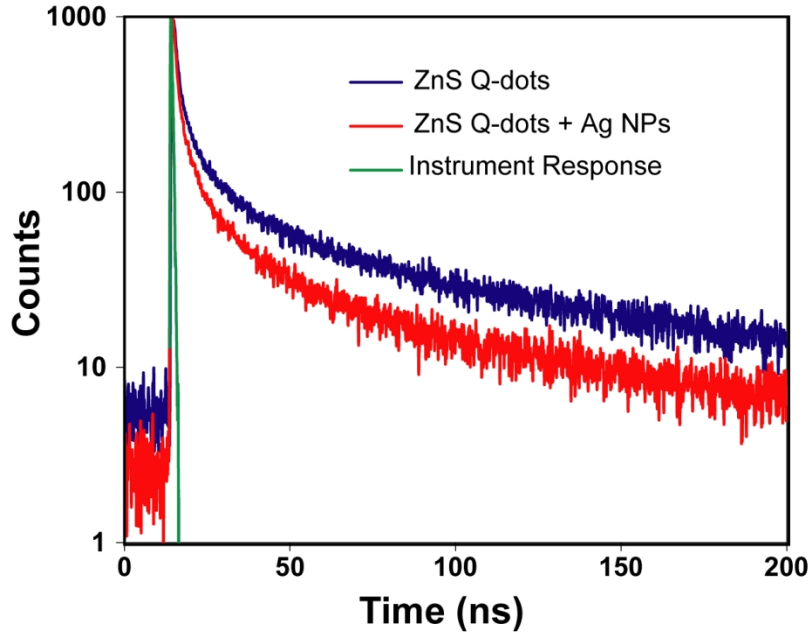

Figure 2.6. Fluorescence decay profile of ZnS Q-dots in absence and presence of Ag NPs.

emission decay profile of the ZnS Q-dots in time resolved fluorescence measurements.[43-44] Time correlated single photon counting (TCSPC) provides an accurate measurement of energy transfer, excluding both ground state complex formation and inner filter effect. **Figure 2.6** shows the emission decay of ZnS Q-dots at 427 nm both in presence and absence of Ag NPs. The resulting fluorescence can be fitted to exponential curve in order to derive the decay time constants, which can be used to calculate the lifetime of the fluorophore. It is evident from **Figure 2.6** that ZnS Q-dots follow a multi exponential decay, characteristic of semiconductor Q-dots.[45] The decay was analyzed using bi-exponential kinetics as given in equation 2.5

$$I(t) = \sum_i \alpha_i \exp(-t/\tau_i) \qquad (2.5)$$

where, α_i and τ_i are the pre-exponential factors and excited-state fluorescence lifetimes associated with the i-th component, respectively. The lifetimes (τ_1 and τ_2) and pre-exponential factors (α_1 and α_2) of ZnS Q-dots emission at different Ag NPs concentration, is summarized in **Table 2.1.** For the

bi-exponential decay the average lifetime $< \tau >$ was determined from the following equation 2.6[28]

$$< \tau >= \sum_i \frac{\alpha_i \tau_i^2}{\alpha_i \tau_i} \qquad (2.6)$$

ZnS nanocrystals show an average lifetime of 47.05 ns in the absence of Ag NPs, which decrease with increase in Ag NP concentration due to the availability of more number of acceptors. The decrease in average lifetime of the ZnS Q-dots confirms the involvement of an additional mode of quenching, other than Coulombic interaction, possibly through energy transfer process between the ZnS Q-dot – Ag NP pair. Moreover, this explains the positive deviation observed in the Stern-Volmer plot.

Table 2.1: Fluorescence life time data obtained using the biexponential model for the ZnS Q-dots in absence and presence of Ag NPs.

Ag NPs/ZnS Q-dots	α_1	τ_1 **(ns)**	α_2	τ_2 **(ns)**	$< \tau >$ **(ns)**	χ^2
0	117	7.55	73.5	55.6	47.05	1.08
1.66×10^{-5}	129	6.60	66.8	52.45	43.65	1.07
3.32×10^{-5}	106.2	6.37	48.4	44.42	35.31	1.09
4.98×10^{-5}	205.3	4.67	53.8	42.89	31.68	1.14

2.5. Conclusion

In summary, water dispersible chitosan stabilized ZnS Q-dots of ca. 3 nm were prepared in an environment friendly method. The interaction of ZnS Q-dots with citrate capped Ag NPs resulted in the fluorescence quenching of the Q-dots in concentration dependent manner. The corresponding Stern-Volmer plot for the present fluorophore-quencher pair indicated mixed nature of quenching with a high K_{sv} value (9×10^9 M^{-1}) which demonstrates the efficient quenching of ZnS Q-dots by Ag NPs. The Coulombic interaction between the positively charged ZnS Q-dots and negatively charged Ag NPs led to the formation of electrostatic complex that contribute to the static mechanism of the quenching process. Furthermore, the involvement of energy transfer process due to excellent spectral overlap between ZnS Q-dots emission and surface plasmon resonance (SPR) band of Ag NPs was confirmed by the time resolved fluorescence measurements. The R_0 value calculated for the present donor-acceptor pair was found to be 18.4 nm which was greater than the generally observed Förster distance. The implication of the present findings may lead to the development of long range FRET – or NSET – based methods for studying biological multicomponent system.

2.6. References

1. W. Zhong, *Anal. Bioanal. Chem*., **2009**, 394, 47–59.
2. A. P. Alivisatos, *J. Phys. Chem.*, **1996**, 100, 13226–13239.
3. A. M. Smith, G. Ruan, M. N. Rhyner, S. Nie, *Anal. Biomed. Eng.*, **2006**, 34, 3–14.
4. I. L. Medintz, H. T. Uyeda, E. R. Goldman, H. Mattoussi, *Nat. Mater.*, **2005**, 4, 435–446.
5. M. Han, X. Gao, J. Z. Su, S. Nie, *Nat. Biotechnol.*, **2001**, 19, 631–635.
6. P. Alviastos, *Nat. Biotechnol.*, **2004**, 22, 47–52.
7. T. Jamieson, R. Bakhshi, D. Petrova, R. Pocock, M. Imani, A. M. Seifalian, *Biomaterials*, **2007**, 28, 4717–4732.
8. X. Li, J. Qian, L. Jiang, S. He, *Appl. Phys. Lett.*, **2009**, 94, 63111–63113.
9. L. Dyadyusha, H. Yin, S. Jaiswal, T. Brown, J. J. Baumberg, F. P. Booy, T. Melvin, *Chem. Commun.*, **2005**, 25, 3201–3203.
10. D. M. Willard, A. V. Orden, *Nat. Mater.*, **2003**, 2:575-576.
11. I. L. Medintz, A. R. Clapp, H. Mattoussi, E. R. Goldman, B. Fisher, J. M. Mauro, *Nat. Mater.*, **2003**, 2, 630–638.
12. K. Ray, R. Badugu, J. R. Lakowicz, *J. Am. Chem. Soc.*, **2006**, 128, 8998–8999.
13. E. Dulkeith, M. Ringler, T. A. Klar, J. Feldmann, A. M. Javier, W. J. Parak, *Nano Lett.*, **2005**, 5, 585–589.
14. A. Murgadoss, A. Chattopadhyay, *Bull. Mater. Sci.*, **2008**, 31, 533–539.
15. J. Zhang, Y. Fu, M. H. Chowdhury, J. R. Lakowicz, *Nano Lett.*, **2007**, 7,2101–72107.
16. P. P. Pompa, L. Martiradonna, A. D. Torre, F. D. Sala, L. Manna, M. D. Vittorio, F. Calabi, R. Cingolani, R. Rinaldi, *Nat. Nanotechnol.*, **2006**, 1, 126–130 .
17. K. Aslan, I. Gryczynski, J. Malicka, E. Matveeva, J. R. Lakowicz, C. D. Geddes *Curr. Opin. Biotechnol.*, **2005**, 16, 55–62
18. K. Aslan, J. R. Lakowicz, C. D. Geddes, *Anal. Bioanal. Chem.*, **2005**, 382, 926–933
19. C. A. Sabatini, R. V. Pereira, M. H. Gehlen, *J. Fluores.*, **2007**, 17, 377–382.
20. H. Nabika, S. Deki, *J. Phys. Chem. B*, **2003**,107, 9161–9164.
21. L. L. Tay, N. Rowell, R. Boukherroub, *Mater. Res. Soc.*, **2005**, 901, 221–226.
22. M. Umadevi, P. Vanelle, T. Terme, B. J. M. Rajkumar, V. Ramakrishnan, *J. Fluores.*, **2009**, 19, 3–10.
23. J. Zhang, Y. Fu, M. H. Chowdhury, J. R. Lakowicz, *J. Phys. Chem. C*, **2007**, 111, 11784–11792.

24. C. S. Yun, A. Javier, T. Jennings, M. Fisher, S. Hira, S. Peterson, B. Hopkins, N. O. Reich, G. F. Strouse, *J. Am. Chem. Soc.*, **2005**, 127, 3115–3119.
25. S. Saini, S. Bhowmick, V. B. Shenoy, B. Bagchi, *J. Photochem. Photobiol. A: Chem.*, **2007**, 190, 335–341.
26. H. C. Warad, C. Thanachayanont, G. Tumcharern, J. Dutta, Proceedings of the 2nd IEEE International Conference on Nano/Micro Engineered and Molecular System, **2007**, Bangkok Thailand.
27. A. T. R. Williams, S. A. Winfield, J. N. Miller, *Analyst*, **1983**, 108, 1067–1071.
28. J. R. Lakowicz, 3rd edition, Principles of Fluorescence spectroscopy, **1999**, Kluwer Academic/Plenum, New York.
29. J. Turkevich, P. C. Stevenson, J. Hillier, *Discuss. Faraday Soc.*, **1951**, 11, 55–75.
30. Q. Xiao, C. Xiao, *Appl. Surf. Sci.*, 2008, 254:6432–6435.
31. P. E. Lippens, M. Lannoo, *Phys. Rev. B*, **1989**, 39, 10935–10942.
32. L. Brus, *J. Phys. Chem.*, **1986**, 90, 2555–2560.
33. M. Mall, L. Kumar, *J. Lumin.*, **2010**, 130, 660–665.
34. M. H. Yousefi, A. A. Khosravi, K. Rahimi, A. Nazesh, *Eur. Phys. J-Appl. Phys.*, **2009**, 45, 10602–10604.
35. Z. S. Pillai, P. V. Kamat, *J. Phys. Chem. B*, **2004**, 108, 945–951.
36. R. A. A. Puebla, R. F. Aroca, *Anal. Chem.*, **2009**, 81, 2280–2285.
37. C. Fan, S. Wang, J. W. Hong, G. C. Bazan, K. W. Plazco, A. J. Heeger, *Proc. Natl. Acad. Sci. U. S. A.*, **2003**, 100, 6297–6301.
38. D. Longa, G. Wua, S. Chen, Radiat. *Phys. Chem.*, **2007**, 76, 1126–1131.
39. W. B. Tan, N. Huang, Y. Zhang, *J. Colloid Interface Sci.*, **2007**, 310, 464–470.
40. M. J. O'Connella, C. K. Chana, W. Lia, R. K. Hicksa, S. K. Doorna, H.L. Wang, *Polymer*, **2007**, 48, 7582–7589.
41. S. K. Ghosh, A. Pal, S. Kundu, S. Nath, T. Pal, *Chem. Phys. Lett.*, **2004**, 395, 366–372.
42. J. Griffin, A. K. Singh, D. Senapati, P. Rhodes, K. Mitchell, B. Robinson, E. Yu, P. C. Ray, *Chem. Eur. J.*, **2008**, 15, 342–351.
43. S. Sarkar, R. Bose, S. Jana, N. R. Jana, N. Pradhan, *J. Phys. Chem. Lett.*, **2010**, 1, 636–640.
44. F. Huang, E. Lerner, S. Sato, D. Amir, E. Haas, A. R. Fersht, *Biochemistry*, **2009**, 48, 3468–3476.
45. G. Williams, P. V. Kamat, *Langmuir*, **2009**, 25, 13869–13873.

Chapter 3

Functional Chitosan Nanocarriers for Potential Applications in Gene Therapy*

This chapter illustrates the synthesis of functional chitosan nanocarriers having ZnS Q-dots as imaging and folic acid as targeting modalities respectively and pCD-UPRT as therapeutic agent. It also presents the potential theranostic applicability of the nanocarriers.

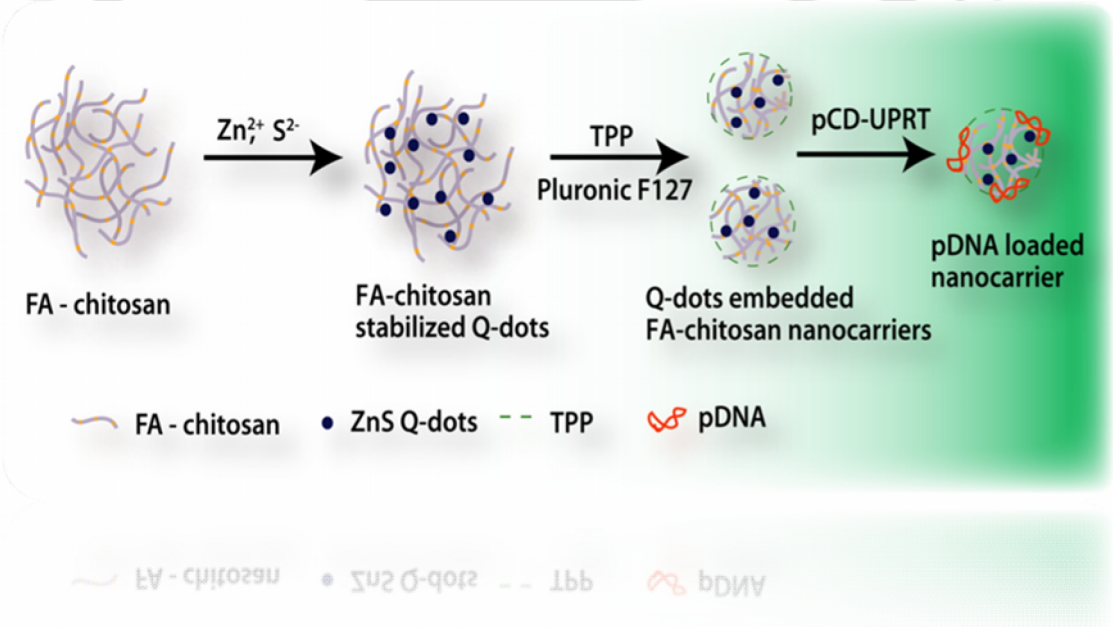

* Much of this work has appeared in print. It is reproduced with permission from *Materials Letters*, 2012, 68, 261–264. Copyright © 2012, Elsevier.

Chapter 3

Functional Chitosan Nanocarriers for Potential Applications in Gene Therapy

3.1. Introduction

Gene therapy is a promising tool, involving transfer of a therapeutic gene into specific cells for the treatment of certain forms of cancers and viral infections. The challenge remains in the development of suitable carrier, namely viral and non-viral vectors; the former exhibit higher transfection efficiency and rapid transcription, but with the evident drawbacks of non-specific targeting, eliciting immune responses and cytotoxicity, however, the latter bear an advantage of superior safety.[1]

Chitosan, a biocompatible polysaccharide has emerged as one of the suitable non-viral vectors for gene therapy.[2] Chitosan nanoparticles has been reported to deliver DNA, where targeting was achieved either by FA conjugation or using cell penetrating peptides,[2, 3] still there is lack of functionalities, to track the delivery process. Though, organic fluorophore has been used to tag polymeric particles, the intrinsic drawback of photobleaching has limited its use in cell labeling. In this respect, semiconductor quantum dots have emerged as an excellent fluorophore due to their outstanding optical properties and resistance to photobleaching.[4] Fluorescent chitosan nanoparticles, incorporating Cadmium (Cd) based quantum dots, has been reported,[5, 6] but the inherent toxicity of Cd^{2+} ions impedes clinical applications. Therefore, there is a requisite for the functional nanocarriers which will be nontoxic, targeted and traceable. The development of such nanocarriers will have tremendous applicability for theranostics.

3.2. Outline of the Research Work

1) Functional chitosan nanocarriers having folic acid and ZnS Q-dots as targeting and imaging modules are synthesized and characterised.
2) The nanocarriers were spherical in shape with size of ~75 nm and fluorescence maxima at 440 nm.
3) Cell viability assay showed that the nanocarriers were non-cytotoxic against U87 MG and HT 29 cells.
4) Presence of ZnS Q-dots within the nanocarriers helped in tracking the uptake process.
5) Gel retardation and DNAse protection assay showed efficient binding of pDNA containing suicide genes to the nanocarriers and stability against degradation respectively.

3.3. Experimental Section

3.3.1. Materials

Chitosan (low MW, >75 % deacetylated), Folic acid, Pluronic F-127, Sodium tripolyphosphate (TPP), 2,3-Bis(2-methoxy-4-nitro-5-sulfophenyl)-2H-tetrazolium-5-carboxanilide (XTT) were purchased from Sigma-Aldrich, USA. N-(3-dimethyaminopropyl)-N'-ethyl carbodiimide hydrochloride (EDC), zinc acetate dihydrate, sodium sulfide, was obtained from Merck, India. Milli-Q ultra-pure water (>18 MΩ cm, Millipore) was used in all experiments.

3.3.2. Synthesis of ZnS Q-dots stabilized by FA-chitosan

Conjugation of FA to chitosan was carried out following previously reported method.[8] The synthesis of FA-chitosan stabilized ZnS Q-dots was done using an inorganic wet-chemical synthesis method as mentioned in chapter 2 with modifications. Briefly, zinc acetate (2 mM) was added to 0.05 % (*w/v*) FA-chitosan solution under constant stirring and heated at 80 °C for 15 min. After cooling down to room temperature, 2 mM of freshly prepared sodium sulfide was added dropwise in an ice bath with continuous stirring which resulted in the formation

of ZnS Q-dots. The as prepared colloidal solution of ZnS Q-dots, was ultrasonicated to remove the dissolved gases, if any, and preserved at room temperature in dark.

3.3.3. Synthesis of chitosan nanocarriers

Method of ionic gelation was adapted to synthesize the chitosan nanocarriers.[10] FA-chitosan stabilized ZnS Q-dots (5 mL) were taken and to it pluronic F127 (0.05 mg mL^{-1}) was added and stirred. Drop-wise addition of TPP (0.14 mg mL^{-1}), under vigorous stirring at pH 4.5 resulted in the appearance of faint milky solution indicating the formation of chitosan nanoparticle. Schematic for the synthesis of the nanocarriers is shown in **Figure 3.1**. Next, the prepared solution was centrifuged at 15000 rpm and the pellet obtained was washed several times and finally dissolved in water to form a colloidal solution of the nanocarriers.

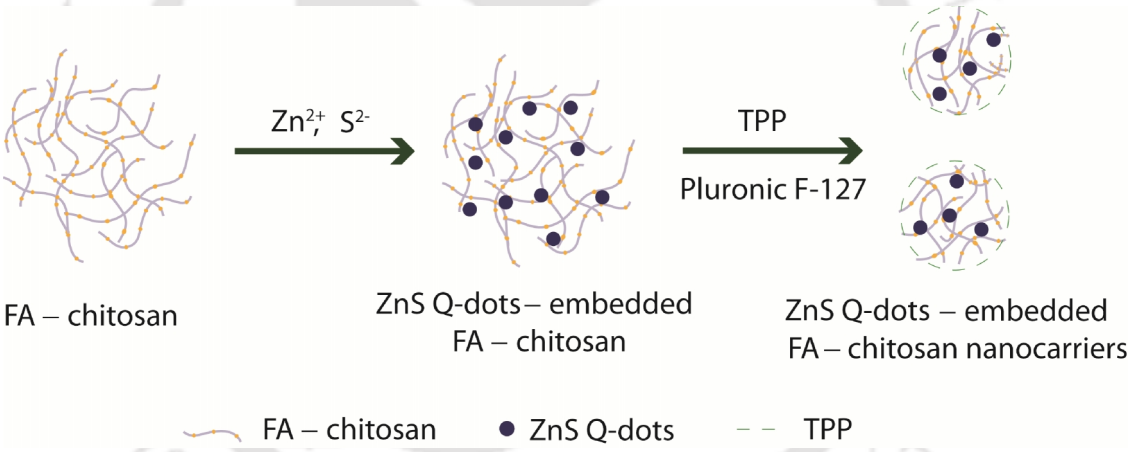

Figure 3.1. Schematic showing the synthesis of the chitosan nanocarriers.

3.3.4. Cell viability assay and Cellular uptake of the nanocarriers

HT 29 (human colon adenocarcinoma) and U87 MG (Human glioblastoma astrocytoma) cell lines were maintained in the DMEM medium supplemented with 10 % FBS, 50 U mL^{-1} penicillin and 50 mg mL^{-1} streptomycin in a humidified atmosphere containing 5 % CO_2 at 37 °C. For the cell viability assay, cells were seeded (10^4 cells/well) into a 96-well microplates and grown overnight. After treating with varying concentrations (0-30 μg mL^{-1}) of the nanocarriers for 24 h,

XTT based cell proliferation assay was carried out according to the manufacturer's protocol to determine the percentage of viable cells. For cellular uptake study, HT 29 cells were seeded in 35 mm cell culture plates and grown for 48 h. It was then incubated with the nanocarriers for 24 h and finally observed under fluorescence microscope (Nikon eclipse Ti) after washing with phosphate buffered saline (PBS; 0.01 M, pH 7.4).

3.3.5. Binding of pCD-UPRT to chitosan nanocarriers and DNAse protection assay

pCD-UPRT (0.2 μg) was incubated with varying concentration (0 - 0.6 μg) of chitosan nanocarriers for 1 h and then electrophoresed in 0.8 % agarose gel at 5 V cm^{-1} and finally visualized in gel documentation system. Protection of complexed pDNA against DNAse degradation was studied after incubating the nanocarriers in presence and absence of 10 U mL^{-1} DNAse I (Promega, USA) for 15 min at 37 °C, according to manufacturer's protocol.

3.3.6. Transfection analysis of HT 29 cell line using chitosan nanocarriers

HT 29 cells were seeded in 6-well cell culture plates and transfected with pCD-UPRT loaded chitosan nanocarriers in serum free media for 12 h. Culture media was then removed and the cells were treated with 10 mM of the prodrug 5-FC in DMEM media for 48 h. Cells treated with 20 μM of 5-FU for 48 h was taken as a positive control. After removing the culture media and washing with PBS, the cells were briefly stained with Acridine Orange/Ethidium Bromide (AO/EB) (10 mg mL^{-1} AO and 10 mg mL^{-1} EB in PBS), in order to detect apoptotic or necrotic nuclei. Finally, the cells were visualized under a fluorescence microscope (Nikon eclipse Ti) for AO and EB stain with blue and green filter respectively.

3.3.7. Instrumentation

UV-Vis and fluorescence spectra were recorded with Perkin Elmer Lambda 25 and Perkin Elmer LS 55 instrument respectively. Fourier Transform Infrared (FTIR) spectroscopy was done using a Perkin Elmer Spectrum One instrument.

Transmission Electron Microscopy was performed in JEOL 2100 UHR-TEM instrument. 5 μL of sample was drop-cast on carbon-coated copper grids and subsequently air-dried before TEM analysis. X-ray diffraction (XRD) pattern were recorded with Brucker D8 Advanced X-ray diffraction measurement system, with Cu Kα source (λ =1.54 Å). Atomic Force microscopy was done using PicoScan™ 2500 (Molecular imaging corporation, USA) in a non-contact mode. Zeta potential and solvated particle size was measured using Delsa™ Nano C (Beckman Coulter) at 25 °C using water as diluent having refractive index of 1.33 and viscosity of 0.8878 cp. Zeta potentials were determined by measuring the electrophoretic mobility of charged particles under an applied electric field. The above instrument used a zeta potential module equipped with a 35 mW two laser diode (658 nm) where the scattered light was detected at a 90^{o} angle. Smoluchowski equation was used to calculate the zeta potential values from the measured velocities.

3.4. Results and Discussion

3.4.1. Functionalization of chitosan with folic acid (FA)

The biofunctionalization of chitosan with folic acid was confirmed by UV-Vis spectroscopy (**Figure. 3.2a**). **Figure 3.2a** showed the absorption spectra of chitosan, FA and FA-chitosan. The characteristic peak in the 280 nm and 370 nm range arising from the π–π* transition of the pterin ring of FA[11] was clearly observed in the FA-chitosan. Since, there was no typical absorption feature of chitosan; the above result confirmed the conjugation process. FTIR spectra of chitosan, FA and FA-chitosan were shown in **Figure 3.2b**. The peaks corresponding to FA was not revealed in the IR spectra of FA- chitosan, which could either due to the broad absorption of chitosan or low modification.

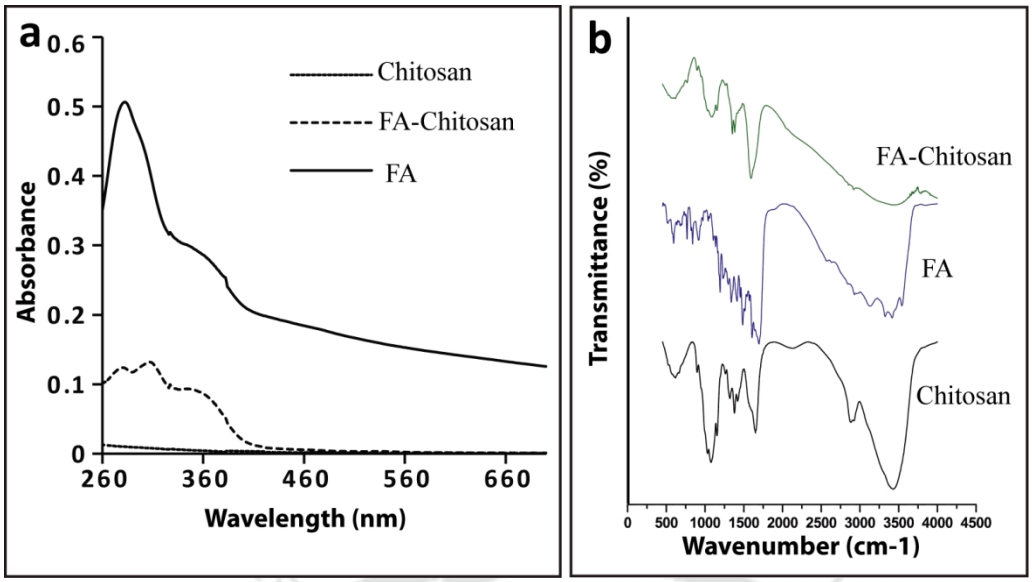

Figure 3.2. (**a**) UV-Vis spectra and (**b**) FTIR spectra of folic acid (FA), chitosan and FA-chitosan.

3.4.2. Synthesis and characterization of ZnS Q-dots using FA-chitosan as stabilizer

The FA-chitosan was then used for the synthesis of ZnS Q-dots. The UV-Vis and fluorescence spectra of the prepared ZnS Q-dots have been shown in **Figure 3.3a**. Absorbance edge at around 300 nm, considerable blue shifting from the 340 nm peak of bulk ZnS was observed,[9] indicating the role of quantum confinement effect. An emission maximum at around 440 nm was detected when the Q-dots were excited at wavelength of 315 nm. The crystallinity of the prepared ZnS Q-dots was demonstrated by the XRD pattern (**Figure 3.4a**) showing characteristic peaks at 28°, 47°, and 56° corresponding to the {111}, {220} and {311} lattice planes of bulk ZnS, respectively.[9]

3.4.3. Synthesis and characterization of ZnS Q-dots embedded chitosan nanocarrier

Next, functional chitosan nanocarriers were prepared from the FA-chitosan stabilised ZnS Q-dots by the method of ionic gelation using the polyanion, TPP. As depicted by the TEM (**Figure 3.3b**) and AFM image (**Figure 3.3d, e, f**), the ZnS Q-dots embedded FA-chitosan nanocarriers were nearly monodisperse and spherical in shape.

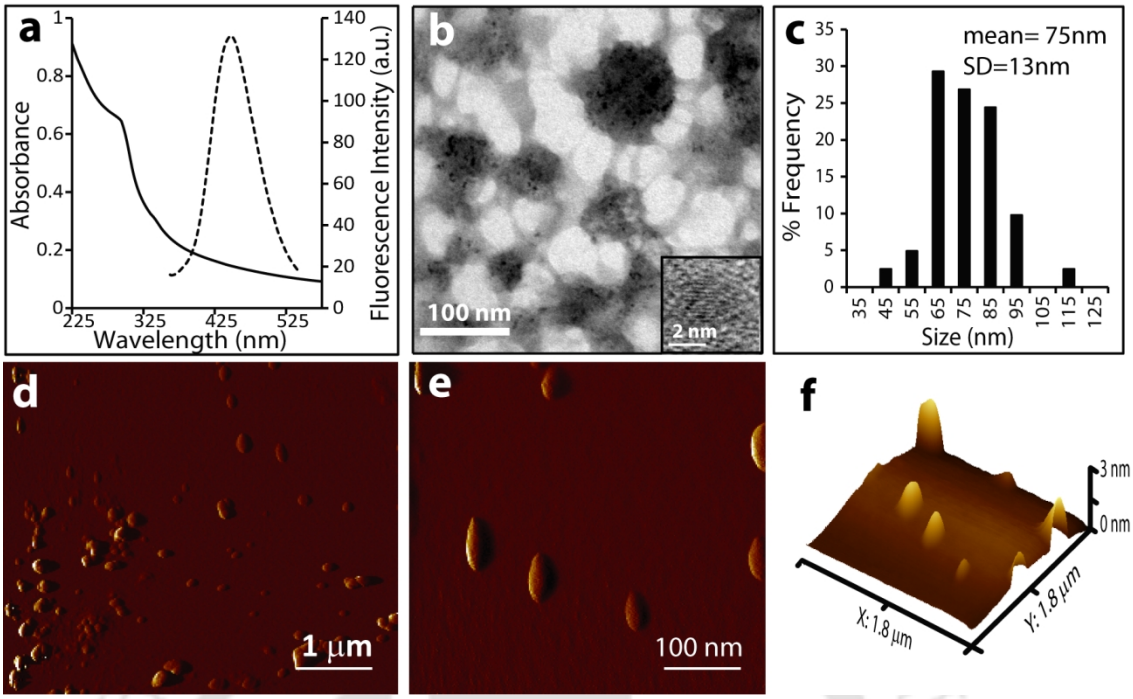

Figure 3.3. (**a**) UV-Vis and Fluorescence spectra of ZnS Q-dots, (**b**) TEM image of ZnS Q-dots embedded chitosan nanocarriers with inset showing the HRTEM of the Q-dots, (**c**) Particle size distribution, (**d-e**) AFM image, (**f**) corresponding 3D view of the nanocarriers.

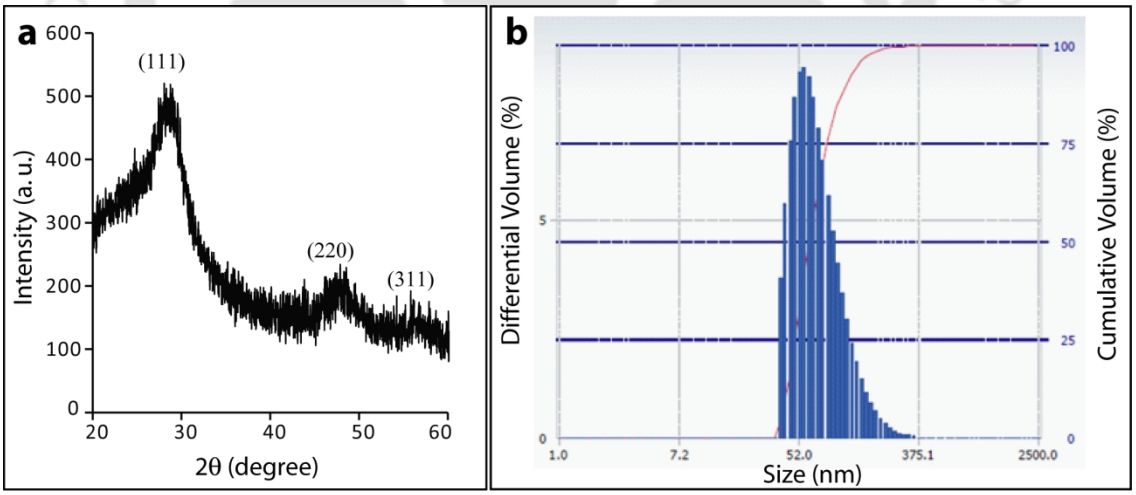

Figure 3.4. (**a**) XRD pattern of the ZnS Q-dots. (**b**) Particle size distribution of chitosan nanocarriers determined by photon correlation spectroscopy.

The TEM image clearly shows the presence of ZnS Q-dots as dark spots embedded within the nanocarriers. The lattice resolved planes of ZnS and size of ~3 nm was seen from the high resolution TEM (HRTEM) of ZnS Q-dots (**Figure 3.3b, inset**). From the particle size distribution (**Figure 3.3c**) obtained from the TEM image, the average sizes of the nanocarriers were determined to be 75 ± 13 nm. The 3D surface view (**Figure 3.3f**) of the nanocarriers is shown in Figure 3.3 e depicting height less than 3 nm. The solvated size of the nanocarriers was determined using photon correlation spectroscopy (**Figure 3.4b**) which yielded a diameter of 134.1 nm for the chitosan nanocarriers (polydispersity index, 0.254). The solvated size was greater than those obtained from TEM/AFM measurement due to the swollen state of the nanocarriers in aqueous environment. The smaller size of the nanocarriers and the use of poloxomer, pluronic F 127 in the synthesis process would minimize the interaction of the nanocarriers with the plasma proteins, reducing opsonisation, and could thereby increase the circulation time of the nanocarriers.[12] Zeta potential of the nanocarriers at 25 °C in water was measured to be +24.65 mV, which was sufficient to render stability to the nanocarriers against aggregation.

3.4.4. Cytotoxicity evaluation and cellular uptake of the prepared nanocarrier

To evaluate the cytotoxicity of the prepared nanocarriers, we have performed the XTT assay. Notably, for both the cell lines tested, more than 95 % of the cells were viable (**Figure 3.5a**) after 24 h of treatment even at the highest concentration of nanocarriers used, thereby confirming its biocompatibility. Next, the cellular uptake of the nanocarriers was studied in HT 29 cells by using fluorescence microscopy. The representative phase contrast and fluorescence micrographs of the cells after 24 h of incubation with the functional nanocarriers, is shown in **Figures 3.5b** and **3.5c** respectively. The uptake of the nanocarriers was confirmed from the blue fluorescence observed (**Figure 3.5c**) which was ascribed to the quantum dots present within the nanocarriers. Though the fluorescence intensity observed (**Figure 3.5c**) was low, but, in comparison to the control cells (**Figure 3.5e**) where no fluorescence was detected, indicated that the fluorescence obtained was indeed due to the cellular internalization of the nanocarriers.

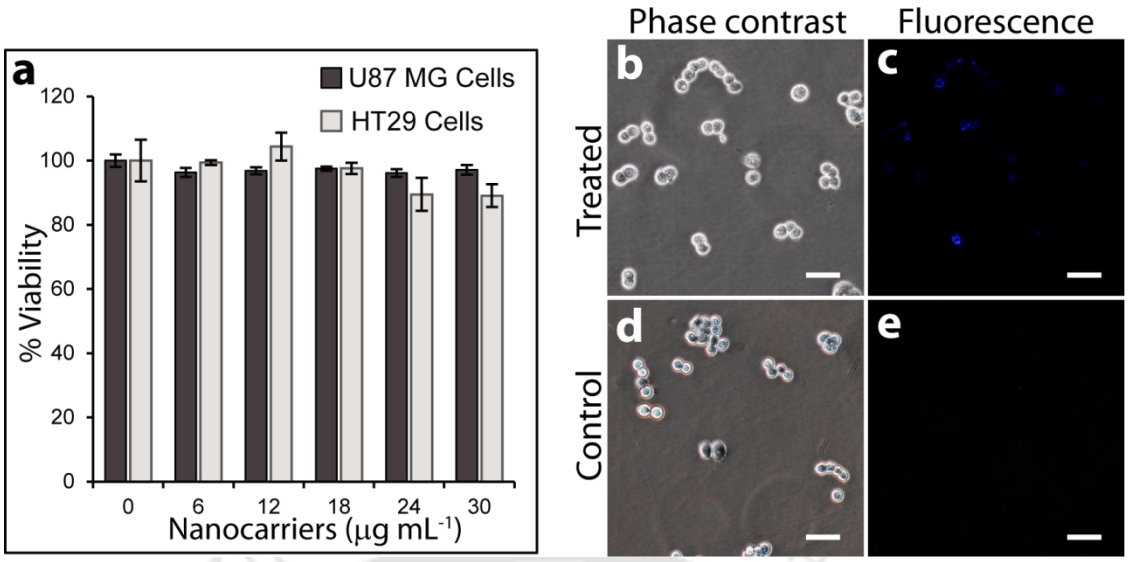

Figure 3.5. (**a**) XTT assay of FA-chitosan nanocarriers at different concentrations against U87 MG and HT 29 cells. Data are presented as the average ± SD. (**b, d**) Phase contrast image and (**c, e**) Fluorescence micrographs of nanocarriers treated and non-treated HT 29 cells, respectively. Scale bar: 50 μm

3.4.5. Binding of pCD-UPRT to chitosan nanocarriers and DNAse protection assay

The gel retardation assay (**Figure 3.6a**) visibly showed that the amount of pDNA in the lanes reduced (lane 2 to lane 7) with increasing concentration of the nanocarriers indicating efficient binding. The bands observed in the wells of lane 2 to lane 7 indicated the complexation of pDNA with the nanocarriers which retarded the movement of the pDNA. Saturation of the nanocarriers with pDNA was observed (Lane 7) for the maximum concentration of nanocarriers (the ratio of nanocarriers/pDNA was 3 μg/μg) used. Lane 1 and lane 8 represented the controls containing naked pDNA and the nanocarriers, respectively. Further, to check the stability of the pDNA during *in vitro* conditions, we carried out DNAse protection assay which showed (**Figure 3.6b**) that binding of pDNA with the chitosan nanocarriers protected the pDNA from degradation (well 4) as compared to naked DNA (lane 2), where no band was seen indicating complete degradation by DNAse. Lane 1 containing only the pDNA and lane 3 containing the pDNA complexed chitosan nanocarriers served as the experimental controls.

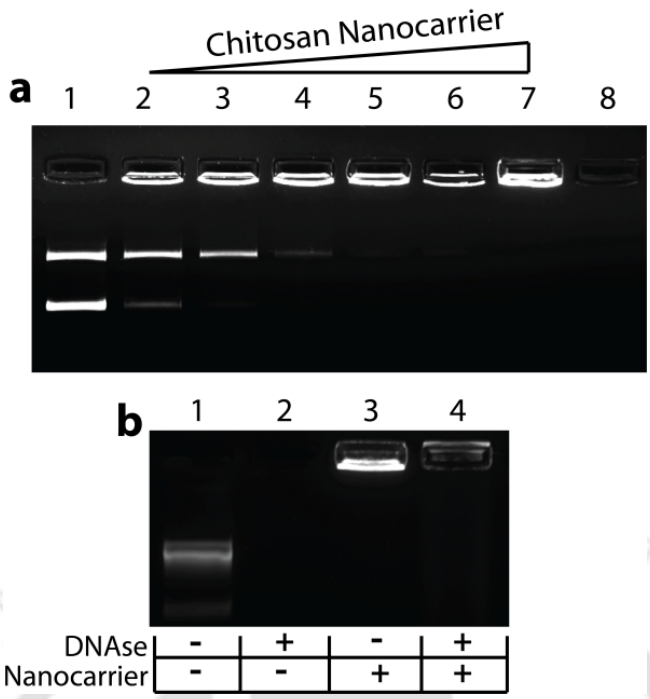

Figure 3.6. (**a**) Gel retardation assay of pCD-UPRT (0.2 μg) incubated with varying concentration (0.1, 0.2, 0.3, 0.4, 0.5, 0.6 μg) of nanocarriers (Lanes 2-7). Lanes 1 and 8 correspond to naked pCD-UPRT and nanocarrier control, respectively. (**b**) DNAse protection assay, Lane 1 and 3 are non-treated pDNA and nanocarriers controls respectively, Lane 2 and 4 represents the samples of Lane 1 and 3 after DNAse treatment.

The zeta potential of the chitosan nanocariers after binding with pDNA was measured to be +23.76 mV. Since, the nanocarriers were already synthesized using the polyanion TPP, the zeta potential of the nanocarriers after binding with pDNA was not much affected.

3.4.6. Transfection analysis of HT 29 cell line using chitosan nanocarriers

The transfecting ability of the chitosan nanocarriers were demonstrated by the induction of cell death in HT 29 cell lines after addition of the prodrug, 5-FC, as revealed from AO/EB staining. The fluorescence microscopic images obtained with blue and green filters post AO/EB dual staining was merged and is shown in **Figure 3.7**. Transient expression of the suicide genes to CD-UPRT enzymes converts the added prodrug 5-FC to 5-FU and other toxic metabolites, which leads

to cell death.[7] **Figure 3.7a** and **3.7b** shows that the untreated and unloaded chitosan nanoarriers treated cells stained green due to the uptake of AO dye and both have well organized chromatin structures indicating normal morphology. On the other hand, in case of pCD-UPRT complexed chitosan nanocarriers treated cells, nuclear uptake of EB was observed as indicated by the orange-red stain of the dye (**Figure 3.7c**) which corroborated compromised cell membrane and cell death. Cells treated with the drug 5-FU showed extensive cell death and served as positive control (**Figure 3.7d**).

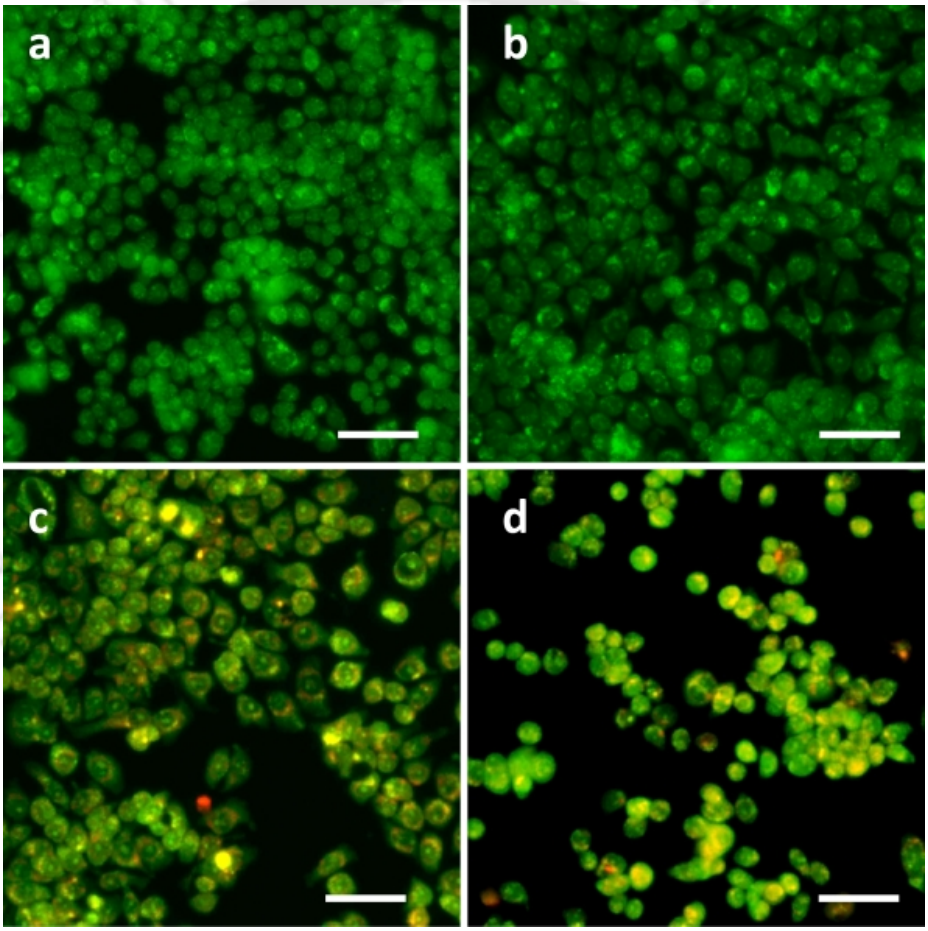

Figure 3.7. Merged fluorescence micrographs of AO/EB dual staining of (**a**) untreated, (**b**) unloaded chitosan nanocarriers, (**c**) pCD-UPRT loaded chitosan nanocarriers treated HT 29 cells, with subsequent treatment with 5-FC for 48 h and (**d**) 5-FU treated HT 29 cells after 48 h of treatment. Scale bar: 100 μm

3.5. Conclusion

In summary, we demonstrated a facile method for preparation of functional chitosan nanocarriers containing folic acid and ZnS Q-dots as targeting and imaging modalities, respectively. The prepared nanocarriers showed no toxicity against the cell lines tested, enabling it to be used for gene delivery. The cellular uptake of the nanocarriers was also demonstrated by fluorescence microscopy. Gel retardation and DNAse protection assay showed efficient binding and stability of pDNA containing the genes for CD-UPRT with the nanocarriers. The functional effect of the nanocarriers in transfecting HT 29 cells can further be explored as a potential non-viral system for gene therapy. Thus, the synthesized multifunctional nanocarriers can suitably be used for theranostic applications.

3.6. References

1. S. D. Patil, D. G. Rhodes, D. J. Burgess, *AAPS J.*, **2005**, 7, E61–E77.
2. H. Q. Mao, K. Roy, V. L. Troung-Le, K. A. Janes, K. Y. Lin, Y. Wang, et al., *J. Cont. Rel.*, **2001**, 70, 399–421.
3. S. Mansouria, Y. Cuieb, F. Winnikb, Q. Shia, P. Lavignea, M. Benderdoura, E. Beaumonta, J. C. Fernandes, *Biomaterials*, **2006**, 27, 2060–2065.
4. X. Michalet, F. F. Pinaud, L. A. Bentolila, J. M. Tsay, S. Doose, J. J. Li, G. Sundaresan, A. M. Wu, S. S. Gambhir, S. Weiss., *Science*, **2005**, 307, 538–544.
5. Q. Nie, W. B. Tan, Y. Zhang, *Nanotechnology*, **2006**, 17, 140–144.
6. L. Li, D. Chen, Y. Zhang, Z. Deng, X. Ren, X. Meng, et al., *Nanotechnology* **2007**, 18, 1–6.
7. P. Gopinath, S. S. Ghosh, *Biotechnol. Lett.*, **2008**, 30, 1913–1921.
8. S. J. Yang, F. H. Lin, K. C. Tsai, M. F. Wei, H. M. Tsai, J. M. Wong, et al., *Bioconjugate Chem.*, **2010**, 21, 679–689.
9. A. Jaiswal, P. Sanpui, A. Chattopahyay, S. S. Ghosh, *Plasmonics*, **2011**, 6, 125–132
10. P. Sanpui, A. Chattopahyay, S. S. Ghosh, *ACS Appl. Mater. Interfaces*, **2011**, 3, 218–228.
11. F. Liu, D. Deng, X. Chen, Z. Qian, S. Achilefu, Y. Gu, *Mol. Imaging Biol.*, **2010**, 12, 595–607.
12. F. Alexis, E. Pridgen, L. K. Molnar, O. C. Farokhza, *Mol. Pharm.*, **2008**, 5, 505–515.

Chapter 4

Quantum Dot Impregnated-Chitosan Film for Heavy Metal Ion Sensing and Removal*

This chapter illustrates the cation exchange mediated chemical transformation of ZnS Q-dots. This rationale was used for sensing and removal of heavy metal ion from water using ZnS Q-dots impregnated chitosan film.

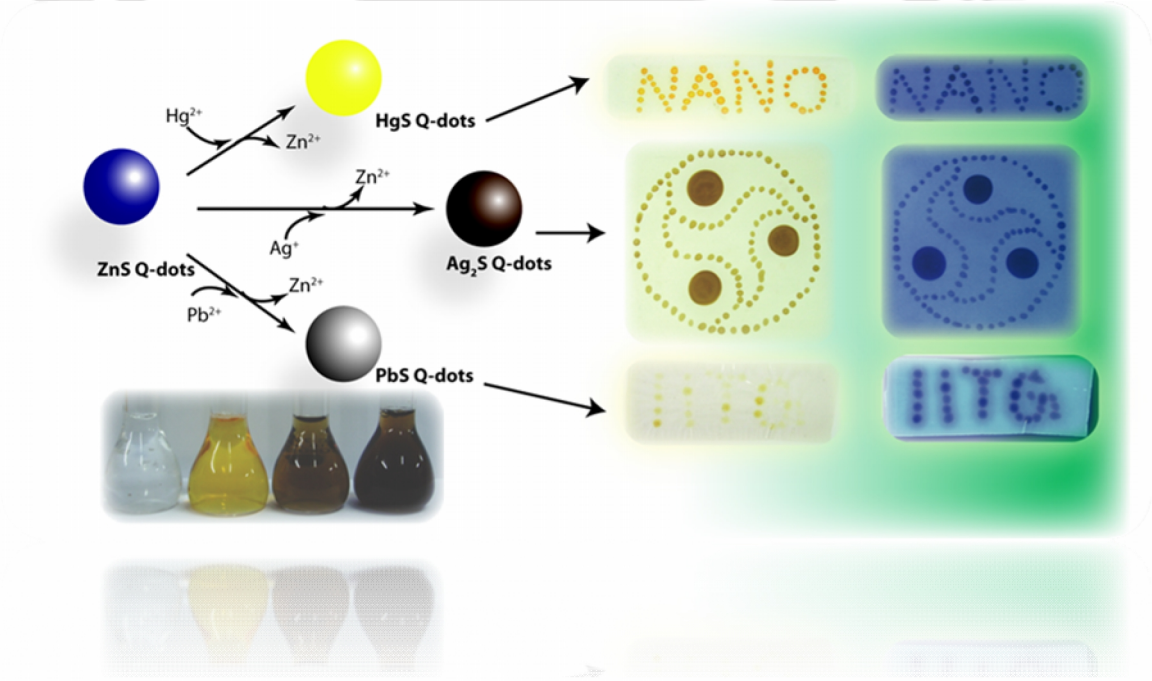

* Much of this work has appeared in print. It is reproduced with permission from *Langmuir*, 2012, 28, 15687−15696. Copyright © 2012, American Chemical Society (ACS Publications).

Chapter 4

Quantum Dot Impregnated-Chitosan Film for Heavy Metal Ion Sensing and Removal

4.1. Introduction

Recently, synthesis of semiconductor nanocrystals (NCs), otherwise known as quantum dots (Q-dots) following a chemical transformation approach has gained pace due to the exquisiteness of the process in altering one NC to another, which is otherwise challenging to prepare independently.[1-12] The method not only enables us to create nanostructures of diverse compositions, but also helps in engineering multicomponent novel nanomaterials/nanostructures having unprecedented shapes and crystal structures.[4-12] In this regard, chemical transformation can be considered as an important toolkit for synthetic chemists having four different categories of solid state chemical transformations *viz.* alloying, replacement reaction, cation exchange reaction and anion exchange reaction[13-14] However, the cation exchange reaction has its uniqueness due to its ability to preserve the original structure/morphology of the starting material.[1, 3, 13-14]

A great deal of research has been carried out by Alivisatos and co-workers on the cation exchange mediated transformation of cadmium (Cd) based NCs.[1, 3-5, 15] It has been shown that cadmium chalcogenide nanostructures can be converted to other metal (Ag, Cu, Pb) chalcogenides simply by adding an excess of the metal ion present in an organic solvent.[1, 3] The ionic nature of the elements present in inorganic semiconductor has been shown to be responsible for the cation exchange process, where the anions serve to preserve the structural framework and the cations remain relatively mobile in the crystal lattice.[1] The propensity of cation exchange reaction depends on the thermodynamic driving force; which decides the direction of reaction and the ability to overcome the activation barrier

for the diffusion of atoms and ions.[13-14, 16] In this regard, the solvation of cations and the relative solubility difference between the reactant and the product, act as determining factors for the thermodynamic favourability of the reaction.[14, 16] Higher solubility product constant of a reactant than that of the ionic solid product in the reaction medium facilitates the forward reaction of ion exchange.[14] Once the above condition is met, the activation barrier remains the limiting factor for the transformation process.

In case of bulk solids, the transformation process is slow because of high activation energies, which impede the movement of atoms and ions in the solid and thus requires extreme reaction conditions.[1, 13-14] However, NCs and nanostructures have large surface to volume ratio which enables statistical averaging of the kinetics, leading to homogeneity and molecule like reaction behaviour.[1, 14, 16] The factors governing the thermodynamic barriers in NCs/nanostructures include the ionicity of the cation-anion interaction, frame of the anion sublattice and the structural differences in the phases of the reactant and the product.[13-16]

The structural changes, if any, in the transformed product could stem from the change in volume and lattice parameters during the reaction.[14, 16] Wark *et al.* have shown that the large fractional volume change (based on bulk lattice parameters) of the reaction can also lead to void formation and fragmentation depending on the degree of lattice stress developed during the transformation.[16] Further, reports by Jeong *et al.* suggest that even changes in the fractional volume of the NCs during the transformation reaction preserves the original morphology of the NCs.[14]

Till date, most of the cation exchange based chemical transformation reactions have been reported for Cd based NCs.[13] Only a few reports are available on the cation exchange in ZnS nano/microstructures.[17-19] Dloczik and Könenkamp have shown the transformation of columnar ZnO to ZnS and then converting the ZnS columns to other metal chalcogenide columns by immersing the tubular structures/films into aqueous solution of the respective metal ions.[17] The complete conversion took several hours and it required elevated temperatures.

Similarly, Yu *et al.* have shown the conversion of ZnS colloidal spheres to CuS/ZnS nanocomposite hollow spheres by ion exchange method and studied its photocatalytic activity.[20] Recently, Pala *et al.* showed that aerogels/xerogels containing ZnS nanoparticle could be used to remediate Pb^{2+} and Hg^{2+} polluted water. The method was able to reduce the heavy metal ion concentration below 15 ppb.[19] However, the reactant and the product particles did not exhibit the property of quantum confinement due to larger sizes and the transformation reaction was demonstrated in either alcohol or alcohol mixed with water organic solvents. The method for preparing the aerogels as well as the technique used for the removal of the contaminated metal ions was cumbersome as large volume of solution needed to be centrifuged to obtain the remediated water. Further, the ability to distinguish between metal ions was not available. Fast and efficient exchange of ions in aqueous medium leading to characteristic Q-dot coloration are useful for sensing and remediation of heavy metal ions, as bulk of the pollutants are present in the aquatic environment.

4.2. Outline of the Research Work

1) We report the fabrication of a composite film consisting of ZnS Q-dots and chitosan, a biopolymer. The film has been demonstrated to be capable of sensing and removal of heavy metal ions such as Hg^{2+}, Pb^{2+} and Ag^{+} from water.
2) The film works on the principle of chemical transformation of ZnS Q-dots into product Q-dots, based on cation exchange reaction in aqueous solution. For example, the biopolymer chitosan stabilized ZnS Q-dots were synthesized and transformed to HgS, Ag_2S and PbS Q-dots in aqueous medium.
3) The transformation into product crystals was accompanied by display of characteristic color corresponding to particular product Q-dot. Thus one could easily identify the presence and removal of a heavy metal ion from water.
4) The transformation reaction was validated by detailed characterization of the cation exchanged Q-dots using absorption and fluorescence

spectroscopy, transmission electron microscopy, X-ray diffraction and atomic absorption techniques.

5) The time of transformation depended on the nature of the product crystals (Q-dots). It was fast in the presence of Hg^{2+} or Ag^{+} (typically <1 s) and slower in the presence of Pb^{2+} (in minutes).
6) Interestingly, the morphology of the reactant Q-dots was maintained in the transformed products with differential volume changes due to the alteration in the crystal lattice parameters (depending on the product Q-dots).
7) Overall, the film could detect individual ions or dominant ions in a mixture of ions by simple display of change in colors.
8) The biofriendly polymer film and the Q-dots have been chosen to be ideal candidates for demonstration of quick and easy sensing and removal of heavy metal ions in water.

4.3. Experimental Section

4.3.1. Materials

Zinc acetate dihydrate [$Zn(CH_3COO)_2.2H_2O$], mercuric chloride ($HgCl_2$), mercuric nitrate ($HgNO_3.2H_2O$), lead nitrate [$Pb(NO_3)_2$], sodium sulphide (Na_2S) and acetic acid (glacial, 99-100%) were purchased from Merck Pvt. Ltd. (India). Silver nitrate ($AgNO_3$) and chitosan were purchased from Sigma-Aldrich chemical Pvt. Ltd. (USA). All chemicals were of AR grade and used as received without any further purification. MilliQ ultra-pure water (>18 MΩ cm) was used for all experiments.

4.3.2. Synthesis of ZnS Q-dots

ZnS Q-dots were prepared following a method reported previously by our group[21-22] and mentioned in chapter 2 with slight modification. Briefly, 21 mg $Zn(CH_3COO)_2.2H_2O$ was added to 9 mL of 0.5 mg mL^{-1} chitosan solution (dissolved in 0.1 % acetic acid) and it was heated at 80 °C for 15 min with continuous stirring. Next, the solution was allowed to cool down to room temperature and then 10 mM Na_2S solution was added dropwise to the above solution (kept in an

ice bath) under vigorous stirring in an ice bath. This resulted in the formation of milky colloidal suspension indicating the formation of ZnS Q-dots. The resulting colloidal dispersion was centrifuged at 20000 rpm for 15 min and the pellet thus obtained was washed with water for 3 times to remove unreacted ions, if any. Finally, it was suspended in 0.1 % acetic acid solution using a sonication bath to obtain a colloidal dispersion of ZnS Q-dots. The synthesized ZnS Q-dots were characterized using transmission electron microscopy (TEM), UV-vis and fluorescence spectroscopy and X-ray diffraction (XRD) measurements. For UV-vis and fluorescence spectroscopy quartz cuvettes of 1 cm path length were used.

4.3.3. Cation exchange reaction for the transformation of ZnS Q-dots

The chemical transformations of the ZnS Q-dots were performed by adding an aqueous solution of the desired metal ion to the ZnS Q-dot dispersions at room temperature and pH 5.5–6.0. For the conversion of ZnS Q-dots to HgS, Ag_2S and PbS Q-dots, a desired amount of the dispersion of ZnS Q-dots was taken in a vial and 5 times excess of Zn^{2+} ions in ZnS Q-dots of the respective heavy metal ion (Hg^{2+}, Ag^{+} and Pb^{2+}) was added to the solution, which resulted in the formation of different coloured solution depending upon the metal ions used. The addition of Hg^{2+} and Ag^{+} ions resulted in the immediate appearance of bright yellow and brown colour solution indicating the cation exchange mediated transformation of ZnS Q-dots. On the other hand, the addition of Pb^{2+} resulted in the formation of brown coloured solution several minutes after addition; the solution turned dark brown after about 6 h, indicating the transformation of ZnS Q-dots to PbS Q-dots. After the completion of the reaction, the Q-dots were centrifuged and the pellet was suspended in 0.1 % acetic acid solution after washing with MilliQ water for three times to remove the unreacted heavy metal ions and the released Zn^{2+} ions in the transformation process. The recovered Q-dots were characterized by TEM, UV-visible spectroscopy and XRD. The elemental compositions of the Q-dots were determined from the energy dispersive X-ray spectroscopy (EDS).

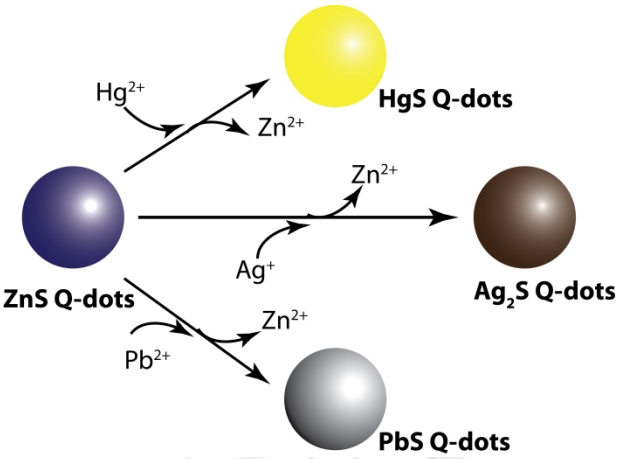

Figure 4.1. Schematic diagram depicting the cation exchange mediated chemical transformation of ZnS Q-dots to HgS, Ag_2S and PbS Q-dots.

4.3.4. Fabrication of ZnS impregnated Chitosan film

5 mg mL^{-1} chitosan solution was prepared in 0.5 % acetic acid and it was filtered to remove insoluble impurities, if any. 5:1 (*v/v)* chitosan solution and (chitosan-stablized) ZnS Q-dots were taken in a conical flask and mixed well using both stirring and sonication. The mixture solution was then poured in a polypropylene plate (1.5 cm height) and kept in an incubator at 37 ^{0}C. After ~48 h the film was separated from the plate and it was removed with the help of forceps. The prepared film was characterized using scanning electron microscopy (SEM), UV-visible spectroscopy and EDS.

4.3.5. Using the fabricated film for heavy metal removal

The ZnS Q-dots impregnated chitosan film was cut into 2 × 2 sq. cm small pieces and was used as a dipstick for the removal of heavy metal ion from solution. Two different concentrations of each of the heavy metal ion solution of 20 mL volume at neutral pH were taken in a tube and the film was completely immersed into it. The film was left immersed at room temperature for 1 h in case of Hg^{2+} and Ag^{+}, whereas, it was dipped for 2 h in case of Pb^{2+} ions. Manual swirling of the solution was done at each 10 min interval. The initial and final concentration of the metal ions along with the Zn^{2+} ion released in the solution was determined using atomic

absorption spectroscopy (AAS). The entire experiment was performed in triplicates and the data is presented as mean ± SD of three independent readings.

4.3.6. Instrumentation

TEM and selected area electron diffraction (SAED) analyses were performed using JOEL 2100 UHR-TEM instrument operating at an accelerating voltage of 200 kV. Sample for TEM was prepared by placing a 5 μL dropcast onto a 300 mesh carbon coated copper grid with subsequent air drying. UV-vis and fluorescence spectroscopy were carried out with Perkin Elmer LS 25 and Perkin Elmer LS 55 spectrophotometers respectively. XRD was recorded with a Brucker D8 Advanced X-ray diffraction measurement system, with Cu Kα source (λ = 1.54 Å). SEM was carried out using a LEO 1430VP SEM, after coating the sample with gold film using Polaron sputter coater. Elemental analysis using EDX spectroscopy was performed with Oxford INCA X-sight equipment attached to the LEO 1430VP SEM. The elemental concentrations of the metal ions in the medium were determined using Varian Inc. AA240 AAS.

4.4. Results and Discussion

4.4.1. Characterization and transformation of ZnS Q-dots

As mentioned in the Experimental Section, ZnS Q-dots were synthesized in aqueous medium using chitosan as the stabilizing agent. The stabilized Q-dots were dispersed in water medium for characterizations and transformation. The UV-vis spectrum of the dispersion is shown in **Figure 4.2a**, which consists of an excitonic edge at 304 nm. The band gap was calculated from the Tauc plot (**Figure 4A.1 a**, *Appendix*) which resulted in a value of 4.09 eV. The band gap increased considerably, in comparison to bulk band gap (3.60 eV) of ZnS semiconductor and thereby indicating the role of quantum confinement.[21, 23] **Figure 4.2b** represent the emission spectrum of the dispersion. At an excitation wavelength of 315 nm the dispersion displayed an emission spectrum with maximum at 438 nm. TEM measurements of the dispersion indicated the presence of NCs with average size of 3.6 ± 0.8 nm (**Figure 4.2c**). XRD measurements supported the formation of ZnS

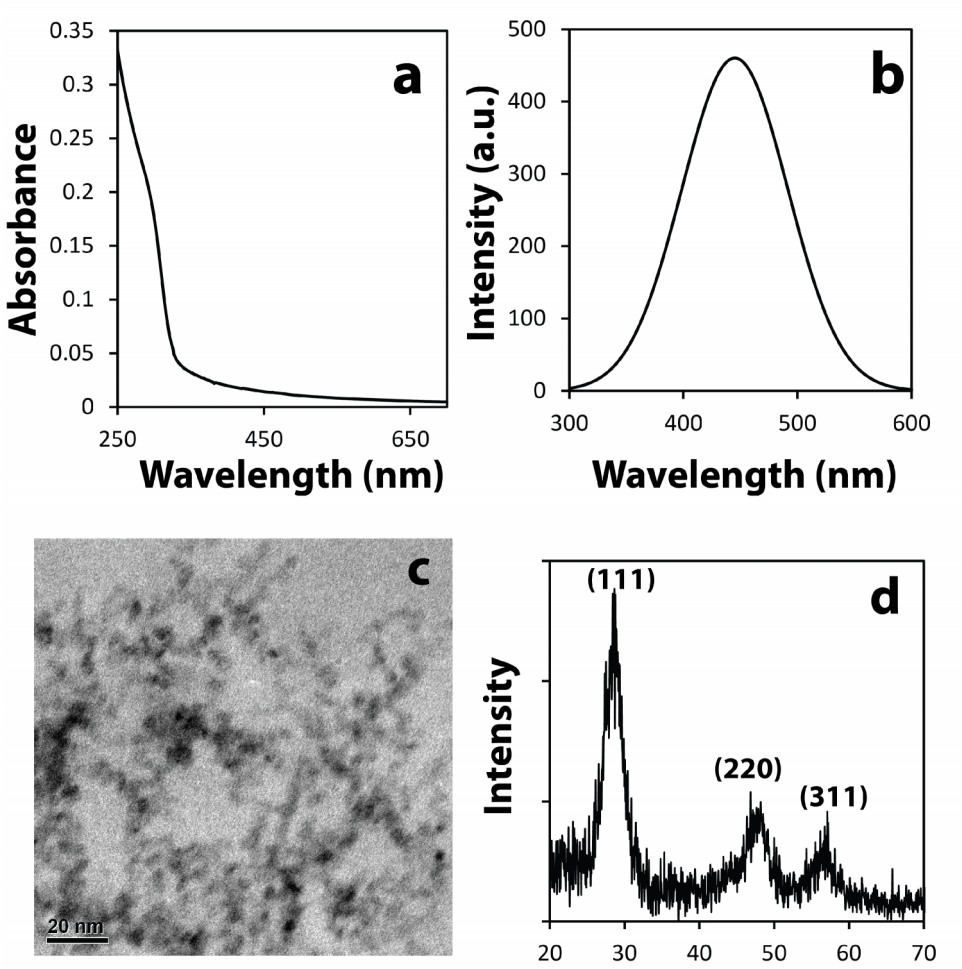

Figure 4.2. (**a**) Absorbance spectrum, (**b**) Fluorescence spectrum, (**c**) TEM image and (**d**) XRD pattern of ZnS Q-dots

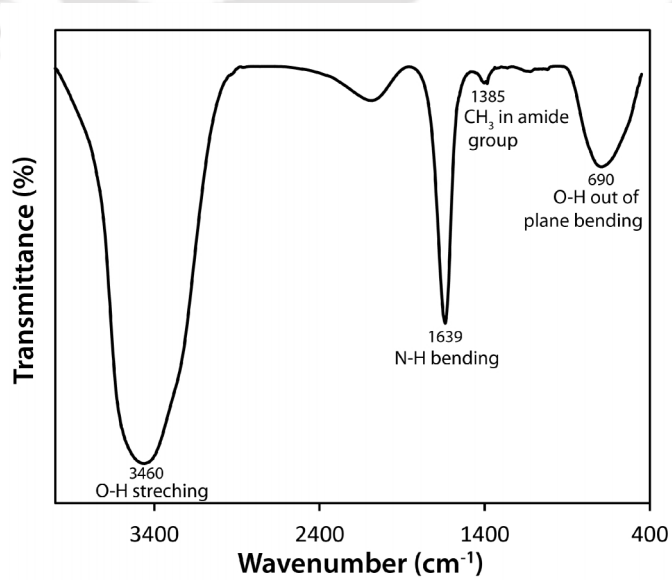

Figure 4.3. FTIR spectrum of chitosan stabilized ZnS Q-dots.

NCs (**Figure 4.2d**). FTIR measurements indicated the presence of chitosan (**Figure 4.3**). Thus the dispersion consisted of ZnS Q-dots along with chitosan.

The dispersion was colorless in nature. However, when an excess of the heavy metal ions, Hg^{2+}, Ag^{+} or Pb^{2+}, was added to the aqueous dispersion of the Q-dots, change in the coloration of the medium could be observed at various times (**Figure 4.4a**, *inset*). For example, after addition of Hg^{2+} or Ag^{+} ions, an instantaneous (in <1 s) appearance of colour could be observed. Addition of Hg^{2+} led to formation of bright yellow color, indicating the formation of HgS; whereas the presence of Ag^{+} ions resulted in brown coloration, possibly due to formation of Ag_2S. This instantaneous nature of cation exchange mediated transformation of Q-dots has been previously reported by Son *et al.* in Cd based NCs. [1] Interestingly, addition of Pb^{2+} ions did not result in an instantaneous colour change, however, the brown colour development indicating the formation of PbS Q-dots, occurred in the time scale of minutes. It took typically about 15–30 min for the appearance of brown colour, depending upon the concentration of the ions used.

Further, the normalized absorption spectra of the heavy metal ion treated samples are shown in **Figure 4.4a**. Treatment of Hg^{2+} ions led to an absorption edge at 500 nm, whereas, treatments of Ag^{+} or Pb^{2+} resulted in a broad absorption spectrum in the UV-vis region (especially up to 650 nm). The absorption spectral features of all the transformed products matched with corresponding Q-dots.[24-29] In all cases, the absorption feature of ZnS Q-dots was not observable, indicating possible complete transformation of the Q-dots in the reaction.

The direct band gaps of the converted Q-dots were also determined using Tauc plot[30-31] (**Figure 4A.1**, *Appendix*) and the results are summarized in **Table 4.1**, along with the bulk band gap of the respective compound. The band gaps of all the Q-dots were higher in comparison to the band gaps of the bulk compound, clearly indicating the role of quantum confinement.[23-29, 31-32] The determined band gaps of the transformed Q-dots were similar to those respective Q-dots reported earlier; which were synthesized separately following organo-metallic or wet chemical synthetic approaches.[23-29, 31-32] The emission of the ZnS Q-dots was

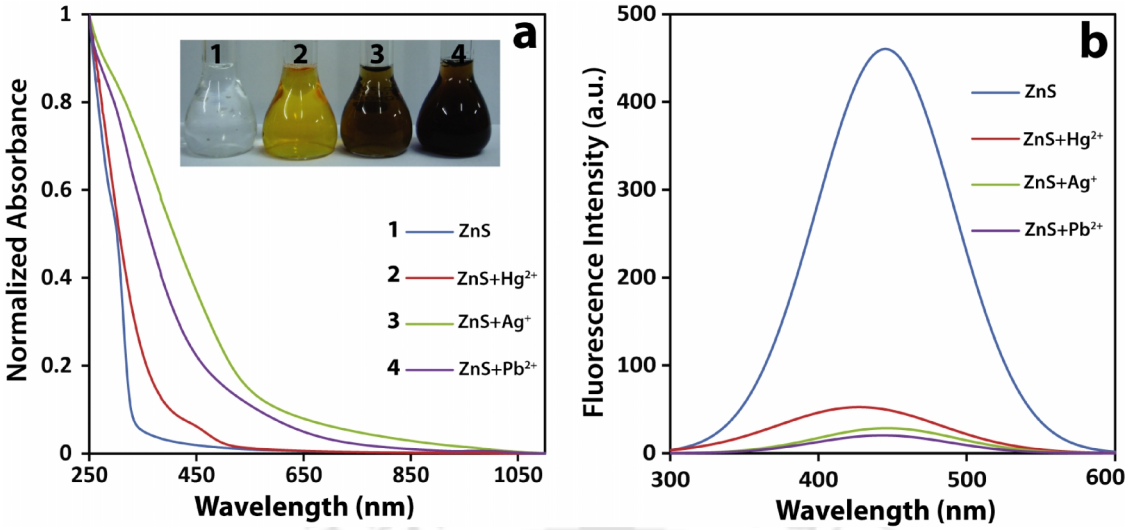

Figure 4.4. (**a**) Normalized UV-vis-NIR spectra of ZnS Q-dots and that of ZnS+Hg^{2+}, ZnS+Ag^{+} and ZnS+Pb^{2+}, with inset showing the appearance (photographs) of the colloidal dispersions in visible light. (**b**) Fluorescence spectra of ZnS Q-dots and that of ZnS+Hg^{2+}, ZnS+Ag^{+} and ZnS+Pb^{2+} solution.

nearly quenched (**Figure 4.4 b**) after the addition of either of the cations. The quenching of fluorescence of Q-dots after undergoing a cation exchange reaction has previously been reported for Cd based Q-dots.[1] Thus the absorption and fluorescence spectroscopic measurements indicated transformations of ZnS Q-dots in the presence of ions in the medium to corresponding product Q-dots.

Table 4.1. Band gap of the semiconductor bulk material studied in the present case along with the calculated band gap of the respective materials at its quantum size using the Tauc plot.

Quantum dots	**Bulk band gap**[21, 23-29, 31] **(direct) (eV)**	**Determined band gap from Tauc plot (eV)**
ZnS	3.60	4.09
HgS	0	2.48
Ag_2S	1.00	2.16
PbS	0.41	1.86

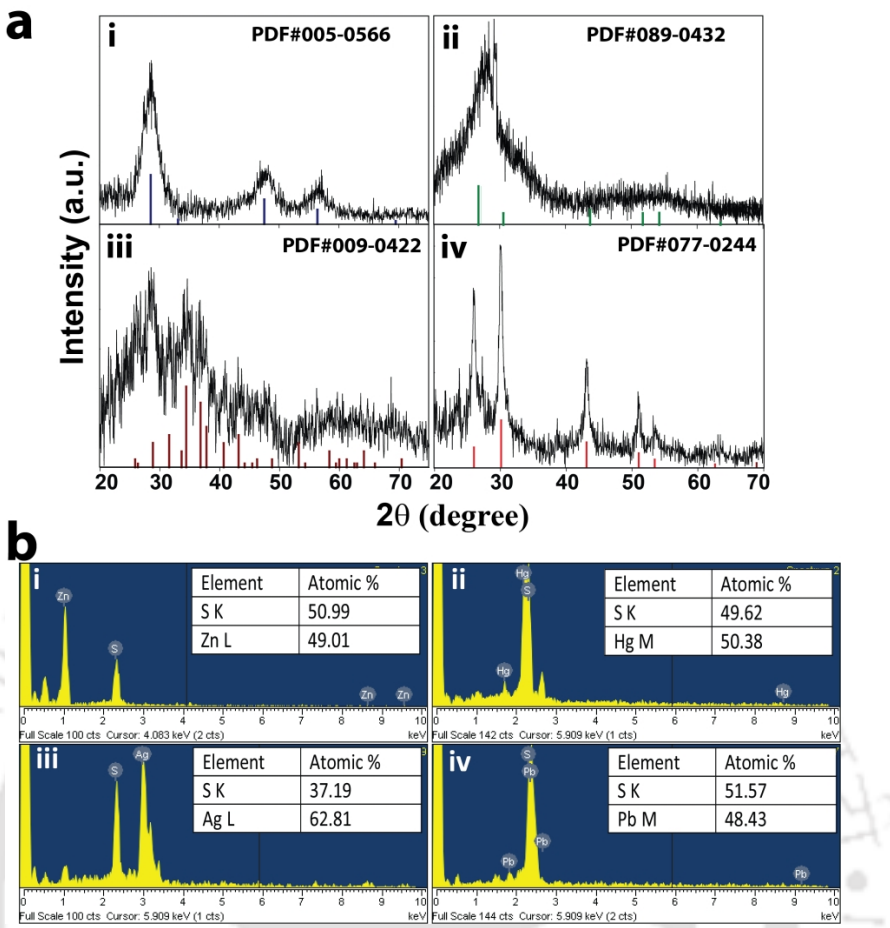

Figure 4.5. a) XRD patterns of (**i**) ZnS Q-dots, and the transformed (**ii**) HgS Q-dots, (**iii**) Ag_2S Q-dots and (**iv**) PbS Q-dots. The lines under the spectra represent the JCPDS pattern for each material. **b**) EDX spectra of the (**i**) reactant ZnS Q-dots and the transformed (**ii**) HgS Q-dots, (**iii**) Ag_2S Q-dots and (**iv**) PbS Q-dots. The inset shows the atomic percentage of the elements present in the respective Q-dots.

Figure 4.5a shows the XRD diffraction patterns and the EDS analyses of the reactant and the cation-treated products respectively. All the peaks were indexed with the JCPDS pattern of the respective compound shown in stick pattern along with the XRD pattern. **Figure 4.5a** (**i**) corresponds to the XRD pattern of as-prepared ZnS Q-dots. As is clear from the figure and the stick pattern the peaks at 28.5°, 47.5° and 56.4° correspond to the {111}, {220} and {311} planes of ZnS in the cubic phase of sphalerite crystal. Addition of either of Hg^{2+}, Ag^{+} or Pb^{2+} led to nearly complete disappearance of the peaks corresponding to ZnS crystal. In addition, new peaks appeared corresponding to crystals of HgS, Ag_2S and PbS respectively. For example, as shown in **Figure 4.5a** (**ii**), the peak at 26.3°

corresponds to {111} plane of HgS (in cubic phase of metacinnabar). Similarly, shown in **Figures 4.5a (iii)** and **4.5a (iv)** are the XRD patterns of the samples treated with Ag^{+} and Pb^{2+} ions and the peaks appear corresponding to lattice planes of Ag_2S (in monoclinic phase of acanthite) and PbS (in cubic phase of galena) respectively. Thus, XRD measurements supported the transformation of ZnS Q-dots into HgS, Ag_2S and PbS crystals upon treatment with Hg^{2+}, Ag^{+} and Pb^{2+} ions respectively. EDS results, shown in **Figure 4.5b**, further supported the transformation of ZnS into the above crystals following treatments with corresponding parent ions. It may be mentioned here that although quantitative measurement of ion concentration in a sample is not possible based on EDS measurements, their relative abundance could be at least indicative. Thus, as shown in the **Figure 4.5b**, the ratio of Pb and S to have been 1:1, Ag and S to have been 2:1 and Pb and S to have been 1:1 in the corresponding crystal could be concluded from the results. The complete conversion cannot be established from these results as minute quantity of amorphous ZnS particles could remain unreacted; even then the results indicated nearly complete transformation of the ZnS Q-dots. The minor peak corresponding to Zn atom in case of **Figure 4.5b (iii)** can possibly be due to the adsorption of the released Zn^{2+} ions or some non-transformed Q-dots. Overall, EDS results supported the transformation of ZnS into product crystals as in the case of XRD measurements.

Further, morphological analyses of the as-synthesized Q-dots and those of the products were carried out using TEM. **Figures 4.6 a, b, c** and **d** show the TEM images of as-synthesized (ZnS) Q-dots along with the products of Hg^{2+}, Ag^{+} and Pb^{2+} treated samples. As is clear from the figures spherical nanoparticles (NPs) were present in all samples. The particle size distributions were obtained from the TEM images and are shown in **Figure 4.6 (i-l)**. The average particle size and standard deviation were calculated directly from the individual sizes, which also are in good agreement with the results of Gaussian fit to the histogram. Also, the size distributions for all the samples were narrow. The sizes of the as synthesized ZnS, and those of samples treated with Hg^{2+}, Ag^{+} and Pb^{2+} were calculated to be 3.6 ± 0.8, 3.9 ± 0.9, 7.3 ± 1.9 and 3.9 ± 0.9 nm respectively. High resolution TEM

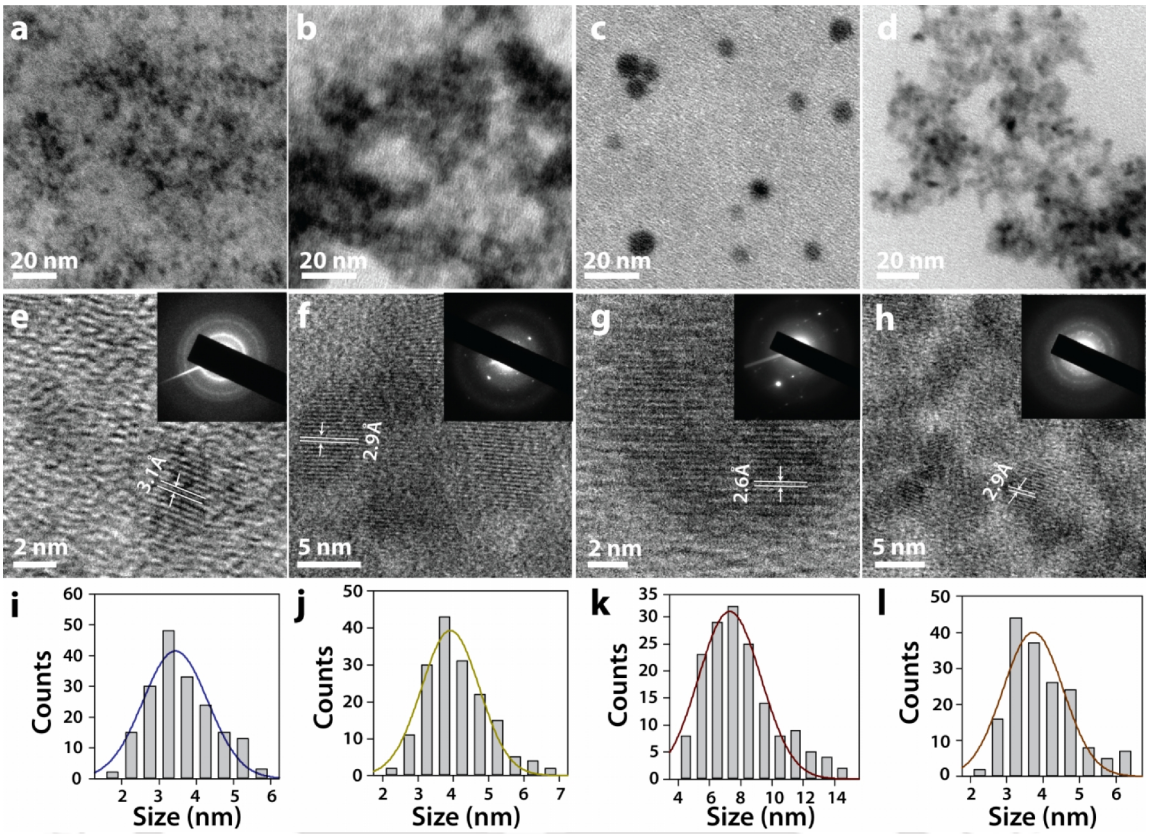

Figure 4.6. (**a-d**) TEM images of the reactant ZnS Q-dots and the transformed HgS, Ag_2S and PbS Q-dots respectively. (**e-h**) HRTEM images of ZnS, HgS, Ag_2S and PbS Q-dots respectively with inset showing the SAED pattern. (**i-l**) The particle size distribution of the ZnS, HgS, Ag_2S and PbS Q-dots respectively along with the Gaussian fit to the respective histogram.

(HRTEM) of the samples (**Figure 4.6 e-h**) and the SAED pattern (**Figure 4.6 e-h**, *inset*) showed clear lattice fringes and crystallinity of all them. The results confirmed the formation of HgS, Ag_2S and PbS NCs as results of reactions between ZnS Q-dots and Hg^{2+}, Ag^{+} and Pb^{2+} respectively. Lattice spacing corresponding to individual NCs is identified in the figures.

Further, a careful analysis of the average sizes and the distributions of particle sizes therein indicated systematic change in the sizes of the particles upon chemical transformation. Additionally, retention of sphericity for all the transformation indicated preservation of morphology of the crystals during the process. Previous reports suggest that the morphology of NCs is often maintained after the transformation reaction,[1, 6-12] which was also observed in the cases

herein. This signifies that during a cation exchange reaction the structural frame of the anionic sub-lattice is preserved with only minor alterations of the anion lattice positions. Therefore, the transformation reaction proceeded by the diffusion of the cations through the anionic sub-lattice. It has been reported that the exchange reaction could initiate and propagate at particular regions of the reactant nanostructure.[16] The rationale behind this was proposed to be due to the difference in the polarity in the facets of NCs as well as the difference in the accessibility (or for that matter inaccessibility) of the reactant cation to the different regions of the NCs due to selective passivation.[16] However, in the present case, the XRD, EDS and TEM results suggested that the transformation reaction was complete and non-selective; as we did not observe any partially exchanged Q-dot neither we had the evidence of a faceted reaction.

The increase in size of the Q-dots with respect to the reactant ZnS Q-dots could be explained on the basis of the change in the lattice parameters while encompassing the transformation reaction. The crystal structure, lattice parameters of the reactant and product Q-dots, and the fractional volume change during the cation exchange process, based on the unit cell volume of the bulk material are summarized in **Table 4.2**.

As the crystal structure of the ZnS Q-dots and that of HgS and PbS Q-dots were all in the same cubic zinc blende phase, only small fractional change in volume could be observed, which was commensurate with the unit cell dimensions of the respective materials. The calculations validated the minor increase in dimensions of the ZnS Q-dots when transformed into HgS and PbS Q-dots, as were observed in the TEM images. Whereas, the transformation of ZnS to Ag_2S Q-dots resulting in significant volume increase, as seen from the TEM micrographs (**Figure 4.6c**), can be attributed to the change in the cubic crystalline phase of ZnS to monoclinic phase of Ag_2S Q-dots. Approximately, two fold increase in the fractional volume change takes place based on the unit cell lattice parameters, thereby, attesting the major size increase in case of Ag_2S Q-dots. It is interesting to note that in spite of significant volume increase in the Ag_2S Q-dots; there was no void formation or fragmentation of the resulting Q-dots,

Table 4.2. Structure, lattice parameters and the fractional volume change for the reactant and the transformed Q-dots in the present study.

Q-dots	Crystal Structure	Lattice Parameters	Unit cell volume $(Å)^3$	ΔV/V
ZnS	Sphalerite (cubic)	a = b= c = 5.406 Å $\alpha = \beta = \gamma = 90^0$	157.99	reactant
HgS	Metacinnabar (cubic)	a = b= c = 5.8537 Å $\alpha = \beta = \gamma = 90^0$	200.58	0.27
Ag_2S	Acanthite (Monoclinic)	a = 9.52, b = 6.93, c = 8.29 Å, $\alpha = \gamma = 90^0$, β=123.87^0	454.11	1.87
PbS	Galena (cubic)	a = b= c = 5.9340 Å $\alpha = \beta = \gamma = 90^0$	208.95	0.32

demonstrating that the transformation reaction required only minor structural change irrespective of prominence of the increase in volume.

The cation exchange transformation reaction majorly depends on the solubility product constant (K_{sp}) of the reactant and the product, which determines the thermodynamic favourability of the reaction. The solubility product of an ionic solid is the equilibrium constant between its solvated and the solid state. The solubility product constant of the different materials investigated in the present study along with the Gibbs free energy change (ΔG^0) for their dissolution into ions and the reduction potential of cations are summarized in **Table 4.3**. The free energy change of solvation depends upon the solubility product according to equation 4.1.

$$\Delta G^0 = -RT \ln K_{sp} \tag{4.1}$$

Table 4.3. Solubility product data, free energy change of solution of the metal sulfides and the reduction potential of the cations studied in the present case at 25^{0}C.

Quantum dots	Solubility Product constant[14], K_{sp}	K_{sp} ratio	ΔG^0 (Dissolution into ions)	Reduction Potential (E^0) of cation[19] (M^{n+}/M) (V)	Difference in reduction Potential (ΔE^0)
ZnS	3.00×10^{-25}	reactant	1.40×10^5	-0.763	-
HgS	6.00×10^{-53}	5.00×10^{27}	2.98×10^5	+0.854	+1.617
Ag_2S	3.00×10^{-50}	1.00×10^{25}	2.83×10^5	+0.79	+1.55
PbS	1.00×10^{-28}	3.00×10^3	1.60×10^5	-0.125	+0.638

The positive value of the free energy change indicates that the dissolution of the metal chalcogenides into respective ions is nonspontaneous, whereas, the reverse reaction is favourable. As it can be seen from **Table 4.3** that the solubility product constant of HgS, Ag_2S and PbS are less; and the free energy is more positive than that of ZnS. The higher value of K_{sp} ratio which denotes the equilibrium constant for the cation exchange reaction; signifies that the exchange reaction goes to completion. Further, the rate of reaction has been ascribed to the difference in the reduction potential of Zn^{2+} and the incoming metal ions.[19] Thus higher difference between the reactant and the product metal cation reduction potential leads to faster exchange reaction.[19] For example, larger positive reduction potential of Hg^{2+} in comparison to that of Pb^{2+} leads to faster reduction. Thus, ZnS Q-dots could spontaneously get converted into the other Q-dots in the order of HgS > Ag_2S > PbS. It is worth mentioning that the above transformation do not occur instantly in case of bulk materials due to large kinetic barrier, whereas, the nano counterpart of the respective materials can cross the kinetic barrier instantaneously depending on K^*_{sp}, the solubility product constant of the NC, which has been defined as,

$$\log K^*_{sp} = \log K_{sp,bulk} + 2\gamma A_m / [3\log(RT)] \quad (4.2)$$

where, K_{sp}, γ and A_m are the solubility product, the surface tension and molar surface area of the solute respectively.[13-14] It is noteworthy to mention that when a mixture of Hg^{2+}, Ag^{+} and Pb^{2+} ions in the same ratio were used, HgS was formed favourably over others. Thus magnitude of solubility product of the product NC plays the key role in deciding how facile the transformation would be.

In order to probe the efficacy of using the Q-dots (ZnS) for sensing and removal of heavy metal ions tests were carried out in the presence of varying concentrations of Hg^{2+} ions in water. For this the ZnS Q-dots (0.43 μM) were dispersed in water as the UV absorbance of the dispersion showed a clear and measureable edge. The UV-vis absorption spectra of the dispersion at varying concentration of Hg^{2+} are shown in **Figure 4.7**. It was observed from the spectra that for 1 – 10 ppm of Hg^{2+} the absorbance edge corresponding to the ZnS Q-dots were prominent (although diminishing systematically) with slight appearance of a background beyond 350 nm. At 25 ppm, it was noticed that the edge corresponding to ZnS Q-dots completely vanished and that of HgS Q-dots started appearing indicating conversion of ZnS to HgS Q-dots. The colour of the solution

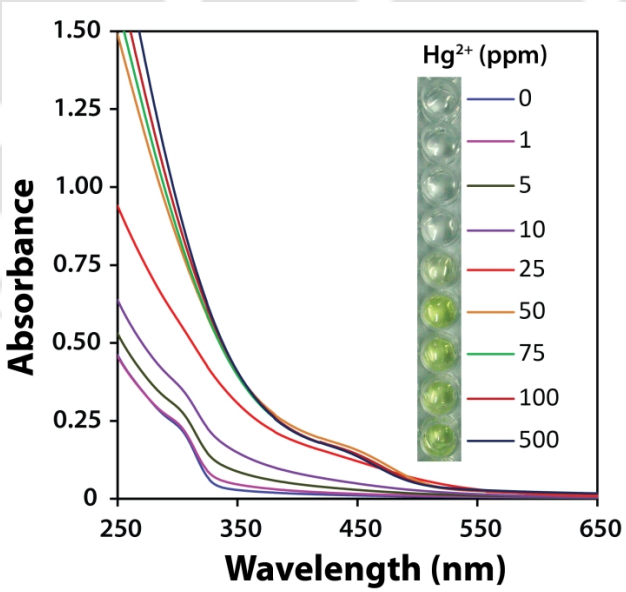

Figure 4.7. Absorption spectra of ZnS Q-dots when treated with varying concentration of Hg^{2+} ions. The right panel images represent the appearance of the samples under visible light illumination, at the concentrations mentioned in the legend (ppm).

also turned to light yellow - the characteristic feature of HgS Q-dots in the present case, which enabled the visible identification of the formation of HgS Q-dots. An array of such transformation of color in the presence of 9 different cells of dispersion is shown in **Figure 4.7** (right panel images). As is clear from the figure, the change of color is apparent when the concentration of Hg^{2+} was 25 ppm or higher.

Further, at a concentration of 50 ppm Hg^{2+}, prominent absorbance edge corresponding to HgS Q-dots along with intense yellow colour of the solution was detected and beyond this concentration no change; either in the peak position or in the colour of the solution indicating the saturation point, where all the ZnS Q-dots present were possibly converted to HgS Q-dots. The result signifies that at this particular concentration of ZnS Q-dots, i.e. 25 ppm of Hg^{2+}, the same ions can be visually detected due to the development of yellow coloration. Thus transformation of Q-dots by ion-exchange reaction could be used for visual detection as well as arresting of heavy metal ions.

We also investigated the possibility of sensing and removal of other divalent and trivalent metal ions using ZnS Q-dots in liquid medium and the results are shown in **Figure 4A.2** (*Appendix*). Addition of divalent cations like Cd^{2+}, Mg^{2+}, Mn^{2+}, Sr^{2+} did not show any immediate colour formation in contrast to the heavy metal ions mentioned above. On the other hand, addition of Cu^{2+} showed brown colour development. The presence of Fe^{2+} and Fe^{3+} ions showed a faint brown colour, which was the intrinsic colour of the salts when dissolved in water. Amongst the tested trivalent ions, Au^{3+} (being present as $AuCl_4^-$) showed dark brown colour formation possibly due to its conversion into sulphide, whereas, Al^{3+} did not show any visible colour development. The formation of colour for the particular metal ions can again be accounted for based on the solubility product constant of the metal sulphide and the reduction potential of the metal ion. None of the ions exhibited prominent coloration as in case of Hg^{2+}, making the process distinct and possibly selective. Hence, the lowest solubility product of the HgS and higher reduction potential of Hg^{2+} ions make the process competent for Hg^{2+} ion detection and removal. It may be mentioned here that the limit of detection of the current sensor was not to the ppb level, as in case of

reported DNA aptamer, antibody or organic ligand based sensors;[33] however, the simple chemistry, along with the use of cheaper biopolymer having the film forming capability and visual colour formation, subsiding the need of sophisticated instrumentation, empowers it to be useful for sensing and removal of the selective heavy metal ions from contaminated water.

4.4.2. Fabrication of ZnS Q-dots impregnated chitosan film and heavy metal ion removal

In order to exploit the ability of the ZnS Q-dots to undergo a cation exchange based chemical transformation reaction, we fabricated chitosan films impregnated with ZnS Q-dots and used it as a simple dipstick tool for sensing and removal of heavy metal ions from contaminated water. Chitosan (poly(1,4-β-D-glucopyranosamine)) is a biocompatible and biodegradable polymer obtained from the deacetylation of chitin (poly-(1,4-β-N-acetyl-D-glucosamine)) found in the shells of crustaceans, which is the second most abundant polysaccharide in nature.[34-35] Chitosan also has the excellent property of forming films with sufficient mechanical properties.[36] The scheme for the fabrication of the chitosan film is shown in **Figure 4.8** and further details are available in the Experimental Section. The SEM image of the fabricated film is shown in **Figure 4.9**. The film showed smooth morphology with a thickness of ~35 μm as measured from SEM and phase contrast micrographs (**Figure 4A.3**, *Appendix*).

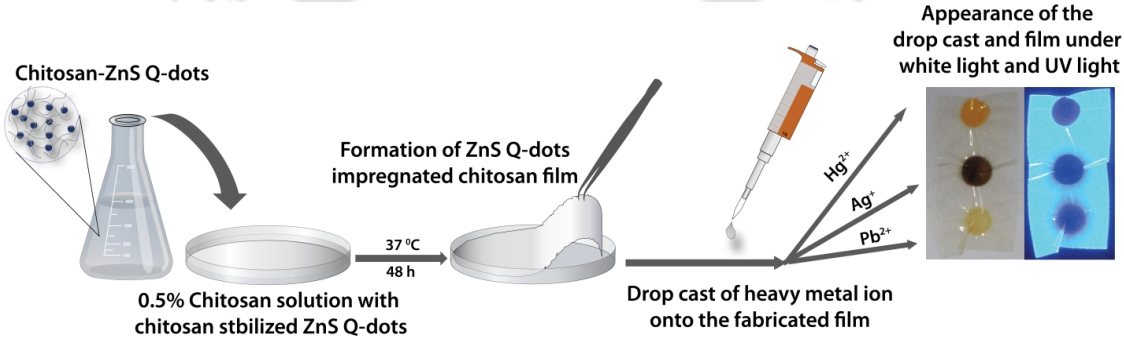

Figure. 4.8. Schematic demonstrating the fabrication of ZnS Q-dots impregnated chitosan film along with the appearance of the drop cast of different metal ions onto the fabricated film under visible and UV light.

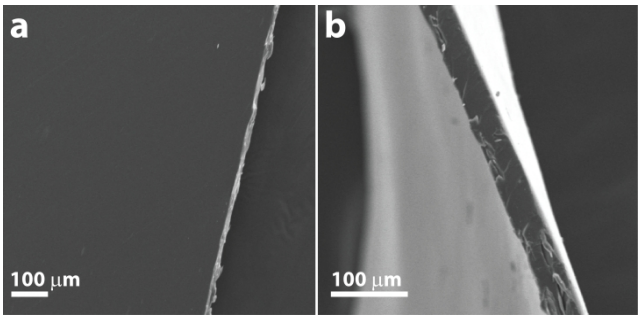

Figure 4.9. SEM images of the chitosan film (**a**) showing smooth morphology and (**b**) the vertical section showing the thickness of ~35 μm.

The presence of ZnS within the film was confirmed by EDS and UV-visible spectroscopic analysis (**Figure 4A.4,** *Appendix*). Also, shown in **Figure 4.8** are the color changes following addition of water containing heavy metal ions (Hg^{2+}, Ag^{+} and Pb^{2+}). The visual appearance of the ZnS Q-dots-chitosan film with the drop cast of different heavy metal ion in visual light and under UV illumination is shown in **Figure 4.8**. The Hg^{2+} ions led to the characteristic yellow colour, whereas, Ag^{+} and Pb^{2+} resulted in dark and light brown coloration, similar to those observed in solution. When the film was observed under UV light, the bright blue fluorescence of the ZnS Q-dots was completely quenched. The drop cast of Pb^{2+} which was only faintly visible, can easily be identified under the UV illumination. Although the photographs shown here were based on drop cast, which was used for easy demonstration of different colours due to different metals, a single film could also be used for removal of single metal or multiple metals by dipping the same in the medium (as described later). The rationale behind the film fabrication was that, that it can suitably be used as a simple dipstick method for the removal of heavy metal ions (Hg^{2+}, Ag^{+} and Pb^{2+}) from aqueous solution. The film can simply be dipped into the contaminated water/sample for a certain period of time and later can be removed easily, enabling the exchange of less toxic Zn^{2+} ions from the film with that of a toxic heavy metal ion from the solution. We have also fabricated chitosan film devoid of the ZnS Q-dots and checked its role for the detection of the metal ions. The drop cast of the different metal ions onto these unloaded films did not show the development of any colour either in visible light or under UV

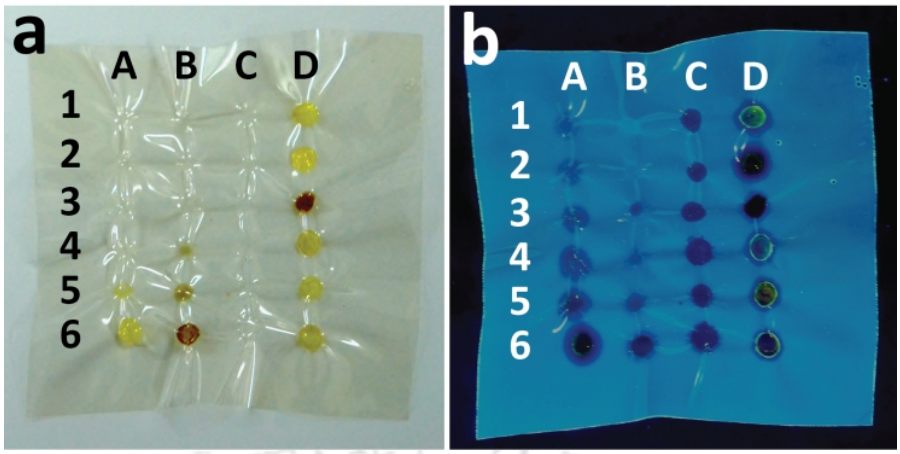

Figure 4.10. Matrix created by the drop cast of different metal ions of varying concentrations as well as mixtures under (**a**) visible and (**b**) UV light. A1-A6, B1-B6 and C1-C6 represent the drop cast Hg^{2+}, Ag^{+} and Pb^{2+} at 5, 10, 25, 50, 100, 500 ppm respectively. D1 and D2 show the drop cast of mixture of Hg^{2+}: Ag^{+} and Hg^{2+}: Pb^{2+} in 1:1 ratio, D3 and D4 are the drop cast of Ag^{+}: Pb^{2+} and Hg^{2+}: Ag^{+} in 1:1 and 1:2 ratio in the order. D5 and D6 represent the mixtures of Hg^{2+}: Ag^{+}: Pb^{2+} in 1:1:1 and 1:2:1 ratios respectively.

illumination (**Figure 4A.5**, *Appendix*). This demonstrated that only the Q-dots impregnated within the films were responsible for the detection of the metal ions.

Figure 4.10 shows the arrays of drop cast of varying concentrations of different metal ions onto the chitosan film under visible and UV light. Columns A–C represent the appearance of the drop cast of Hg^{2+}, Ag^{+} and Pb^{2+} in increasing concentration along the rows 1–6 (5 – 500 ppm). Hg^{2+} and Ag^{+} ions were identified in the visible illumination in the 50–500 ppm concentration range due to the development of yellow and brown color respectively, whereas no visual color was identified at lower concentrations. When observed under UV light, spots of Hg^{2+} and Ag^{+} even at the concentration of 5 ppm and 25 ppm respectively was observed. Pb^{2+} ions, which did not formed any visual coloration under white light at the range of concentration being tested, were easily identified under UV illumination even at the lowest concentration of 5 ppm. When mixtures of the different metal ions were used for the drop cast, then the formation of color was based on the solubility product constant. The mixtures containing the Hg^{2+} ions led to the development of yellow color, deserting the effect of other metal ions

Table 4.4. Initial and final concentrations of the heavy metal ions (Hg^{2+}, Ag^{+} and Pb^{2+}), amount of Zn^{2+} released and the percentage removal of the respective metal ions using ZnS Q-dot impregnated chitosan films.

Heavy Metal ion	Initial concentration (C_i) (ppm)	Final concentration (C_f) (ppm)	Amount removed (C_i-C_f) (ppm)	Amount of Zn^{2+} released (ppm)	% Removal (C_i-C_f)/ C_i ×100
Hg^{2+}	9.17 ± 0.25	5.23 ± 0.11	3.93 ± 0.37	4.85 ± 0.72	42.90
	19.77 ± 1.17	8.67 ± 1.21	11.1 ± 2.37	8.6 ± 0.25	56.16
Ag^{+}	8.18 ± 0.44	3.68 ± 0.29	4.5 ± 0.73	1.87 ± 0.29	55.03
	17.78 ± 1.19	6.54 ± 0.34	11.24 ± 1.54	4.96 ± 0.34	63.22
Pb^{2+}	8.01 ± 0.19	4.67 ± 0.23	3.34 ± 0.42	2.55 ± 0.38	41.68
	20.68 ± 0.42	15.53 ± 0.1	5.15 ± 0.53	4.15 ± 0.69	24.89

(D1-D2 and D4-D6). Similarly, the mixture of Ag^{+} and Pb^{2+} caused the appearance of brown coloration (D3), characteristic of Ag^{+} ions in the present case.

As a proof of principle to determine the heavy metal ion removal capacity of the fabricated film, we dipped a 2 × 2 sq. cm film in two different concentrations; each of which consisted of either of Hg^{2+}, Ag^{+} and Pb^{2+} aqueous solution. The initial and final concentrations of the respective metal ions were determined using AAS and the results are summarized in **Table 4.4**. In order to accredit that the removal mechanism involved cation exchange reaction, the concentration of Zn^{2+} in each of the sample was also monitored. Additionally, the AAS data was also corrected by subtracting the amount of Zn^{2+} released, if any, by diffusion or other means from the film to the solution, in order to demonstrate the sole role of cation exchange reaction in the transformation process. It was observed from the AAS data that about 50% of the Hg^{2+} ions were removed from the solution within 1 h duration, whereas, more than 60% of Ag^{+} ions were removed within the same time period. The amount of Zn^{2+} ions released were almost similar to those of Hg^{2+} and Pb^{2+} removed and was nearly half the amount in case of Ag^{+}; maintaining the stoichiometric ratio. In case of Pb^{2+} ions, nearly

40% of the ions were removed in 2 h duration from the initial concentration of ~8 ppm, whereas, removal was only 24 % in case of 20 ppm initial concentration of Pb^{2+} ion. The difference in the transformation could be correlated with the difference in reduction potential between the Zn^{2+} cation and the contaminant metal cation. The more is the difference between the reactant and the incoming metal cation, the faster is the transformation.[13] The above results suggest that the present system could be used as a suitable method for the efficient removal of Hg^{2+} and Ag^{+} cations, whereas, it can also be used to remove Pb^{2+} ions but in extended period of time.

Since chitosan is a known for adsorbing metal ions,[37] blank adsorption experiment using chitosan film in absence of the ZnS Q-dots was performed. Interestingly, it was observed that only negligible amount, if any, of the heavy metal ions were removed from their aqueous solution via adsorption onto the film surface (**Table 4.5**), under conditions as used for Q-dot impregnated films. Thus, removal of the metal ions from the aqueous solution was mainly based on the cation exchange mediated chemical transformation of the ZnS Q-dot impregnated within the chitosan film.

Table 4.5. Initial and final concentrations of the heavy metal ions (Hg^{2+}, Ag^{+} and Pb^{2+}) and the amount of ions adsorbed using chitosan films in absence of the ZnS Q-dots. The minor difference in the concentrations of Hg^{2+} could be considered as experimental error.

Heavy Metal ion	Initial concentration (C_i) (ppm)	Final concentration (C_f) (ppm)	Amount adsorbed (C_i-C_f) (ppm)
Hg^{2+}	5.45 ± 1.6	6.65 ± 0.21	-
	17.4 ± 2.7	15.5 ± 0.14	1.9
Ag^{+}	9.3 ± 0.63	8.65 ± 0.4	0.65
	23.34 ± 0.4	19.7 ± 0.8	3.64
Pb^{2+}	7.6 ± 0.24	6.87 ± 0.25	0.73
	17.3 ± 0.3	17.1 ± 0.08	0.2

4.5. Conclusion

We have demonstrated the cation exchange mediated chemical transformation of ZnS Q-dots in an aqueous solution. The ZnS Q-dots synthesized using the biopolymer chitosan as the stabilizing agent underwent a cation exchange reaction leading to the formation of stable colloidal HgS, Ag_2S and PbS Q-dots, which are sometimes difficult to synthesize in the aqueous phase. The transformed products retained the morphology of the reactant Q-dots and showed quantum confinement effect. The transformation reaction was based on the difference in the solubility product constant of the reactant and the product materials enabling the conversion of a material having higher K_{sp} to that of having a lower K_{sp} The transformed HgS and PbS Q-dots showed minor volume change, whereas, Ag_2S showed significant volume expansion which was explained on the basis of difference in lattice parameters of the reactant and the product Q-dots. The ZnS Q-dots impregnated chitosan film showed the ability to visually detect and remove the heavy metal ions from aqueous solution. The removal capacity of the fabricated film was demonstrated using AAS and the findings suggests its potential applicability in environmental remediation. The present system could be used in designing of a heavy metal ion removal filtration system utilizing the film forming property of chitosan along with the excellent capability of the ZnS Q-dots to undergo cation exchange reaction. The transformed Q-dots could have important applications in the optoelectronic fields due to its simple synthesis in aqueous medium. Further, our fabricated chitosan films impregnated with the ZnS Q-dots enabled us to use it for a simple dipstick method for the removal of heavy metal ions from contaminated water.

4.6. References

1. D. H. Son, S. M. Hughes, Y. Yin, A. P. Alivisatos, *Science*, **2004**, 306, 1009–1012.
2. H. Li, M. Zanella, A. Genovese, M. Povia, A. Falqui, C. Giannini, L. Manna, *Nano Lett.*, **2011**, 11, 4964–4970.
3. J. M. Luther, H. Zheng, B. Sadtler, A. P Alivisatos,. *J. Am. Chem. Soc.*, **2009**, 131, 16851–16857.
4. R. D. Robinson, B. Sadtler, D. O. Demchenko, C. K. Erdonmez, L. W. Wang, A. P. Alivisatos, *Science*, **2007**, 317, 355–358.
5. B. Sadtler, D. O. Demchenko, H. Zheng, S. M. Hughes, M. G. Merkle, U. Dahmen, L.W. Wang, A. P. Alivisatos, *J. Am. Chem. Soc.*, **2009**, 131, 5285–5293.
6. M. Casavola, M. A. van Huis, S. Bals, K. Lambert, Z. Hens, D. Vanmaekelbergh, *Chem. Mater.*, **2012**, 24, 294–302.
7. C. Zhao, F. Liu, W. Kang, Y. Su, D. Wang, Q. Shen, *Cryst. Growth Des.*, **2011**, 11, 2084–2090.
8. A. M. Smith, S. Nie, *J. Am. Chem. Soc.*, **2011**, 133, 24-26.
9. K. Miszta, D. Dorfs, A. Genovese, M. R. Kim, L. Manna, *ACS Nano*, **2011**, 5, 7176–7183.
10. P. K. Jain, L. Amirav, S. Aloni, A. P. Alivisatos, *J. Am. Chem. Soc.*, **2010**, 132, 9997–9999.
11. K. Lambert, B. D. Geyter, I. Moreels, Z. Hens, *Chem. Mater.*, **2009**, 21, 778–780.
12. B. Mukherjee, A. Peterson, V. Subramanian, *Chem Commun.*, **2012**, 48, 2415–2417.
13. G. D. Moon, S. Ko, Y. Min, J. Zeng, Y. Xia, U. Jeong, *Nano Today*, **2011**, 6, 186–203.
14. G. D. Moon, S. Ko, Y. Min, J. Zeng, Y. Xia, U. Jeong, *ACS Nano*, **2010**, 4, 2307–2319.
15. D. O. Demchenko, R. D. Robinson, B. Sadtler, C. K. Erdonmez, A. P. Alivisatos, L. W. Wang, *ACS Nano*, **2008**, 2, 627–636.
16. S. E. Wark, C. H. Hsia, D. H. Son, *J. Am. Chem. Soc.*, **2008**, 130, 9550–9555.
17. L. Dloczik, R. Konenkamp, *Nano Lett.*, **2003**, 5, 651–653.
18. E. Thimsen, Q. Peng, A. B. F. Martinson, M. J. Pellin, J. W. Elam, *Chem. Mater.*, **2011**, 23, 4411–4413.
19. I. R. Pala, S. L. Brock, *ACS Appl. Mater. Interfaces*, **2012**, 4, 2160–2167.
20. J. Yu, J. Zhang, S. Liu, J. Phys. Chem. C, **2010**, 114, 13642–13649.
21. A. Jaiswal, P. Sanpui, A. Chattopadhyay, S. S. Ghosh, *Plasmonics*, **2011**, 6, 125–132.
22. A. Jaiswal, A. Chattopadhyay, S. S. Ghosh, *Mater. Lett.*, **2012**, 68, 261–264.

23. D. Denzler, M. Olschewski, K. Sattler, *J. Appl. Phys*., **1998**, 84, 2841–2845.
24. W. Wichiansee, M. N. Nordin, M. Green, R. J. Curry, *J. Mater. Chem.*, **2011**, 21, 7331–7336.
25. J. Yang, J. Y. Ying, *Chem. Commun.*, **2009**, 3187–3189.
26. H. Pan, X. Tao, C. Maoa, J-J. Zhua, F. Liang, *Talanta*, **2007**, 71, 276–281.
27. P. Peng, B. Sadtler, A. P. Alivisatos, R. J. Saykally, *J. Phys. Chem. C*, **2010**, 114, 5879–5885.
28. M. S. Leo´n-Vela´zquez, R. Irizarry, M. E. Castro-Rosario, J. Phys. Chem. C, **2010**, 114, 5839–5849.
29. I. Moreels, K. Lambert, D. Smeets, D. D. Muynck, T. Nollet, J. C. Martins, F. Vanhaecke, A. Vantomme, C. Delerue, G. Allan, Z. Hens, *ACS Nano*, **2009**, 10, 3023–3030.
30. Z. Khan, M. Khannam, N. Vinothkumar, M. De, M. Qureshi, *J. Mater. Chem*, **2012**, 22, 12090-12095.
31. Y. Y. Kim, D. Walsh, *Nanoscale*, **2010**, 2, 240–247.
32. K. A. Higginson, M. Kuno, J. Bonevich, S. B. Qadri, M. Yousuf, H. Mattoussi, *J. Phys. Chem. B*, **2002**, 106, 9982–9985.
33. G. Aragay, J. Pons, A. Merkoci, *Chem. Rev.*, **2011**, 111, 3433–3458.
34. H. Yi, L. Q. Wu, W. E. Bentley, R. Ghodssi, G. W. Rubloff, J. N. Culver, G. F. Payne, *Biomacromolecules*, **2005**, 6, 2881–2894.
35. P. Sanpui, A. Chattopadhyay, S. S. Ghosh, *ACS Appl. Mater. Interfaces*, **2011**, 3, 218–228.
36. S. Sharma, P. Sanpui, A. Chattopadhyay, S. S. Ghosh, *RSC Adv.*, **2012**, 2, 5837–5843.
37. W. S. W. Ngah, L.C. Teong, M. A. K. M. Hanafiah, *Carbohydr. Polym.*, **2011**, 83, 1446–1456.

Chapter 5

One Step Synthesis of Carbon dots by Microwave Mediated Caramelization of Poly(ethylene glycol)*

This chapter illustrates a rapid, simple and one step method for the synthesis of carbon dots using poly(ethylene glycol), both, as precursor and passivating agent. The C-dots possessed low cytotoxicity and were able to enter cells making them suitable candidate for bioimaging and biolabeling applications.

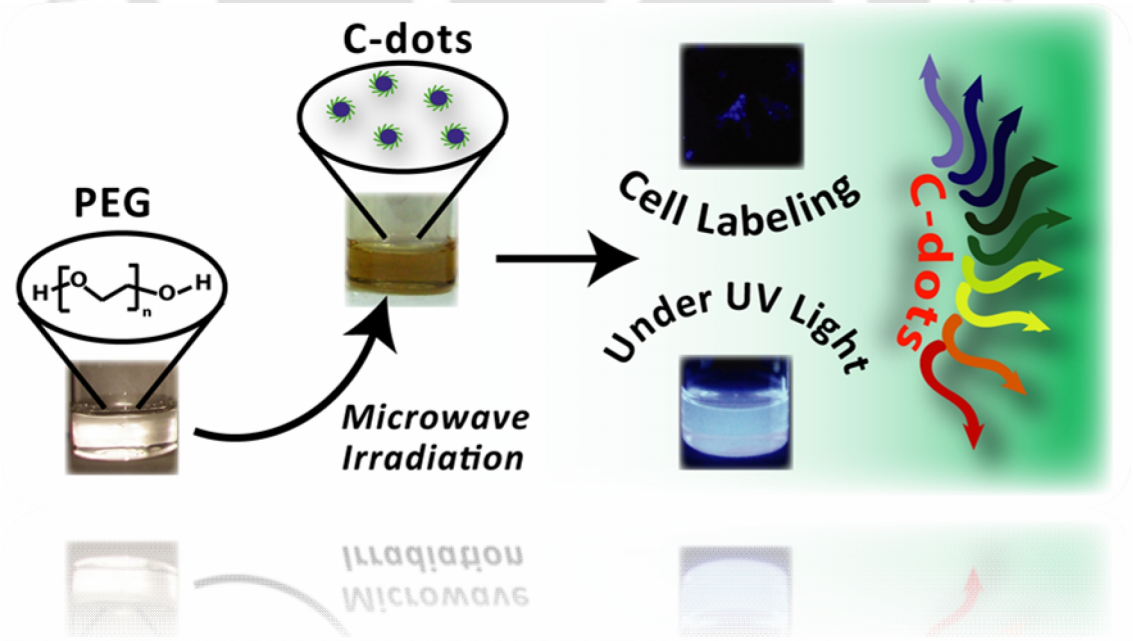

* Much of this work has appeared in print in *Chemical Communications*, 2012, 48, 407–409. It is reproduced with permission from The Royal Society of Chemistry, Copyright © 2012.

Chapter 5

One Step Synthesis of Carbon dots by Microwave Mediated Caramelization of Poly(ethylene glycol)

5.1. Introduction

Recently, carbon dots (C-dots) have emerged as a promising fluorophore owing to its extraordinary photoluminescent properties and biocompatibility.[1] In striking contrast to semiconductor quantum dots (Q-dots), which are generally made up of heavy metals and thus cytotoxic towards mammalian cells, C-dots have the advantage of chemical inertness and greatly reduced cytotoxicity.[1, 2] C-dots possess stable photoluminescence that is free from photobleaching and excitation dependent emission spectra, which make them the appropriate candidate for future 'nanolight' with potential applications in bioimaging, biolabeling and development of optoelectronic devices.[1] However, the phenomenon of C-dot associated photoluminescence is yet to be understood completely. Reports suggest that the reason behind the photoluminescence might be the presence of surface energy–trapping sites on the C-dots and their radiative recombination.[1, 3] The emission from C-dots is very low for unpassivated surface; but the passivation of the C-dots with polymers or other organic molecules can increase the quantum yield (QY) by several folds.[3]

In the last few years, the focus has been on the development of various methods for synthesizing these 'nanolights'. Top down approaches, involving chemical oxidation of arc-discharge [4] and candle soot[5] using nitric acid, laser ablation[3] and electrochemical oxidation of graphite,[2] are currently being used as state-of-the-art methods to synthesize C-dots. However, these processes involve complex and extreme synthesis conditions, are time and energy consuming, and need expensive starting materials or apparatus. On the other hand, in the bottom

up approach, microwave pyrolysis of different carbohydrates either in presence or in absence of any surface passivating agent and dehydration of carbohydrates with subsequent surface passivation have been reported to produce C-dots with sufficient QY.[6, 7] For example, Wang *et al.* have reported the synthesis of C-dots from glycerol, glycols and other saccharides, and showed that the presence of an inorganic ion was required to obtain C-dots with photoluminescence.[7] On the other hand, Zhu *et. al.* have demonstrated that irradiation of glucose in presence of PEG with microwave resulted in the formation of monodispersed C-dots.[6] Although the authors claimed that PEG acted only as the passivizing agent, it was not clear from their study whether the source of carbon in C-dots was glucose, PEG or both. Also, the toxicity of the C-dots synthesized in these studies was not tested against mammalian cells. Surprisingly, there are no reports, to the best of our knowledge, demonstrating a polymer to be used as a source of carbon for preparing C-dots in spite of the well–established biocompatibility of several polymers.

5.2. Outline of the Research Work

1) We report in this chapter a new one-step method of synthesis of carbon dots (C-dots) using poly (ethylene glycol), PEG as the source of carbon as well as the stabilizer (passivizing agent) of the C-dots.
2) This is for the first time that a polymer has been used as the source of carbon for the C-dots. In addition, the polymer is biocompatible and is popular for biomedical application. This would make the application appealing.
3) The method for the generation of C-dots is simple as it involves microwave heating of an aqueous solution of PEG for a few minutes.
4) The generated C-dots, with average sizes of 4.5 ± 0.9 nm, have been characterized by UV-visible and fluorescence spectroscopy, time-resolved fluorescence spectroscopy, transmission electron microscopy and X-ray diffraction. The properties of the C-dots were commensurate with those of small particles sizes.

5) Poly acrylamide gel electrophoresis results indicated possible separation of smaller particles with narrower size distribution (of sizes 1.4 ± 0.4 nm) from the rest.
6) The generated C-dots were found to be non-cytotoxic to mammalian cells thus making their applications appealing.
7) Further, the C-dots were found to be efficient in labeling mammalian cells.
8) Their high photostability and photoluminescence and (along with) non-cytotoxicity make them suitable candidates for applications in biodiagnostics and drug delivery (to act as a probe also).

5.3. Experimental Section

5.3.1. Synthesis of C-dots

PEG 200 (Merck, India Pvt. Ltd.) and ultrapure MilliQ water (>18 MΩ cm) were mixed in 3:1 ratio (*v/v*) in a glass vial yielding a transparent solution. The solution was then heated in 900 W domestic microwave oven (Onida) for varying time period, which resulted in the formation of C-dots, indicated by the development of golden yellow color.

5.3.2 Characterization of C-dots

Transmission electron microscopy (TEM) measurements were performed in JEOL 2100 UHR-TEM instrument at a maximum accelerating voltage of 200 kV. 5 μL of sample was drop-cast on carbon-coated copper grids and subsequently air-dried before TEM analysis. UV-Vis and fluorescence spectra were recorded with a Perkin Elmer Lambda 25 and a Perkin Elmer LS 55 instruments respectively. Time-resolved fluorescence intensity decay of the C-dots was recorded using a Life Spec II spectrofluorimeter (Edinburgh Instrument). The sample was excited by 375 nm laser, and the decay was measured in a time scale of 0. 024410 ns/channel. The decay curves were analyzed by FAST software, provided by Edinburgh Instrument along with the fluorescence instrument. The generated curve for intensity decay was fitted in the function given in equation 5.1

$$I(t) = \sum_i \alpha_i \exp(-t/\tau_i) \tag{5.1}$$

where, α_i is the initial intensity of the decay component i, having a life time of τ_i. The average lifetimes of C-dots were calculated using the following equation 5.2

$$< \tau >= \sum_i \frac{\alpha_i \tau_i^2}{\alpha_i \tau_i} \tag{5.2}$$

X-ray diffraction (XRD) patterns were recorded with a Brucker D8 Advanced X-ray diffraction measurement system, with Cu Kα source (λ =1.54 Å).

5.3.3. Electrophoretic separation of C-dots

The prepared C-dots were loaded to a 20 % poly(acrylamide) gel containing SDS as the denaturing agent and electrophoretic separation was carried out at 200 V at proper cooling conditions in a vertical gel electrophoresis unit (Hoefer®). After electrophoresis, the gel was visualized by illumination using a UV trans-illuminator (λ = 312 nm).

5.3.4. Cell Culture and viability assay

HT 29 cells (human colon adenocarcinoma) was procured from National Center for Cell Sciences (NCCS), Pune, India and were cultured in Dulbecco's modified Eagle's medium supplemented with penicillin (50 units mL^{-1}), streptomycin (50 mg mL^{-1}), and 10 % (*v/v*) fetal bovine serum. Cells were maintained in 5 % CO_2 humidified incubator at 37 ^oC.

For the cell viability assay, cells were seeded (10^4 cells/well) into a 96-well microplate and grown overnight. After treating with varying concentrations of the C-dots for 24 h, 2,3-Bis(2-methoxy-4-nitro-5-sulfophenyl)-2H-tetrazolium-5-carboxanilide (XTT) (Sigma-Aldrich, USA) based cell proliferation assay was carried out according to the manufacturer's protocol to determine the percentage

of viable cells based on the mitochondrial activity of the cells. The percentage cell viability of the nontreated cells (control) was taken as 100 %. All measurements were collected in triplicate and the values are expressed as mean ± standard deviation (SD).

For cellular labelling study, HT 29 cells were seeded in 35 mm cell culture plate and grown for 48 h. It was then incubated with the C-dots in DMEM medium for 24 h. Then, the medium was removed and the cells were washed with PBS for 3 times. Finally, 1 mL of PBS was added to the plate and the cells were observed under epifluorescence microscope (Nikon eclipse Ti).

5.3.5. Quantum Yield (Q.Y.) determination of C-dots

Quantum yield was measured according to established procedure[1] by using quinine sulfate in 0.10 M H_2SO_4 solution as the standard. The absorbance was measured on a Perkin Elmer LS 55 Spectrophotometer. Absolute values are calculated according to the following equation 5.3

$$Q = Q_R \frac{m}{m_R} \frac{n^2}{n_R^2} \quad (5.3)$$

where, Q is the quantum yield, m is the slope of the plot of integrated fluorescence intensity *vs* absorbance and n is the refractive index (taken here as 1.33, the refractive index of distilled water). The subscript R refers to the reference fluorophore, quinine sulphate solution. In order to minimize re-absorption effects, absorbance in the 10 mm quartz cuvette was kept below 0.15 at the excitation wavelength of 375 nm.

5.4. Results and Discussion

5.4.1. Synthesis and Characterization of C-dots

The synthesis of C-dots is based on a rapid one-step method through microwave–mediated caramelization of aqueous PEG 200 solution. Irradiation of the aqueous

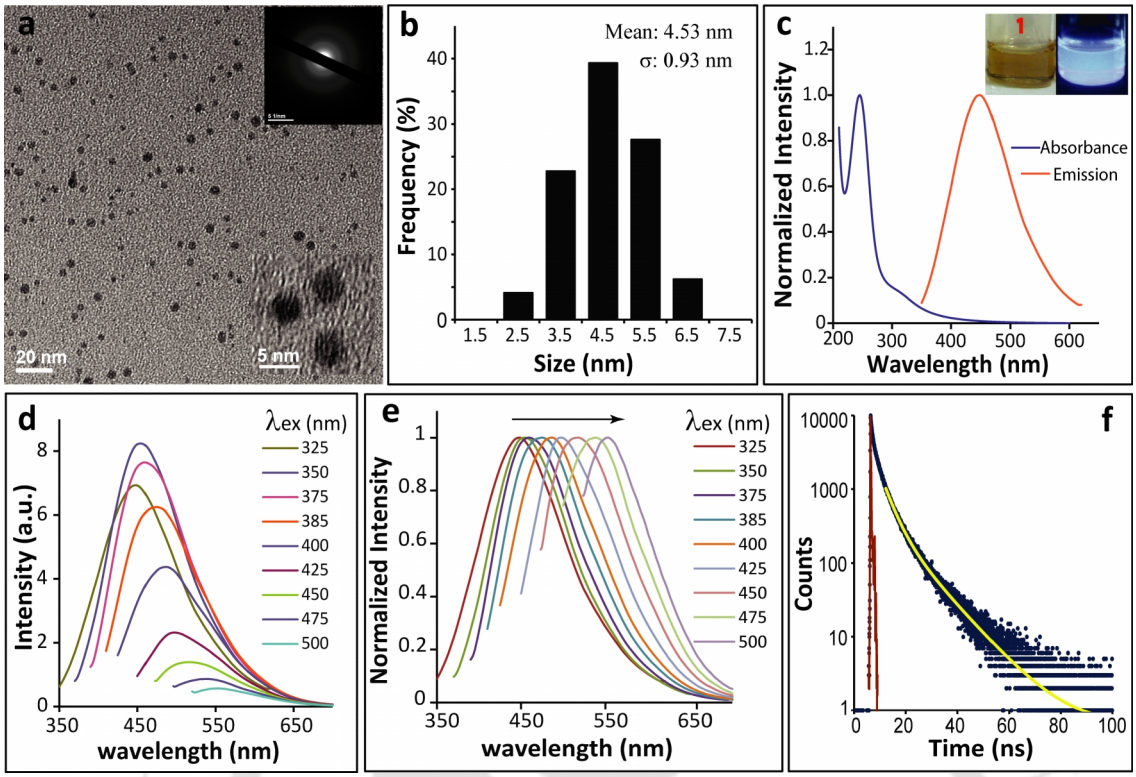

Figure5.1. (**a**) TEM image and (**b**) corresponding particle size distribution of as prepared C-dots. (**c**) Absorbance and emission spectra of the C-dots; (inset) appearance of C-dots in (1) white and (2) UV light. (**d** and **e**) Excitation dependent emission spectra and (**f**) Fluorescence decay profile (λ_{ex} = 375 nm and λ_{em} = 475 nm) of C-dots.

PEG solution by microwave in a 900 W domestic microwave oven for 10 min resulted in the formation of golden-yellow colored solution indicating the formation of C-dots. Transmission electron microscopic (TEM) images of C-dots (**Figure 5.1a**) demonstrated well dispersed and spherical NPs. However, the high resolution TEM (HRTEM) image of the C-dots did not reveal any clear lattice fringes, indicating amorphous nature of the C-dots. This was further supported by corresponding selected area electron diffraction (SAED) pattern (**Figure 5.1a,** *inset*). The average size of the C-dots was determined to be 4.5 ± 0.9 nm from the particle size distribution, as shown in **Figure 5.1b**. Experiments with higher than 600 Da molecular weight polymers did not yield any discernable C-dots.

Figure 5.1c presents the absorption and emission spectra of the as prepared C-dots. The absorption spectrum shows an edge at around 325 nm and a

Table 5.1. Fluorescence Life-time data obtained using the bi-exponential model for the C-dots

	Value	SD	χ^2
τ_1 (ns)	3.77×10^{-9}	5.73×10^{-11}	1.01
τ_2 (ns)	1.11×10^{-8}	1.22×10^{-10}	
α_1	713.2	8.09	
α_2	317.3	8.80	

sharp narrow peak at 245 nm which is ascribed to the π–π* transition of nanocarbon.[10] When these C-dots were excited at excitation edge of 325 nm, an emission peak at 445 nm was observed (**Figure 5.1c**). It should be mentioned here that the PEG solution itself is non-emissive in the visible region, confirming the bright fluorescence to be originating from the synthesized C-dots. Interestingly, with increase in the excitation wavelength from 350 nm to 500 nm, the emission from C-dots gradually shifted to higher wavelength accompanied with decreased fluorescence intensity (**Figures 5.1d and 5.1e**). This bathochromic shift of emission from C-dots has also been reported previously.[1, 3, 6-7] The exact mechanism behind the generation of fluorescence from C-dots is still an enigma. However, the quantum confinement of the passivized surface energy traps is thought to be responsible for the strong fluorescence exhibited by the C-dots.[3]

Figure 5.1f represents the fluorescence decay profile of C-dots which shows double exponential decay kinetics (**Table 5.1**). The average life time $<\tau>$ was calculated to be 7.94 ns, using equation 5.2, which corroborates with earlier reports.[1, 6] The short lifetime of the fluorescence of these C-dots is also indicative of the radiative recombination of the excitons giving rise to fluorescence.[6] The QY of the present C-dots, at an excitation wavelength of 375 nm, was determined to be 1.6 % using quinine sulphate (QY = 54 %) as standard (**Figure 5.2**). It is worth noting that, though QY of the present C-dots was lower than those prepared by pyrolysis of ethylene diamine-tetraacetic acid (EDTA) salts[10] and organo-silane functionalized C-dots,[12] however, it was significantly similar to those produced by nitric acid oxidation of soot [5] and microwave assisted synthesis methods.[6, 7]

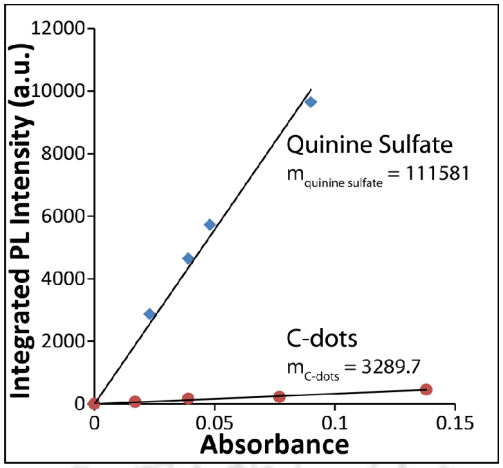

Figure 5.2. Integrated fuorescence intensity versus absorbance plot of C-dots and quinine sulphate.

Electron spin resonance (ESR) studies with the as-synthesized C-dots discounted the possibility of formation of radical species in the dots (**Figure 5A.1,** *Appendix*). The X–ray diffraction (XRD) pattern of C-dots showed a wide peak at 4.1 Å (**Figure 5.3a**) similar to that observed previously by Bourlinos *et al.*[12] **Figure 5.3b** shows the Raman spectrum of the C-dots showing an intense peak at ~1400 cm^{-1} and two shoulders. The spectrum was deconvoluted and it presented three different peaks at 1230, 1396 and 1515 cm^{-1} (**Figure 5.3c**). The peak at 1396 cm^{-1} corresponds to the D-band of carbon, while that at 1515 cm^{-1} to the G-band of graphitic carbon. The intense D-band indicated the presence of disordered carbon. A hump seen at ~1230 cm^{-1} could possibly due to hexagonal diamond or sp^3-rich phase.

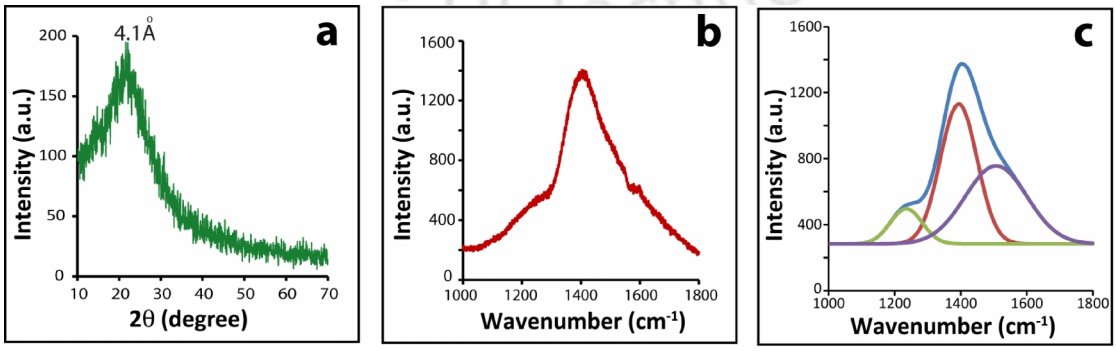

Figure 5.3. (**a**) XRD pattern of the synthesized C-dots, (**b**) Raman spectrum of the C-dots and (**c**) its deconvoluted spectra.

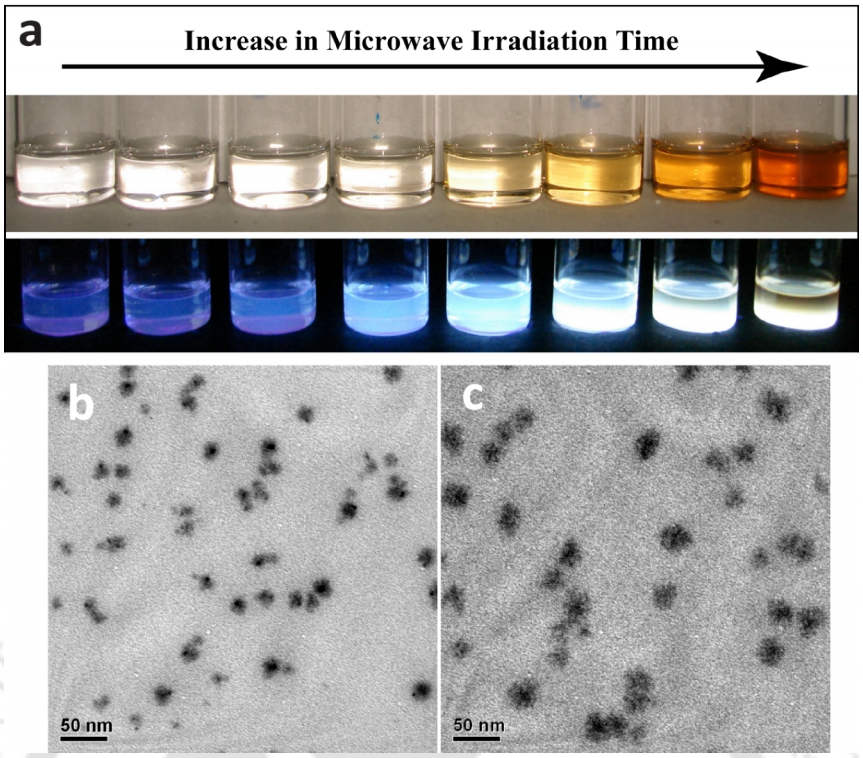

Figure 5.4. (**a**) Digital images showing the effect of microwave irradiation on aqueous PEG leading to the formation of C-dots. ***Top Panel:*** illuminated with white light, ***Bottom Panel:*** with UV light (302 nm). TEM images of C-dots formed after (**b**) 30 min and (**c**) 45 min of microwave irradiation.

The effect of microwave irradiation on the synthesis of C-dots was also studied. **Figure 5.4a** (*top panel*) shows the appearance of the aqueous PEG solution observed under white light after heating in a microwave oven at steps of 2 min. The caramel color started to develop only after 8 min of irradiation, and it was clearly visible in the sample irradiated for 10 min. Further heating of the sample led to dark brown coloration. The appearance of the same samples under UV light (**Figure 5.4a**, *bottom panel*) showed the bright blue emission starting from the sample heated for 6 min. In case of the sample heated for 14 min, emission was not prominent, which could either due to the increase in concentration of the dots or because of the formation of larger sized particles or agglomerates. The morphological analysis of the samples prepared after 30 min and 40 min interval, using TEM clearly showed the presence of larger sized and agglomerated particles (**Figure 5.4b**). Therefore, TEM results corroborated the formation of larger sized C-dots when the samples were subjected to longer microwave irradiation time.

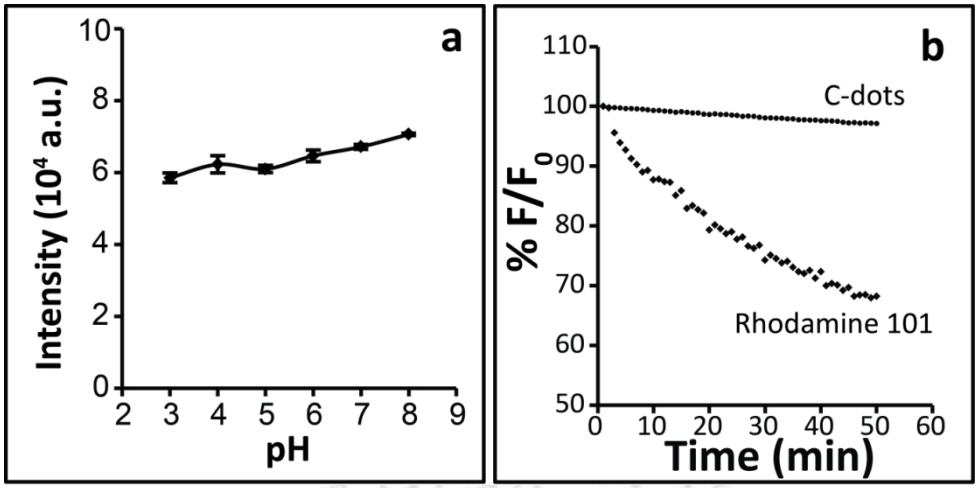

Figure 5.5. (**a**) Effect of pH on the fluorescence intensity of C-dots. All the values are average of three independent readings with ± standard deviation (SD) as error bars. (**b**) The effect of photoirradiation time on the fluorescence intensity of C-dots and the organic fluorophore Rhodamine 101.

The effect of pH on the fluorescence property of C-dots were also investigated (**Figure 5.5a**). The integrated fluorescence intensity did not change significantly in the pH range 3 – 8, indicating the potential application of the present C-dots in a wide range of pH. Further studies on the photostability (**Figure 5.5b**) revealed that the fluorescence of the present C-dots remained almost constant under continuous irradiation with a fluorescence–decrease (F/F_0) rate of only 0.06% per minute. In comparison, the fluorescence of one of the most commonly used organic fluorophore, rhodamine 101, decreased at a rate of 0.59% per minute with photoirradiation time. The excellent resistance to photobleaching exhibited by the present C-dots could lead to remarkable bio–labelling and bioimaging applications where the conventional organic fluorophores suffer from poor photostability.

5.4.2. Electrophoretic separation of C-dots

In an attempt to resolve the C-dots based on their size, denaturing poly(acrylamide) gel electrophoresis (PAGE) of as prepared C-dots was carried out. When the gel was viewed in white light, no band was observed (**Figure 5.6a**).

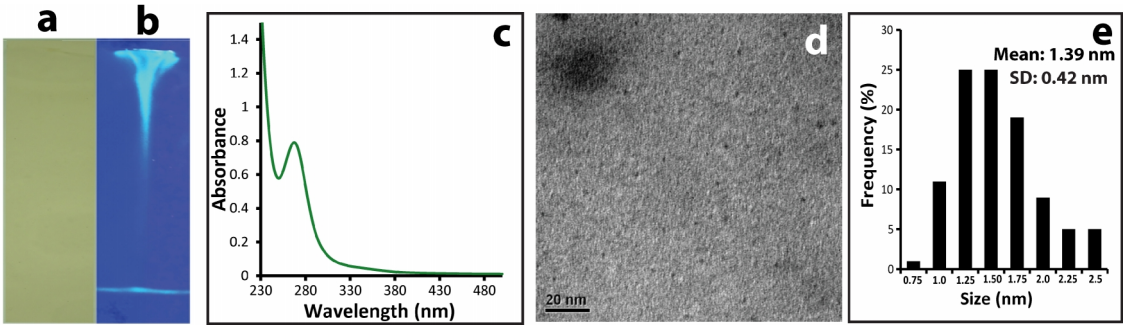

Figure 5.6. Separation of C-dots in poly(acrylamide) gel illuminated by (**a**) white and (**b**) UV light; (**c**) UV-vis spectra of the C-dots obtained from the excised fluorescent band of PAGE. (**d**) TEM image and (**e**) particle size distribution of the separated C-dots.

However, UV–illumination revealed the presence of a sharp well-separated blue fluorescent band and a smear below the well (**Figure 5.6b**). In order to examine the nature of the particles present in the band, the fluorescent band was carefully excised from the gel and eluted using MilliQ ultrapure water. Absorption spectroscopy of the eluate (**Figure 5.6c**) revealed similar feature as that of as–prepared C-dots sample at sub 300 nm, confirming the presence of C-dots in the band. TEM analysis (**Figure 5.6d**) demonstrated the presence of C-dots with average size of 1.4 ± 0.4 nm in the eluate. In other words, we were successful in separating smaller C-dots (~1.4 nm) from the as prepared sample by PAGE. The blue fluorescent smear below the well of the gel also indicated the presence of larger C-dots. The extent of smear appeared on gel increased with the microwave irradiation time, indicating the formation of larger particles.

5.4.3. Cell viability assay and cell labeling

In addition to the stable and tunable fluorescence, low cytotoxicity is an indispensable parameter for future applications of C-dots especially in live cell labeling. *In-vitro* toxicity of the C-dots prepared in the present study was examined by XTT based cell viability assay. It is important to mention here that the concentration of initial PEG solution used for preparing C-dots was considered as the concentration of C-dots as it was difficult to quantify the amount of C-dots present in as–prepared sample. Varying concentrations of C-dots were incubated

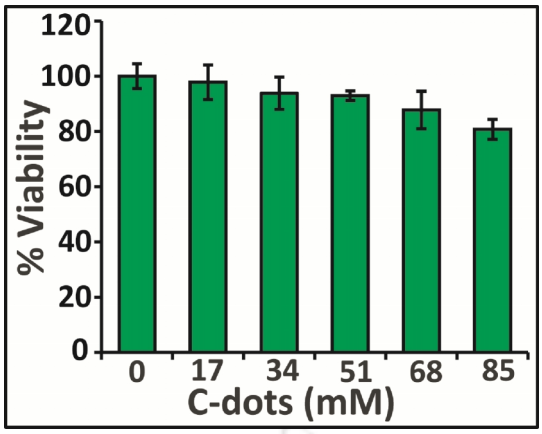

Figure 5.7. Viability (%) of HT 29 cells after 24-h treatment with C-dots as calculated from XTT assay.

with human colon adenocarcinoma HT 29 cells cultured in DMEM media in standard cell culture conditions. After 24 h of incubation, viability of the cells was determined and the results are shown in **Figure 5.7c**. More than 90 % cells were viable when incubated with 51 mM or lesser C-dots. Moreover, the cell viability was more than 80% even at C-dot concentration as high as 85 mM. The results clearly indicated low toxicity of the C-dots. The excellent biocompatibility demonstrated by the present C-dots could be attributed to PEG, the starting material for synthesizing C-dots, and the chemical inertness of C-dots which does not allow the release of any toxic species, unlike the conventional semiconductor Q-dots.[2]

The advantages of reduced cytotoxicity and enhanced photo-stability of the present C-dots can easily be exploited in successful imaging as well as labeling applications both *in-vitro* and *in-vivo*. As a 'proof–of–concept', we incubated HT 29 cells with as prepared C-dots for overnight and then, after repeated washing with phosphate buffer saline (PBS, pH 7.4), observed the cells under fluorescence microscope. HT 29 cells, incubated with C-dots, showed bright blue and green fluorescence under UV and blue light excitation (**Figure 5.8**, *top panel*) whereas no visible fluorescence was detected in 'control' cells (i.e. without C-dot incubation) (**Figure 5.8**, *bottom panel*). This clearly demonstrates the potential of the presently synthesized C-dots to label live cells.

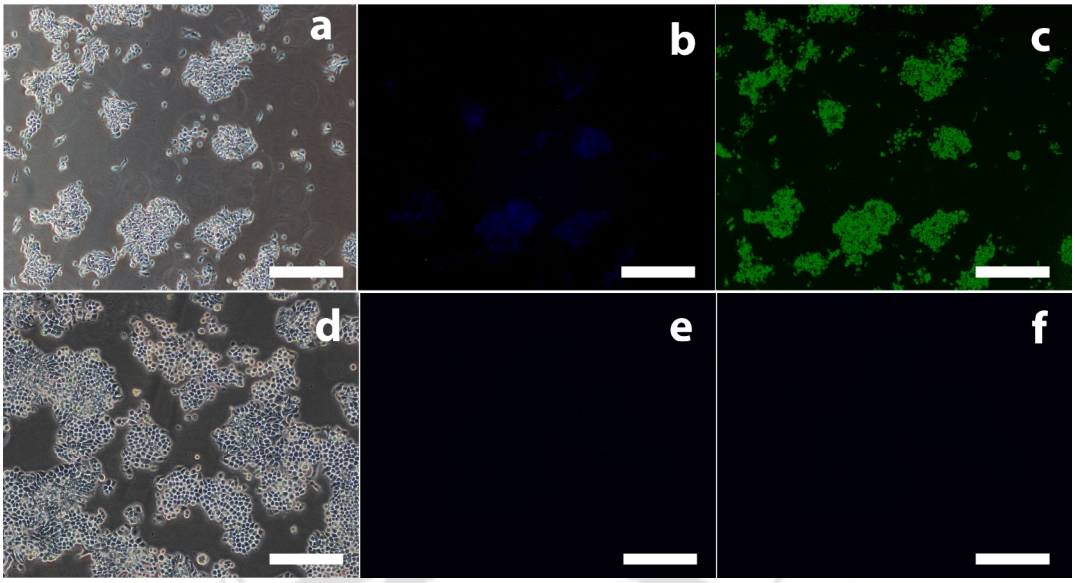

Figure 5.8. (**a**) Phase contrast and epifluorescence image of cell lines treated with C-dots under (**b**) UV excitation and (**c**) blue excitation. (**d**) Phase contrast and epifluorescence microscopic image of Untreated HT 29 cell under (**e**) UV excitation and (**f**) blue excitation respectively. Scale bar: 200 μm

5.5. Conclusion

In summary, we have developed a simple one step microwave mediated synthesis of C-dots using PEG, a biocompatible polymer, as a sole source of carbon and passivizing agent. The resulting C-dots were well–dispersed and showed excitation tunable luminescence, high photostability and suitability for their use in varying pH conditions. Low cytotoxicity of these C-dots and the ability of PEG to be conjugated with other biomolecules make the prepared C-dots a potential candidate for biological and biomedical applications.

5.6. References

1. S. N. Baker, G. A. Baker, *Angew. Chem. Int. Ed.*, **2010**, 49, 6726–6744.
2. Q. L. Zhao, Z. L. Zhang, B. H. Huang, J. Peng, M. Zhang, D. W. Pang, *Chem. Commun.*, **2008**, 5116–5118.
3. Y. P. Sun, B. Zhou, Y. Lin, W. Wang, K. A. S. Fernando, P. Pathak, M. J. Meziani, B. A. Harruff, X. Wang, H. Wang, P. G. Luo, H. Yang, M. E. Kose, B. Chen, L. M. Veca, S.Y. Xie, *J. Am. Chem. Soc.*, **2006**, 128, 7756–7757.
4. X. Xu, R. Ray, Y. Gu, H. J. Ploehn, L. Gearheart, K. Raker, W. A. Scrivens, *J. Am. Chem. Soc.*, **2004**, 126, 12736–12737.
5. H. Liu, T. Ye, C. Mao, *Angew. Chem. Int. Ed.*, **2007**, 46, 6473–6475.
6. H. Zhu, X. Wang, Y. Li, Z. Wang, F. Yanga, X. Yang, *Chem. Commun.*, **2009**, 5118–5120.
7. X. Wang, K. Qu, B. Xu, J. Ren, X. Qu, *J. Mater. Chem.*, **2011**, 21, 2445–2450.
8. F. M. Veronese, G. Pasut, *Drug. Discov. Today*, **2005**, 10, 1451–1458.
9. A. S. Karakoti, S. Das, S. Thevuthasan, S. Seal, *Angew. Chem. Int. Ed.*, **2011**, 50, 1980–1994.
10. D. Pan, J. Zhang, Z. Li, C. Wu, X. Yana, M. Wu, Chem. Commun., **2010**, 46, 3681–3683.
11. A. B. Bourlinos, A. Stassinopoulos, D. Anglos, R. Zboril, M. Karakassides, E. P. Giannelis, *Small*, **2008**, 4, 455–458.
12. F. Wang, Z. Xie, H. Zhang, C. Y. Liu, Y. G. Zhang, *Adv. Funct. Mater.*, **2011**, 21, 1027–1031.
13. H. Peng, J. Travas–Sejdic, *Chem. Mater.*, **2009**, 21, 5563–5565.

Chapter 6

Synthesizing Gold Nanoparticles using Carbon dots*

This chapter presents a simple, room temperature based method for the synthesis of gold nanoparticles, employing C-dots as catalyst. The influence of varying concentration of the Au precursor and C-dots was studied which demonstrated the formation of Au NPs of different sizes and morphologies.

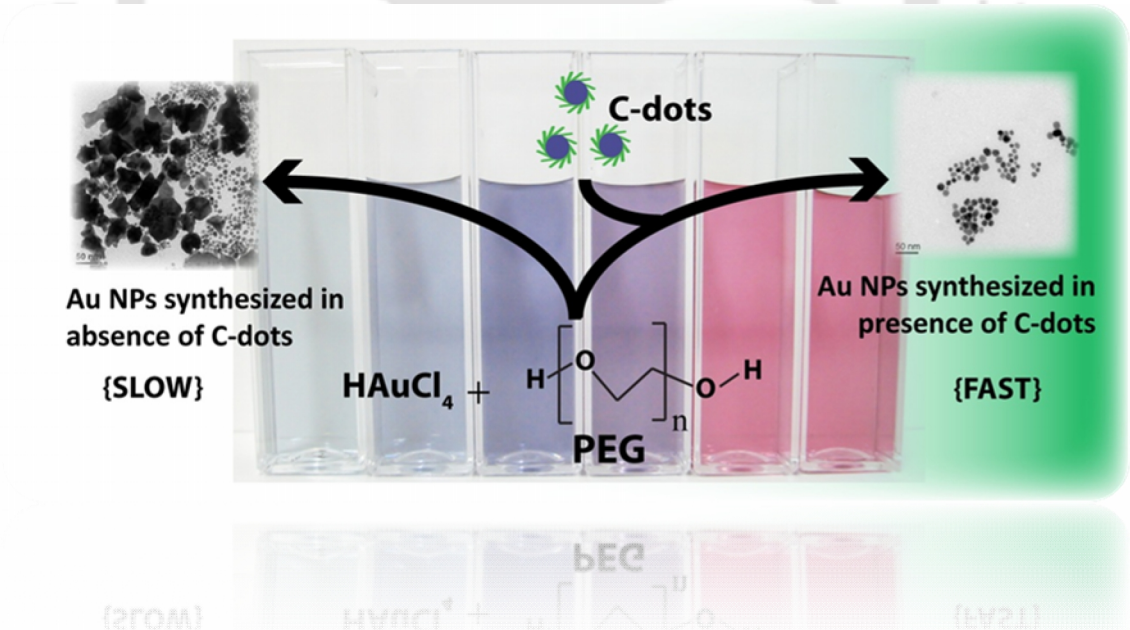

* To be communicated

Chapter 6

Synthesizing Gold Nanoparticles using Carbon dots

6.1. Introduction

Since the serendipitous discovery of carbon dots (C-dots) by Screivens *et al.* while electrophoresing the sample of SWCNT,[1] enormous research has been carried out on the synthesis and isolation of these amazing nanodots.[2-3] C-dots have the fascinating properties of excitation tunable emission, excellent water solubility, are non-cytotoxic and photostable and the surface functionalities offer ease of bioconjugation which make them a suitable candidate for biological applications.[2-5] From the time of its discovery, several applications of these nanodots have appeared. C-dots have been employed for bioimaging,[2-6] gene delivery,[7] in optoelectronic devices,[8-10] in sensing and analytical applications,[11-15] and in photocatalysis.[3, 16-17] Though the semiconductor quantum dots (Q-dots) have superior optoelectronic properties, but its toxicity due to the presence of heavy metal ions[18-21] and the involvement of extreme reaction conditions[22-24] impedes its applicability. In this regard, the benign nature of the C-dots and simple and inexpensive method of synthesis proffer them a protagonist role in various applications.[2-3]

Recently, Kang *et al.* reported the photocatalytic applications of the C-dots in conjunction with semiconductor materials.[3] They designed TiO_2/C-dots and SiO_2/C-dots photocatalytic system and harnessed the entire visible spectrum of the sunlight for degrading organic dyes.[25] They demonstrated that electrons can shuttle along the C-dots which accounts for the efficient photocatalysis. On similar line, they demonstrated the superior photocatalytic activity of an array of C-dots based composite such as C-dots/ZnO, C-dots/Fe_2O_3, C-dots/Ag_3PO_4, C-dots/Ag/Ag_3PO_4 etc.[26-28] Mitra *et al.* and Qin *et al.* demonstrated the use of C-dots

for the reduction of metal ions to form metal nanoparticles (NPs).[29-30] Mitra *et al.* showed that matrix of C-dots can reduce $AuCl_4^-$ to Au NPs in presence of PEG, only after irradiating the reaction mix with microwave. The produced Au NPs were polydisperse with 20–40 nm in size. Report by Qin *et al.* illustrated that irradiating an ethanolic mixture of Au precursor and carbon nitride dots with a high pressure mercury vapor lamp (λ = 254 nm) for 1 h, results in the formation of Au NPs. In the methodology demonstrated by both the groups, irradiation of the metal precursor was a requisite for the formation of Au NPs.

The development of newer methods for the synthesis of Au NPs has been one of the fascinating areas of research in the field of nanotechnology.[31-34] The reason behind this trend is its biocompatibility, easy surface modification, and most importantly its unique size and shape tunable LSPR spectra.[31-34] Au NPs represent an ideal class of nanomaterial used for chemical and biological sensing with tremendous applications in nanomedicine.[35-39] Au NPs can readily adsorb and cause agglomeration of proteins which can be used as delivery vehicle.[40-42] Immuno-Au NPs prepared from conjugating antibodies to the Au NP surface can be used as a probe for antigens on cell surface and could also be used for the selective delivery of therapeutic agents.[43-44]

6.2. Outline of the Research Work

1) We report the room temperature synthesis of Au NPs using C-dots as catalyst in poly(ethylene glycol) (PEG).
2) The synthesis methodology does not require any irradiation of the reaction mixture for the reduction of the metal precursor and it yields smaller sized particles of ~ 15 nm, mostly octahedron in shape.
3) The effect of varying concentration of the Au precursor and C-dots on the synthesis methodology was studied which demonstrated the variation in particle size and shape with change in either of the precursor or catalyst concentration.
4) Time resolved absorbance study for the synthesis of Au NPs showed the sigmoidal behavior for the autocatalytic growth having the lagging phase of induction period.

5) The stability of the prepared Au NPs were also determined which showed that at optimum concentration of the precursor and C-dots, the particles were stable and did not settle down for several days.

6.3. Experimental Section

6.3.1. Materials

Poly(ethylene glycol) 200 was purchased from Merck India Pvt. Ltd. $HAuCl_4$ were purchased from Sigma Aldrich USA. All chemicals employed were of AR grade and were used as received without further purification. Milli Q ultra-pure water (>18 MΩ cm) Millipore were used in all experiments.

6.3.2. Instruments

UV-Vis spectra were recorded with Perkin Elmer Lambda 25 instrument. Transmission Electron Microscopy was performed in JEOL 2100 UHR-TEM instrument. 5 µL of sample was drop-cast on carbon-coated copper grids and subsequently air-dried before TEM analysis. Agarose gel electrophoresis was carried out in Bangalore Genei horizontal electrophoretic system. XRD analysis was done employing Brucker D8 Advanced X-ray diffraction measurement system, with Cu Kα source (λ = 1.54 Å).

6.3.3. Synthesis of Carbon dots

C-dots were prepared using method reported in chapter 5. Briefly, 3:1 ratio of PEG:water was taken in a 15 mL glass vial and it was heated in a domestic microwave for 10 min. This resulted in the appearance of golden yellow color solution, in otherwise colorless solution, indicating the formation of C-dots. The C-dots were purified by dialysing the as prepared solution using a 1 KDa dialysis membrane, against Milli Q water for 48 h. The dialysed sample was then dried in an oven at 50 °C and was weighed to determine the concentration of C-dots. This was used as a reference sample to plot the standard curve in order to determine the concentration of the C-dots in the as prepared sample using absorbance spectroscopy.

6.3.4. Synthesis of Au NPs

2 mL of the as prepared sample (9.28 mg mL^{-1} C-dots) were taken in a 15 mL glass vial and to it 50 μL of $HAuCl_4$ solution (125 μM) was added and mixed well. Immediately the volume was made up to 4 mL using ultrapure Milli Q water and was kept for stirring in dark at room temperature. After few minutes, the color of the solution turned wine red indicating the formation of Au NPs. To study the effect of varying concentration of the gold precursor solution, the desired amount of the $HAuCl_4$ solution was added and the volume was made up to 4 mL and identical methodology, as used for the 50 μL sample was followed for the synthesis of Au NPs. The synthesized Au NPs were characterized using absorbance spectroscopy and Transmission Electron Microscopy (TEM).

6.3.5. Effect of varying concentration of C-dots

In order to study the effect of using varying concentration of C-dots on Au NP synthesis, different amount of C-dots were taken in a glass vial and the volume was made to 2 mL using PEG 200. To this 50 μL of the $HAuCl_4$ solution (125 μM) was added, followed with a volume make up till 4 mL and stirring in dark condition. The synthesized Au NPs were analyzed using UV-visible spectroscopy and TEM study.

6.3.6. Agarose gel Electrophoresis

Agarose gel electrophoresis was carried out to demonstrate the size variation of Au NPs resulting from the synthesis procedure involving varying concentration of the Au precursor. 0.5 % agarose gel was prepared by dissolving agarose powder in 1 × Tris Borate EDTA (TBE) buffer and melting agarose powder in microwave leading to the formation of clear solution. The solution was then poured into the gel casting tray and comb was placed at the middle of the gel and left at room temperature until the gel was formed. The casted gel was then place in the gel tank containing 1 × TBE buffer. Samples were loaded into the gel wells and were allowed to run at 5 Vcm^{-1} for 45 min. Gel pictographs were taken using a digital camera.

6.4. Results and Discussion

6.4.1. Synthesis and characterization of Au NPs using C-dots

Figure 6.1 a and **b** shows the TEM image of the Au NPs synthesized using 125 μM of gold precursor and 2 mL of as prepared C-dots having concentration of 9.28 mg mL^{-1} in PEG. It can be seen from the electron micrographs that majority of the particles were of octahedron shape. The selected area electron diffraction pattern (**Figure 6.1c**) revealed the crystallinity of the synthesized Au NPs which were indexed to the various lattice planes of the Au crystal. The high resolution TEM (HRTEM) of the Au NP (**Figure 6.1d**) and its corresponding Inverse Fast Fourier Transform (IFFT) image (**Figure 6.1e**) exposed the clear lattice fringes of 0.23 nm matching well with the expected d-spacing of the {111} plane of bulk gold crystal.[45-46] The particle size distribution, obtained from the TEM images of the Au NPs is shown in **Figure 6.1f,** form which the average size was calculated to be 15 ± 3.3 nm.

Figure 6.2 shows the XRD pattern of the synthesized Au NPs showing peaks at 38.3°, 44.1° and 64.7° corresponding to the {111}, {200} and {220} planes of the pure crystalline face-centered cubic (fcc) Au.[34, 47] The intensity ratio of the diffraction peaks of {200} and {111} planes was calculated to be 0.21, which was lower than the bulk value of 0.53.[47] The lower value of the ratio suggested the abundance of the {111} planes in the Au nanoparticles.

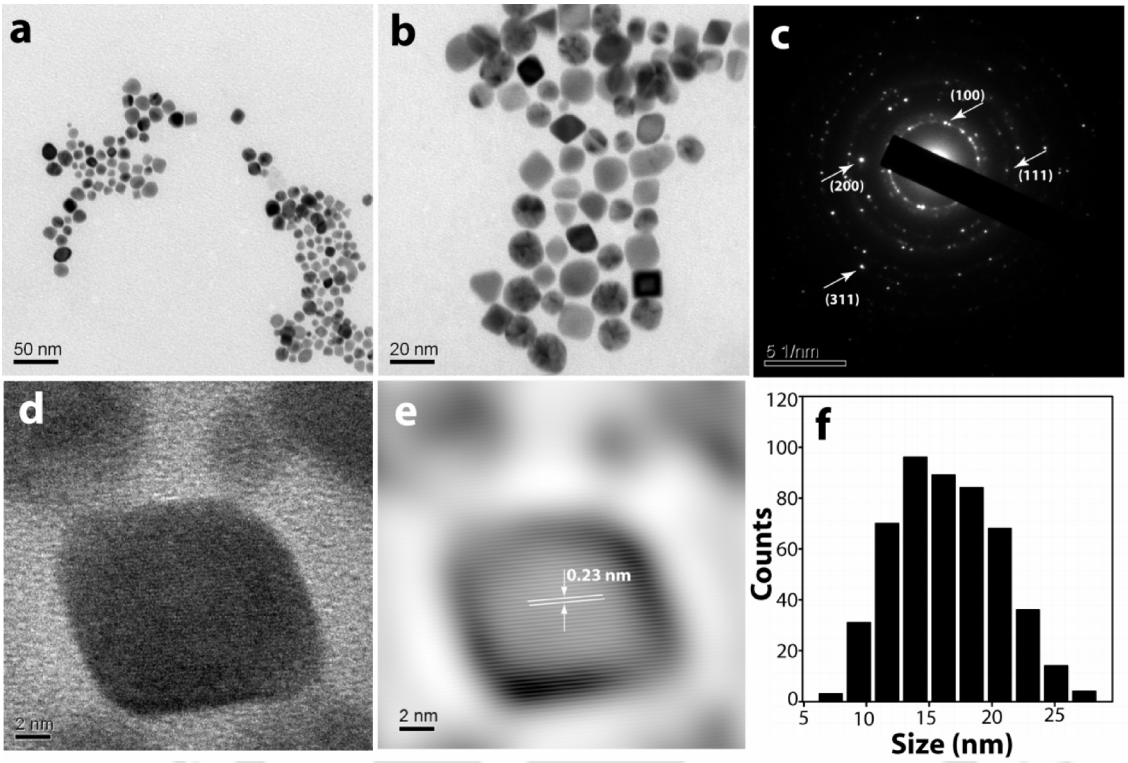

Figure 6.1. (**a-b**) TEM images of Au NPs synthesized using 125 μM of Au precursor, (**c**) corresponding SAED pattern of the Au NPs. (**d**) HRTEM and (**e**) corresponding IFFT image of Au NPs. (**f**) Particle sized distribution of the prepared Au NPs.

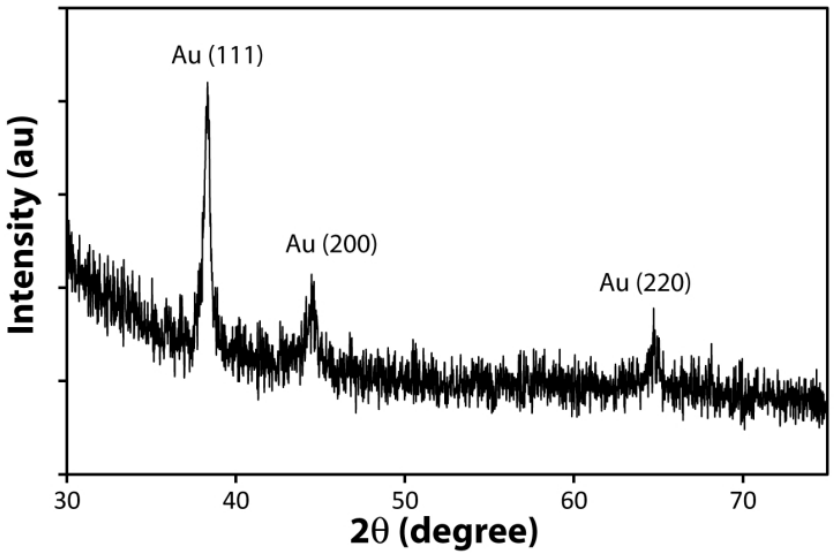

Figure 6.2. XRD pattern of the synthesized Au NPs.

6.4.2. Effect of varying concentration of Au precursor on Au NP synthesis

The effect of varying concentration of the gold precursor on the synthesis of the Au NPs was also studied. **Figure 6.3a** shows the UV visible spectra of the Au NPs synthesized at different [$HAuCl_4$] concentrations. At 125 μM concentration of the Au precursor, the localized surface plasmon resonance (LSPR) peak was observed at 545.2 ± 4.4 nm. The peak was observed at higher wavelength than that reported for spherical Au NPs of the corresponding sizes.[48] The rationale behind the shift could be attributed to the presence of octahedral Au NPs.[34] It is well established that the LSPR peak position and surface polarization of charges for simple geometrical shapes in case of metallic nanoparticles depends both on shape symmetry and corner sharpness. In case of octahedron particles, the surface charge tends to accumulate at the sharp corners leading to enhanced charge separation arising from the polarization of electron density relative to the lattice of positive ions. This enhanced charge separation reduces the restoring force for electron oscillation causing the resonance to occur at lower frequency, which manifests as a bathochromic shift in the extinction spectra of the particle.[34] Additionally, the presence of PEG, which slightly increases the refractive index of the medium could also be a reason behind the shift of the LSPR peak.[49] The extinction spectra of the Au NPs at varying concentrations 62.5, 250, 375, 500, 625 and 700 μM shows shift in the LSPR peak position. For 62.5–375 μM concentration of the Au precursor, the peak was narrow and the intensity increased in the order, whereas, for 500–700 μM of Au Precursor the LSPR peak was broader and the peak intensity was also reduced. **Figure 6.3b** shows the variation in the LSPR peak for different concentration of the Au precursor. It is clear from **Figure 6.3b** that the LSPR peak shift was minimal till 250 μM of the precursor concentration, whereas, there was a dramatic increase in the LSPR peak wavelength for 375–700 μM concentration of Au precursor. The LSPR peak position for different samples at varying concentration of Au precursor is shown in **Table 6.1**.

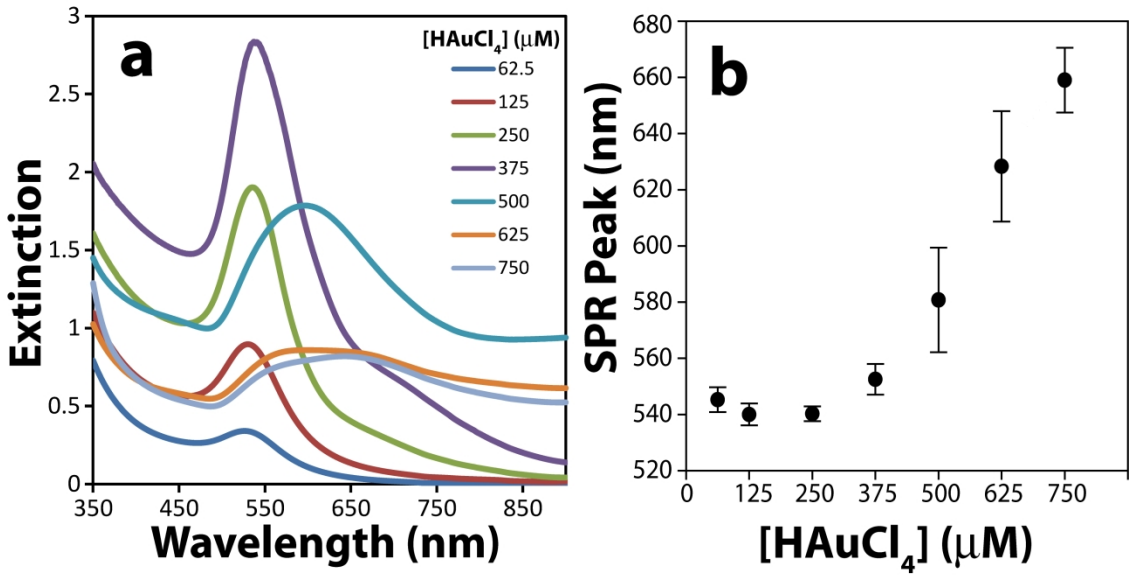

Figure 6.3. (**a**) Extinction spectra of the synthesized Au NPs using different concentration of the Au precursor. (**b**) The LSPR peak wavelength from figure 6.3a plotted as a function of the Au precursor concentration.

Table 6.1. Concentration of Au precursor used for different samples, the precursor:C-dots ratio, the corresponding mean size of the synthesized particles with its LSPR peak wavelength and the induction time required for the evolution of the LSPR peak.

Sample	$[HAuCl_4]$ (μM)	[C-dots] (mg mL^{-1})	[C-dots] / $[HAuCl_4]$ (mg mL^{-1} μM^{-1})	LSPR Peak (nm)	Size (nm)	~Induction Time (min)
1	62.5	9.28	0.158	545.2 ± 4.4	14 ± 2.3	1.7
2	125	9.28	0.074	540.0 ± 3.9	15 ± 3.3	1.8
3	250	9.28	0.037	540.2 ± 2.6	28 ± 6.0	3
4	375	9.28	0.025	552.5 ± 5.4	41.5 ± 11	5.5
5	500	9.28	0.018	580.7 ± 18.6	74 ± 15	10.5
6	625	9.28	0.015	628.3 ± 19.6	–	–
7	700	9.28	0.013	659 ± 11.5	–	–

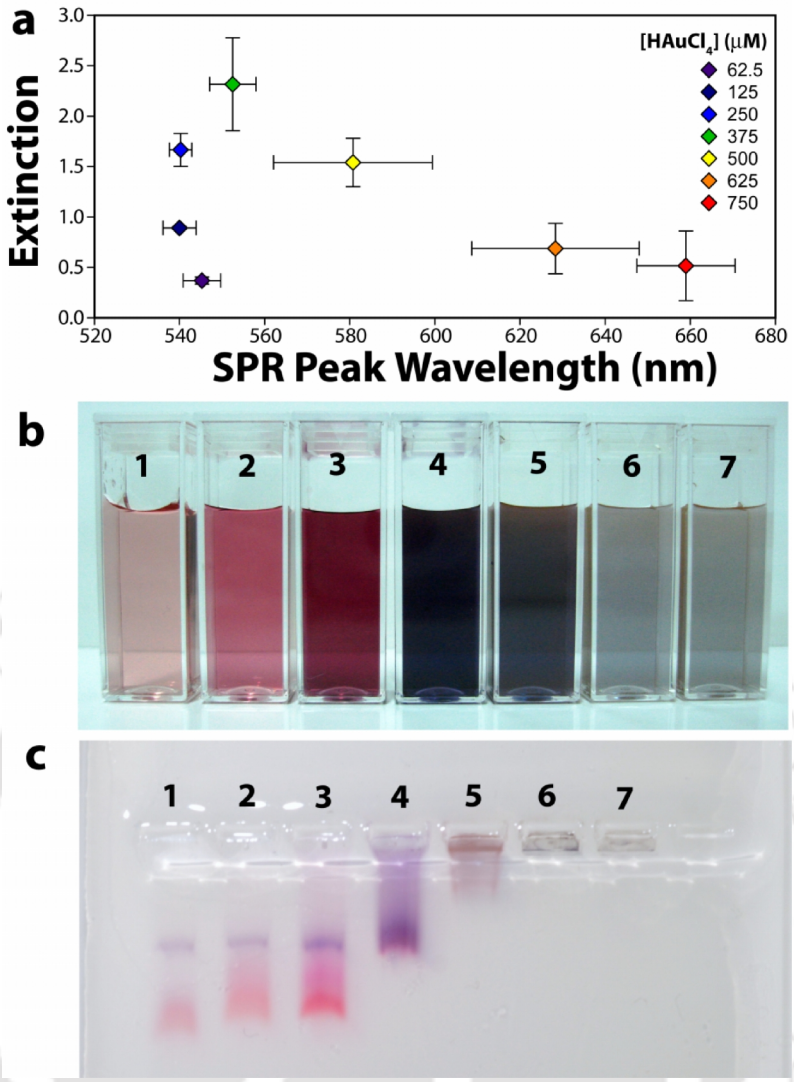

Figure 6.4. (**a**) Scatter plot of the LSPR peak and the extinction as a function of the Au precursor concentration. (**b**) Digital images of the Au NP colloidal solutions prepared with different Au precursor concentrations. (**c**) Digital image of the agarose gel after the Au NPs from the different samples were electrophoresed.

Figure 6.4a shows the scatter plot for LSPR peak position and the intensity of extinction for the different concentration of Au precursor used in the present case. It shows clear spread of the variation in the LSPR peak with change in the precursor concentration. Till 250 μM precursor concentration, the LSPR peak positions were clustered in a narrow region with systematic increase in the amount of extinction for increasing Au precursor concentration. For 375 μM concentration there was substantial peak shift but the increase in the extinction was not in proportion as in case for the lower concentrations. The reason behind

this could be attributed to the increase in the particle size instead of the proportionate increase in the concentration of the particle. On similar lines, for the 500–700 μM concentrations, there was decrease in extinction accompanied by peak broadening and substantial shift in the LSPR peak position. **Figure 6.4b** shows the appearance of the Au NP colloidal solution under visible light. Samples 1–3 evidently displayed the characteristic wine red color of the smaller Au NP colloids. Samples 4 and 5 showed dark purple and brown coloration demonstrating the formation of larger particles and possibly of different morphologies. On the other hand, the samples 6 and 7 showed faint grey coloration indicting the formation of larger sized particles and aggregates of Au NPs. To resolve the particles based on the sizes, all the seven samples were electrophoresed in a 0.5 % agarose gel (**Figure 6.4c**). On the application of electric field, samples 1–3 migrated the maximum distances in contrast to samples 4 and 5 manifesting the presence of comparatively smaller sized particles. Faint band observed lagging behind in the lanes 1–3 could be due to the presence of few larger particles. Samples 6 and 7 did not show any visible band in the corresponding lanes; however, particles were seen to be stuck in the wells and possibly could not migrate from the wells due to larger sizes.

The TEM images, SAED pattern and the particle size distribution of the Au NPs synthesized using varying concentration of Au Precursor is shown in **Figure 6.5** and **Figure 6.6**. For the 62.5 and 250 μM concentration of the precursor, the particles were mostly octahedron with few triangular plates in case of the later. The average size of the particles calculated from the particle size distribution obtained from the transmission electron micrographs were 14 ± 2.3 and 28 ± 6 nm. However, in case of 375 and 500 μM concentration of the precursor molecule, TEM images showed the presence of decahedron particles along with triangular plates and with few octahedron particles. The average sizes of the particles were calculated to be 41.5 ± 11 nm and 74 ± 15 nm respectively. The reason behind the formation of polyhedral particles with plates could be attributed to the lesser amount of C-dots available for the increased concentration of the Au precursor. This decrease in the ratio of C-dots to the Au precursor (**Table 6.1**) could drop the

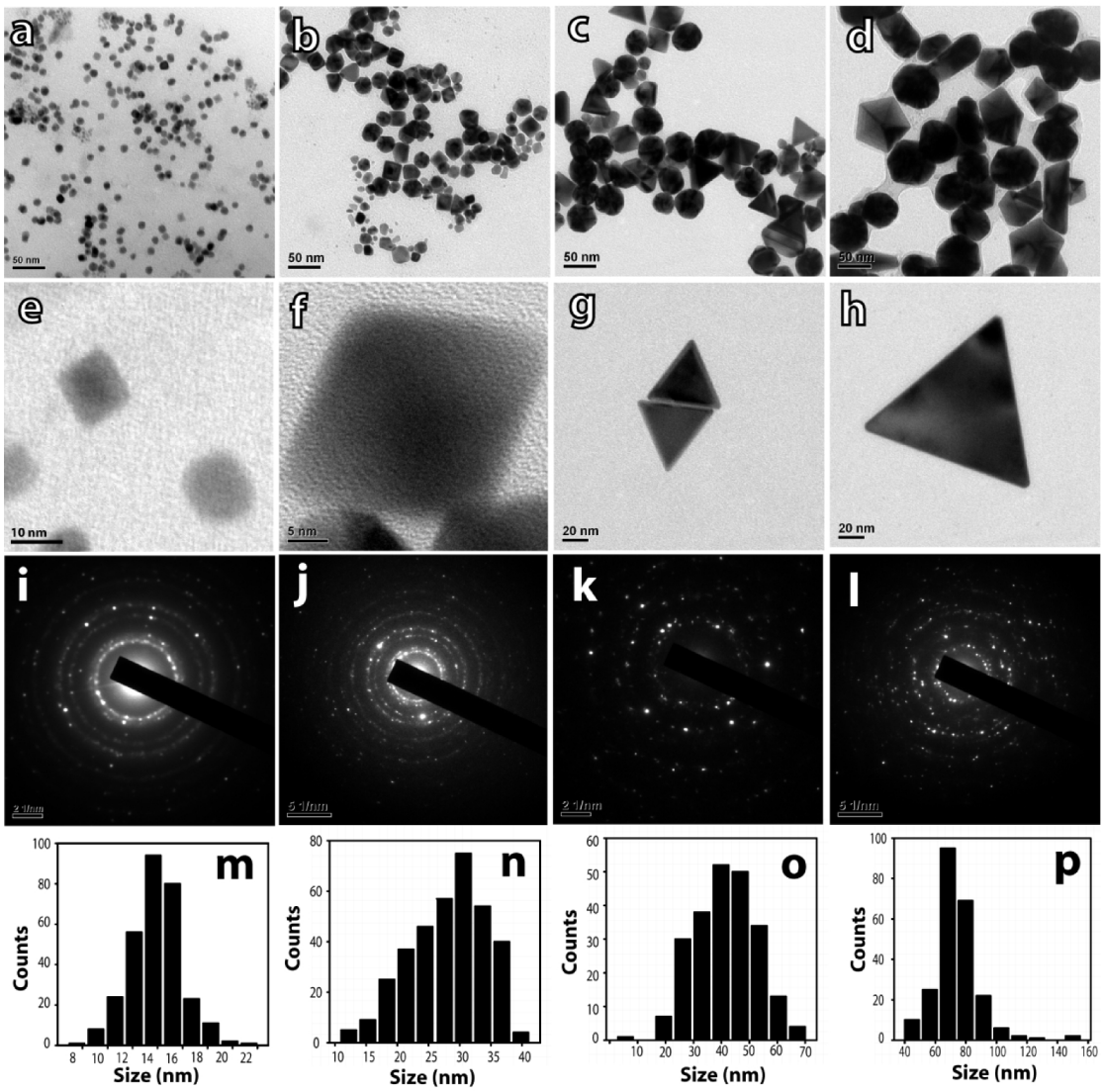

Figure 6.5. (**a-d**) TEM images (low magnification), (**e-h**) magnified TEM images, (**i-l**) SAED pattern and (**m-p**) the particle sized distribution of the Au NPs synthesized using 62.5, 250, 375 and 500 μM Au precursor respectively.

rate of reduction, which may result in the formation of multiply twined nuclei or nucleus with stacking faults, leading to the formation of decahedron particles and triangular plates.[34] For further increased concentration of the Au precursor, larger clumps of particles with no proper geometry were observed (**Figure 6.6**). The SAED pattern of all the Au NP synthesized at varying concentration of the precursor molecule showed the crystalline nature of the particles (**Figure 6.5 i–l** and **Figure 6.6 c–d**).

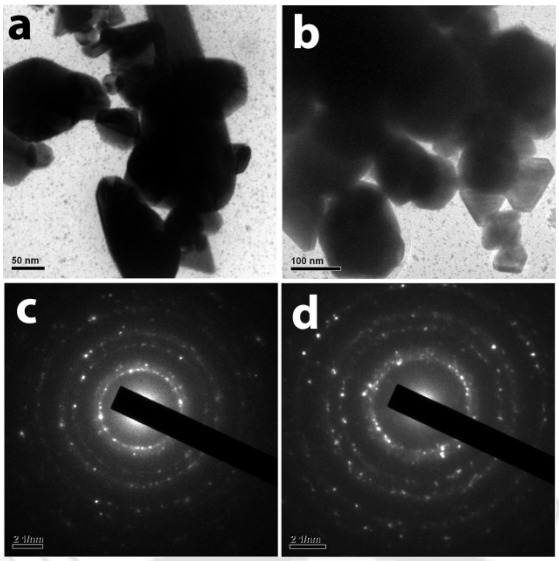

Figure 6.6. (**a-b**) TEM image and (**c-d**) SAED pattern of the Au NPs synthesized with 625 and 750 μM Au precursor concentration.

6.4.3. Time resolved study of the formation of Au NPs

The formation of Au NPs for different concentration of the Au precursor was monitored using absorption spectroscopy. **Figure 6.7** shows the time dependent extinction spectra for the formation of Au NPs, recorded at an interval of 3 min for a total period of 90 min for each of the samples. As can be seen from **Figure 6.7a**, the LSPR peak corresponding to the formation of Au NPs using 62.5 μM Au precursor, appeared at 6 min, which increased sharply at the next 3 min interval and attained saturation within the time span of 90 min. In case of the precursor concentration of 125 μM, a minor but distinct feature of the LSPR peak of the Au NPs was observed in the 6 min time span. The LSPR peak substantially increased at the 9 min interval and it gradually kept increasing for few cycles demonstrating the increase in the concentration of the particles and finally saturated within 90 min. It is to be noted here that the LSPR signature peaks of the Au NPs in case of 250, 375 and 500 μM concentration of Au precursor, appeared only at 9, 12 and 15 min. The reason behind the delay in the appearance of the LSPR peak could be attributed to the decrease in the C-dots to [$HAuCl_4$] concentration ratio which leads to increase in the induction time for the formation of gold nuclei.

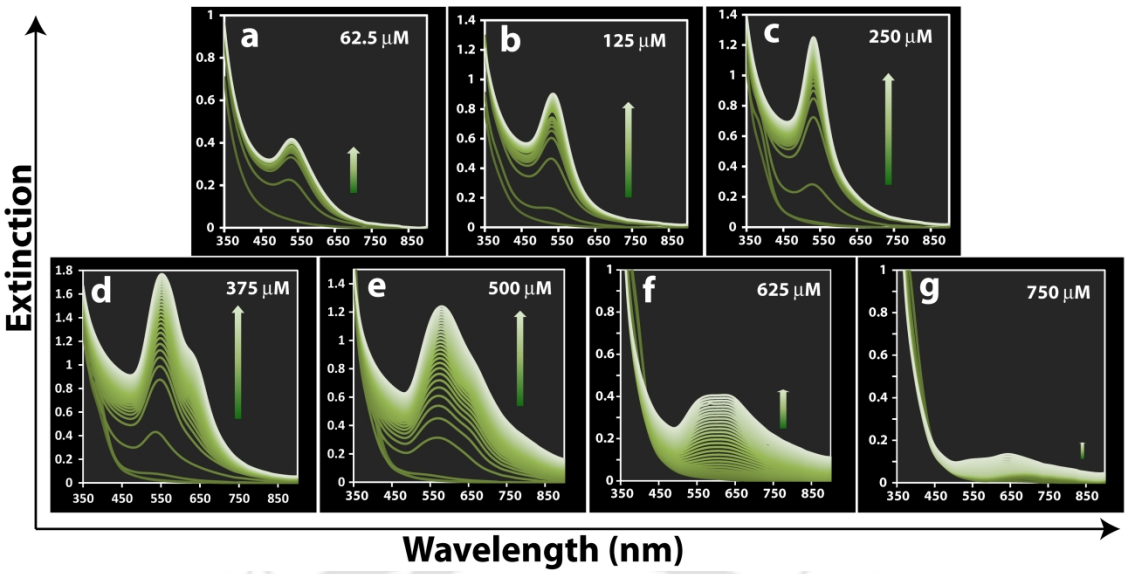

Figure 6.7. Evolution of extinction spectra during the synthesis reaction at varying concentration of the Au precursor as mentioned in the figure.

It is worth noting that the LSPR peak positions for 375 and 500 μM precursor concentration were shifted to higher wavelength compare to that for lower precursor concentration, demonstrating the formation of larger particles. The growth of particles with time can easily be identified by the shift in the peak position with respect to time for samples 3, 4 and 5 (**Figure 6.7c–e**). Samples 6 and 7 corresponding to the Au precursor concentration of 625 and 700 μM showed the appearance of broad peak, only after several minutes of induction time demonstrating the formation of large sized particles without any typical geometry.

Additionally, we have also monitored the temporal evolution of the plasmon band for different concentration of the Au precursor by recording the change in the extinction at a fixed wavelength of 535 nm at every 3 s interval (**Figure 6.8**). It is noteworthy that the change in the absorbance with time cannot be directly correlated with the amount of NPs formed, as during the formation of Au NPs, the size of particles changes and causes variation in the extinction coefficient of the particles.[50]

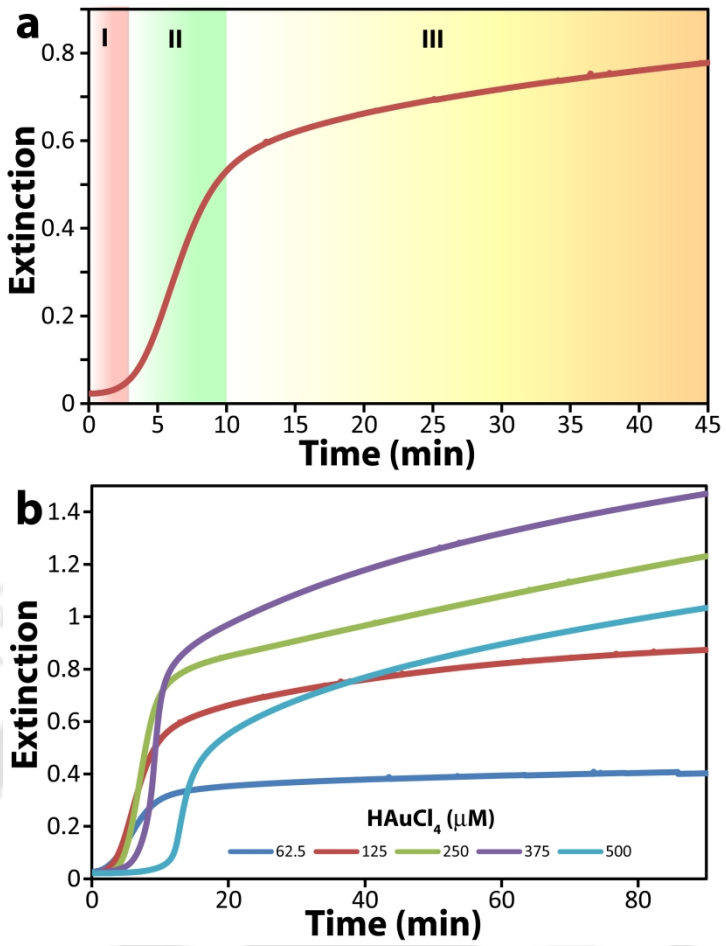

Figure 6.8. (**a**) Temporal evolution of the extinction spectrum recorded at an interval of 3 s for 125 μM Au precursor concentration. The curve is divided into three distinct regions and marked with different colors for easy identification. (**b**) Comparative account of the time dependent extinction spectra for the synthesis of Au NPs using different concentration of the Au precursor.

Therefore, the change in the extinction value with time is not solely responsible for the increase in the concentration of the particles. However, such changes can be used for comparing the global kinetic behavior of reaction.[50] The curve obtained for the change in extinction with respect to time was typically sigmoidal in shape, demonstrating the well-known autocatalytic growth of Au NPs as demonstrated by the Finke and Watzky model.[51-55] The curve can be divided into three regions as shown in the **Figure 6.8a**. Region I (marked with red color) which appears as a lagging phase represents the formation of Au (I) ions by the electron transfer process to the metal precursor (Au (III)) from the reducing agent and subsequent formation of the Au nuclei. The region II (marked with green

color) shows faster change in the extinction value with time, demonstrating the autocatalytic growth of the Au nucleus into seeds and NPs.[51, 55] Once the concentration of atoms drops below the minimum saturation level, no further nucleation takes place, however, the atoms generated by the ongoing precursor reduction will lead to the growth of the nanocrystals to larger sizes until a level of equilibrium is achieved,[34] as seen from the region III of the curve (marked with orange color). In the present case, PEG acts as reductant and it is known to be a weak reducing agent,[29, 56] therefore, the rate of formation of Au (I) ions, or in other words the induction time are expected to be slow which leads to the evolution of Au nuclei. Nevertheless, the presence of C-dots, which is reported to be an electron mediator,[25, 57] accelerates the electron transfer process. It is worth mentioning that with decrease in the concentration of the Au precursor, the induction time reduces (**Table 6.1**), which could be due to the increase in the ratio of C-dots to Au precursor. As C-dots is known to shuttle electrons,[25] increase in the C-dots/[HAuCl4] ratio enhances the rate of reduction and hence reduces the induction time. The induction time required for the formation of Au NPs at different Au precursor concentration is also summarized in **Table 6.1**.

6.4.4. Effect of varying concentration of C-dots on Au NP synthesis

The influence of varying concentration of C-dots on the synthesis of Au NPs was also studied. The Au precursor concentration was fixed to 125 μM while the amount of C-dots was varied from 0 – 9.28 mg mL^{-1}. **Figure 6.9a** shows the extinction spectra of the Au NPs synthesized at different C-dots concentrations. When C-dots were not used in the reaction medium, no sharp feature of the plasmon band of Au NPs was observed. A broad background extending till the NIR region was noticed which could be attributed to the formation of larger sized agglomerates and featureless particles. At the lowest concentration of C-dots (2.32 mg mL^{-1}) used, the extinction spectra showed a broad band in the 550–750 nm region. With further increase in the concentration of C-dots till 4.64 mg mL^{-1} the signatures of the LSPR band of Au NPs started to appear and the plasmon band width also decreased. At 6.96 mg mL^{-1} and 9.28 mg mL^{-1} concentration of the C-

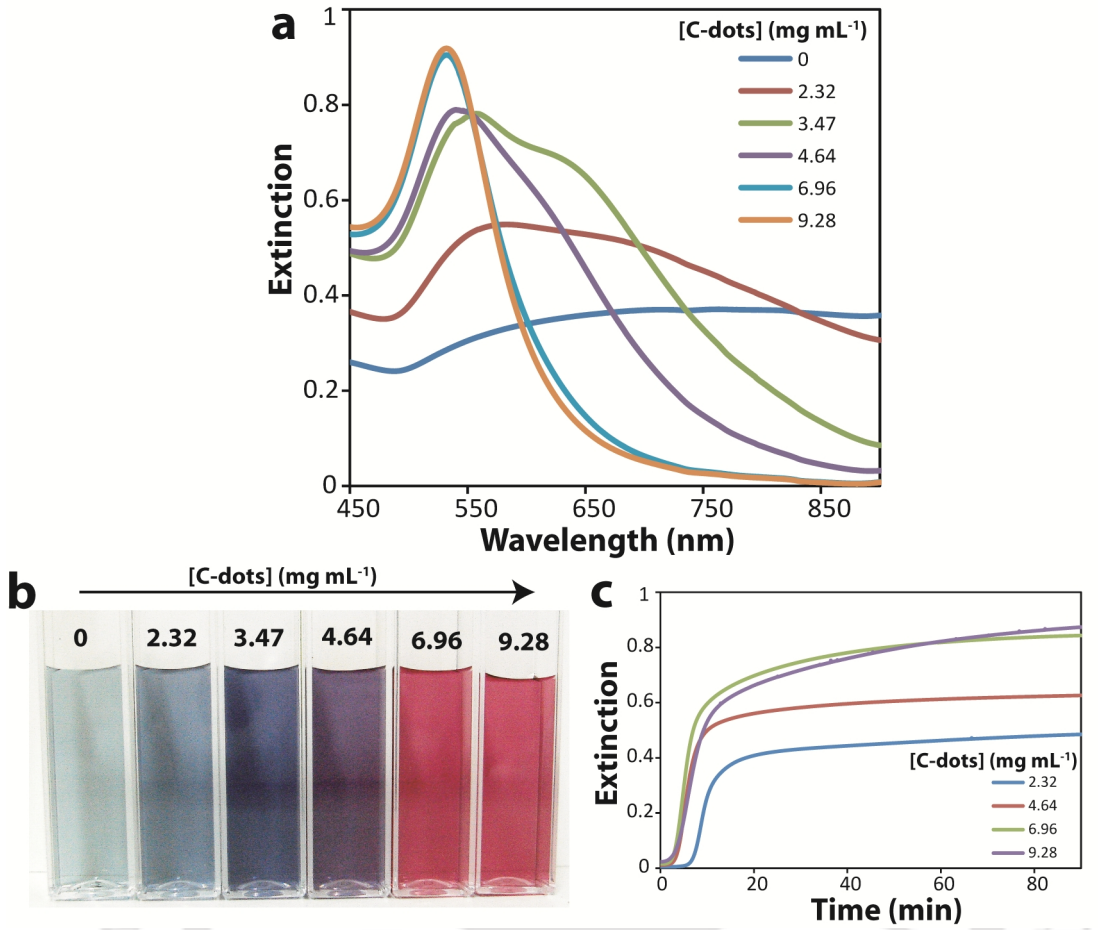

Figure 6.9. (**a**) Extinction spectra of the Au NPs synthesized with varying concentration of C-dots. (**b**) Digital images of the Au NP colloidal solution prepared with different amounts of C-dots. (**c**) Temporal evolution of the extinction of the Au NPs for different concentration of C-dots, taken at an interval of 3 s.

dots, well defined sharp LSPR peak emerging from monodisperse Au NPs were observed. **Figure 6.9b** shows the appearance of the colloidal solution of Au NP formed at different concentration of C-dots, under visible light. It can be clearly seen from the figure that the wine red color, the characteristic feature of small sized Au NPs are obtained only in case of the samples containing higher amount of C-dots. **Figure 6.9c** shows the time dependent change in the extinction of the reaction medium for the synthesis of Au NPs at four different concentrations of the C-dots. The spectra follow the similar sigmoidal pattern as observed for varying concentration of the Au precursor, demonstrating the autocatalytic nature of growth of Au NPs as discussed above. The induction time was more for the lowest

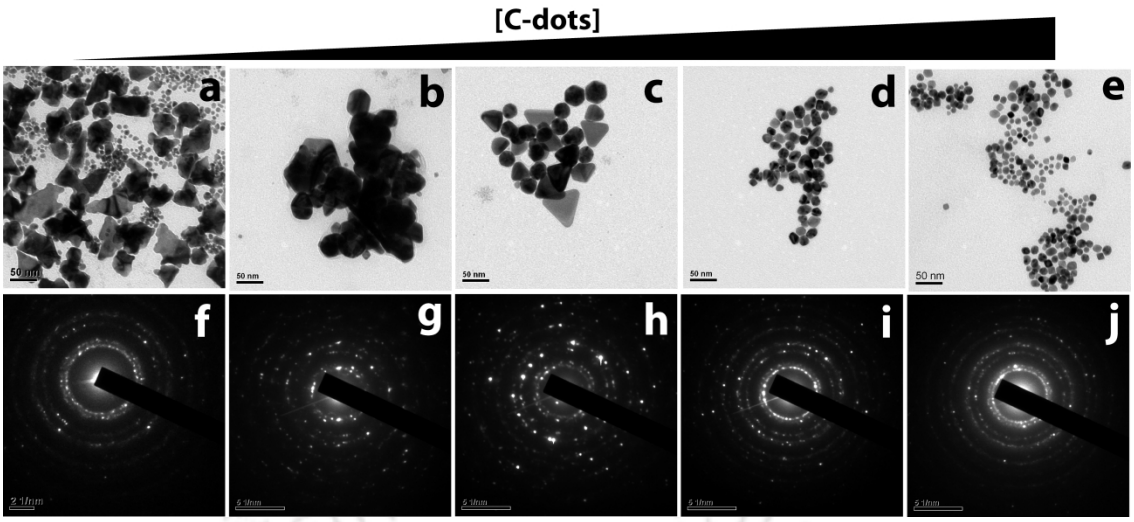

Figure 6.10. TEM mages of the Au NP synthesized using (**a**) 0, (**b**) 2.32, (**c**) 4.64, (**d**), 6.96 and (**e**) 9.28 mg mL^{-1} of C-dots, (**f-j**) the corresponding SAED pattern of the prepared Au NPs.

concentration of C-dots, which gradually reduced with the increase in the C-dots concentration leading to increase in the C-dots/Au precursor ratio. The induction time was almost similar for two highest concentrations of C-dots tested in the present case. The curve for the 2.32 mg mL^{-1} C-dots saturated at lower extinction value for the same Au precursor concentration because of the formation less number of nuclei leading to the formation of larger particles, which thereby, resulted in broad LSPR band with diminished intensity. With increasing C-dots concentration the saturation point for the extinction also increased and it was almost similar for the final two concentrations of the C-dots. This result suggested that 6.96 mg mL^{-1} and 9.28 mg mL^{-1} C-dots resulted in the formation of nearly same amount of the Au nuclei whose growth into Au NPs resulted in similar concentration of the particles, which was reflected from the time based extinction spectra of the Au NPs.

Figure 6.10 shows the TEM images and SAED pattern of the Au NPs synthesized using different concentration of the C-dots and fixed concentration of Au precursor. In absence of C-dots and at the lowest concentration the Au NPs were of larger sizes and irregular shapes (**Figure 6.10a** and **b**). At 4.64 mg mL^{-1} concentration of C-dots the Au NPs formed were mostly of two different morphologies, either decahedron or triangular plates (**Figure 6.10c**). At 6.96 mg

mL^{-1} of C-dots, the particles formed were much smaller than that obtained with the previous concentrations but were larger as compared to those obtained using 9.28 mg mL^{-1} of C-dots. Additionally, for these concentrations, the particles were of regular shapes, mostly with octahedron morphology. The SAED pattern of all the samples demonstrated the presence of crystalline Au particles.

As mentioned earlier, PEG is known to be a mild reducing agent;[29-56] therefore, it was able to reduce the Au precursor in the present situation. However, at room temperature, it takes long hours for the reduction of the Au precursor and mostly clumps of larger sized particles were formed (**Figure 6.10a**). Whereas, the addition of C-dots to the reaction medium drastically reduces the induction time to only few minutes depending on the C-dots-Au precursor ratio. Further, the particles formed were of regular shapes and of smaller sizes. This indicates that C-dots possibly acts as a catalyst by reducing the induction time for the Au NP formation which subsequently results in the formation of large number of nuclei leading to the formation of smaller sized Au NPs. Previous report suggests that C-dots have the capability of shuttling electrons.[25, 29, 57] Therefore, in the present case, C-dots could act as a mediator in the transfer of electron from PEG to the Au precursor, leading to the formation of Au NPs. It is noteworthy that since the reaction was carried out under dark conditions, the possibility of C-dots acting as a photocatalyst can be ruled out. The formation of Au NPs under similar conditions, but in visible light, does not showed any difference in the kind of Au NPs formed which also proved that C-dots acts as a catalyst but not as photocatalyst in the present case.

6.4.5. Stability of the synthesized Au NPs

In order to use metallic NPs for biological applications, the stability of the colloids remains a major concern. We have performed the stability test for the synthesized Au NPs for 15 days using UV-Vis spectroscopy. **Figure 6.11** shows the normalized extinction *vs* time plot of Au NPs synthesized with different concentration of the Au precursor. For 62.5 and 125 μM Au precursor concentration, no major change in the peak position was observed even till 15 days indicating the stability of the

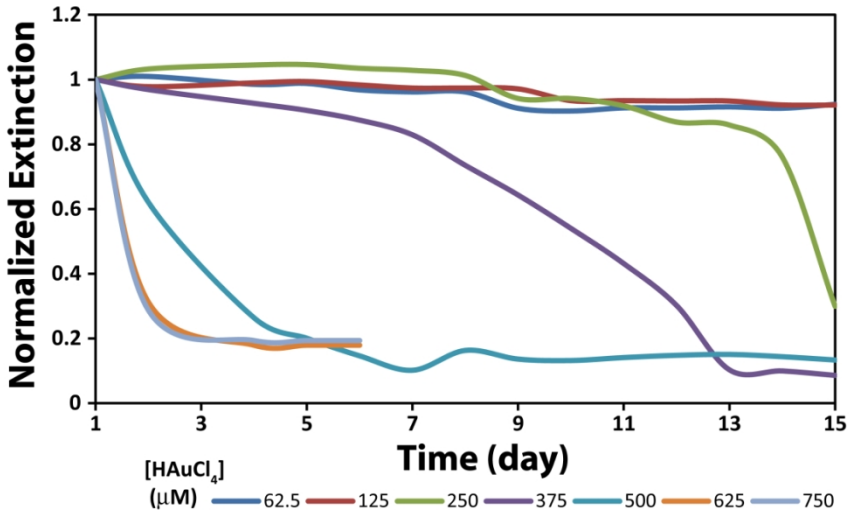

Figure 6.11. Normalized extinction *vs* time plot at the LSPR peak wavelength for Au NPs synthesized using different concentration of Au precursor.

particles. For 500, 625 and 700 μM precursor concentrations the particles were unstable and it settled down very fast, within 2 days for 625 and 700 and in 4 days of synthesis for 500 μM $HAuCl_4$. For 250 and 375 μM concentrations, the particles were stable for 2 and 1 week respectively, after which they started to settle down.

6.5. Conclusion

We developed a simple room temperature based methodology for the synthesis of Au NPs using C-dots in PEG. In contrast to previous reports our procedure is independent of ultraviolet or microwave irradiation. The synthesized particles were well separated with mean size of 15 ± 3.3 nm. The influence of varying concentration of the Au precursor and the C-dots catalyst resulted in the formation of different sized particles with diverse morphologies. Time resolved extinction spectroscopy unveiled the sigmoidal pattern of particle growth with a distinct lagging phase and were according to the Finke and Watzky model. The synthesized Au NPs were stable for several days for the lower concentrations of the Au precursor used. Overall, the applicability of C-dots to act as a catalyst in the synthesis of Au NPs without the involvement of photo or microwave irradiation was demonstrated which may further the research in the catalytic property of C-dots.

6.6. References

1. X. Xu, R. Ray, Y. Gu, H. J. Ploehn, L. Gearheart, K. Raker, W. A. Scrivens, *J. Am. Chem. Soc.*, **2004**, 126, 12736–12737.
2. S. N. Baker, G. A. Baker, *Angew. Chem. Int. Ed.*, **2010**, 49, 6726–6744.
3. H. Li, Z. Kang, Y. Liu, S.-T. Lee, *J. Mater. Chem.*, **2012**, 22, 24230–24253.
4. Z. Liu, *Theranostics*, **2012**, 2, 235–237.
5. P. G. Luo, S. Sahu, S.-T. Yang, S. K. Sonkar, J. Wang, H. Wang, G. E. LeCroy, L. Cao, Y.-P. Sun, *J. Mater. Chem. B*, **2013**, DOI 10.1039/C3TB00018D
6. P. Huang, J. Lin, X. Wang, Z. Wang, C. Zhang, M. He, K. Wang, F. Chen, Z. Li, G. Shen, D. Cui, X. Chen, *Adv. Mater.*, **2012**, *24*, 5104–5110.
7. C. Liu, P. Zhang, X. Zhai, F. Tian, W. Li, J. Yang, Y. Liu, H. Wang, W. Wang, W. Liu, *Biomaterials*, **2012**, *33*, 3604–3613.
8. F. Wang, Y. Chen, C. Liu, D. Ma, *Chem. Commun.*, **2011**, *47*, 3502–3504.
9. X. Guo, C.-F. Wang, Z.-Y. Yu, L. Chen, S. Chen, *Chem. Commun.,* **2012**, *48*, 2692–2694.
10. J. Wang, C.-F. Wang, S. Chen, *Angew. Chem. Int. Ed.*, **2012**, *51*, 9297–9301.
11. Y. Dong, R. Wang, H. Li, J. Shao, Y. Chi, X. Lin, G. Chen, *Carbon*, **2012**, *50*, 2810–2815.
12. H. Gonçalves, P. A. S. Jorge, J. R. A. Fernandes, J. C. G. Esteves da Silva, *Sens. Actuators B: Chem.*, **2010**, *145*, 702–707.
13. A. Salinas-Castillo, M. Ariza-Avidad, C. Pritz, M. Camprubí-Robles, B. Fernández, M. J. Ruedas-Rama, A. Megia-Fernández, A. Lapresta-Fernández, F. Santoyo-Gonzalez, A. Schrott-Fischer, L. F. Capitan-Vallvey, *Chem. Commun.*, **2013**, *49*, 1103–1105.
14. J. C. G. Esteves da Silva, H. M. R. Gonçalves, *TrAC Trends in Analytical Chemistry*, **2011**, *30*, 1327–1336.
15. Y. Wang, S. Wang, S. Ge, S. Wang, M. Yan, D. Zang, J. Yu, *Anal. Methods*, **2013**, *5*, 1328–1336.
16. H. Li, R. Liu, S. Lian, Y. Liu, H. Huang, Z. Kang, *Nanoscale*, **2013**, DOI 10.1039/C3NR00092C.
17. H. Li, X. He, Z. Kang, H. Huang, Y. Liu, J. Liu, S. Lian, C. H. A. Tsang, X. Yang, S.-T. Lee, *Angew. Chem. Int. Ed.*, **2010**, *49*, 4430–4434.
18. E. Chang, N. Thekkek, W. W. Yu, V. L. Colvin and R. Drezek, *Small*, **2006**, 2, 1412–1417.
19. A. M. Derfus, W. C. W. Chan and S. N. Bhatia, *Nano Lett.*, **2004**, 4, 11–18.
20. W.-H. Chan, N.-H. Shiao, P.-Z. Lu, *Toxicol. Lett.*, **2006**, 167, 191–200.

21. M. Green, E. Howman, *Chem. Commun.*, **2005**, 121–123.
22. L. Qu, X. Peng, *J. Am. Chem. Soc.*, **2002**, 124, 2049–2055.
23. C. B. Murray, D. J. Norris, M. G. Bawendi, *J. Am. Chem. Soc.*, **1993**, 115, 8706–8715.
24. D. V. Talapin, A. L. Rogach, A. Kornowski, M. Haase, H. Weller, *Nano Lett.*, **2001**, 1, 207–211.
25. H. T. Li, X. D. He, Z. H. Kang, H. Huang, Y. Liu, J. L. Liu, S. Y. Lian, C. H. A. Tsang, X. B. Yang and S. T. Lee, *Angew. Chem. Int. Ed.*, **2010**, 49, 4430–4434
26. H. C. Zhang, H. Ming, S. Lian, H. Huang, H. Li, L. Zhang, Y. Liu, Z. Kang, S. T. Lee, *Dalton Trans.*, **2011**, 40, 10822–10825.
27. H. C. Zhang, H. Huang, H. Ming, H. T. Li, L. L. Zhang, Y. Liu, Z. H. Kang, *J. Mater. Chem.*, **2012**, 22, 10501–10506.
28. H. Yu, H. C. Zhang, H. T. Li, H. Huang, Y. Liu, H. Ming, Z. H. Kang, *New J. Chem.*, **2012**, 36, 1031–1035.
29. S. Mitra, S. Chandra, P. Patra, P. Pramanik, A. Goswami, *J. Mater. Chem.*, **2011**, 21, 17638–17641.
30. X. Qin, W. Lu, G. Chang, Y. Luo, A. M. Asiri, A. O. Al-Youbi, X. Sun, *Gold Bull.*, **2012**, 45, 61–67.
31. S. Guo, E. Wang, *Anal. Chim. Acta*, **2007**, *598*, 181–192.
32. S. Eustis, M. A. El-Sayed, *Chem. Soc. Rev.*, **2006**, *35*, 209–217.
33. M. Grzelczak, J. Pérez-Juste, P. Mulvaney, L. M. Liz-Marzán, *Chem. Soc. Rev.*, **2008**, *37*, 1783–1791.
34. Y. Xia, Y. Xiong, B. Lim, S. E. Skrabalak, *Angew. Chem. Int. Ed.*, **2009**, *48*, 60–103.
35. L. A. Dykman, N. G. Khlebtsov, *Acta Naturae*, **2011**, *3*, 34–55.
36. C. J. Murphy, A. M. Gole, J. W. Stone, P. N. Sisco, A. M. Alkilany, E. C. Goldsmith, S. C. Baxter, *Acc. Chem. Res.,* **2008**, *41*, 1721–1730.
37. L. Dykman, N. Khlebtsov, *Chem. Soc. Rev.*, **2012**, *41*, 2256–2282.
38. N. Khlebtsov, V. Bogatyrev, L. Dykman, B. Khlebtsov, S. Staroverov, A. Shirokov, L. Matora, V. Khanadeev, T. Pylaev, N. Tsyganova, G. Terentyuk, *Theranostics*, **2013**, *3*, 167–180.
39. E. C. Dreaden, A. M. Alkilany, X. Huang, C. J. Murphy, M. A. El-Sayed, *Chem. Soc. Rev.*, **2012**, *41*, 2740–2779.
40. A. G. Tkachenko, H. Xie, D. Coleman, W. Glomm, J. Ryan, M. F. Anderson, S. Franzen, D. L. Feldheim, *J. Am. Chem. Soc.*, **2003**, *125*, 4700–4701.
41. M. M.-C. Cheng, G. Cuda, Y. L. Bunimovich, M. Gaspari, J. R. Heath, H. D. Hill, C. A. Mirkin, A. J. Nijdam, R. Terracciano, T. Thundat, M. Ferrari, *Curr. Opin. Chem. Biol.*, **2006**, *10*, 11–19.

42. R. Khandelia, A. Jaiswal, S. S. Ghosh, A. Chattopadhyay, *Small*, **2013**, DOI 10.1002/smll.201203095.
43. J. Chen, F. Saeki, B. J. Wiley, H. Cang, M. J. Cobb, Z.-Y. Li, L. Au, H. Zhang, M. B. Kimmey, X. Li, Y. Xia, *Nano Lett.*, **2005**, *5*, 473–477.
44. X. Yang, S. E. Skrabalak, Z.-Y. Li, Y. Xia, L. V. Wang, *Nano Lett.*, **2007**, *7*, 3798–3802Y.
45. Li, S. Liu, T. Yao, Z. Sun, Z. Jiang, Y. Huang, H. Cheng, Y. Huang, Y. Jiang, Z. Xie, G. Pan, W. Yan, S. Wei, *Dalton Trans.*, **2012**, *41*, 11725–11730.
46. Y. Lu, J. Y. Huang, C. Wang, S. Sun, J. Lou, *Nat. Nanotechnol.*, **2010**, *5*, 218–224.
47. C. Li, K. L. Shuford, Q.-H. Park, W. Cai, Y. Li, E. J. Lee, S. O. Cho, *Angew. Chem. Int. Ed.*, **2007**, *46*, 3264–3268.
48. C. Ziegler, A. Eychmüller, *J. Phys. Chem. C*, **2011**, *115*, 4502–4506.
49. Y. B. Zheng, B. K. Juluri, X. Mao, T. R. Walker, T. J. Huang, *J. Appl. Phys.*, **2008**, *103*, 014308(1)–014308(9).
50. C. E. Hoppe, M. Lazzari, I. Pardiñas-Blanco, M. A. López-Quintela, *Langmuir*, **2006**, *22*, 7027–7034.
51. M. A. Watzky, R. G. Finke, *J. Am. Chem. Soc.*,**1997**, *119*, 10382–10400.
52. J. Polte, T. T. Ahner, F. Delissen, S. Sokolov, F. Emmerling, A. F. Thünemann, R. Kraehnert, *J. Am. Chem. Soc.*, **2010**, *132*, 1296–1301.
53. B. Streszewski, W. Jaworski, K. Pacławski, E. Csapó, I. Dékány, K. Fitzner, *Colloids Surf.A Physicochem. Eng. Asp.*, **2012**, *397*, 63–72.
54. K. Pacławski, B. Streszewski, W. Jaworski, M. Luty-Błocho, K. Fitzner, *Colloids Surf. A Physicochem. Eng. Asp.*, **2012**, *413*, 208–215.
55. M. Wojnicki, E. Rudnik, M. Luty-Błocho, K. Pacławski, K. Fitzner, *Hydrometallurgy*, **2012**, *127-128*, 43–53.
56. D.-H. Chen, Y.-W. Huang, *J. Colloid Interf. Sci.*, **2002**, *255*, 299–302.
57. W. Shi, Q. Wang, Y. Long, Z. Cheng, S. Chen, H. Zheng and Y. Huang, *Chem. Commun.*, **2011**, 47, 6695–6697.

Chapter 7

Conclusion and Future Outlook

This chapter briefly presents the summary of the present study and scope for future work.

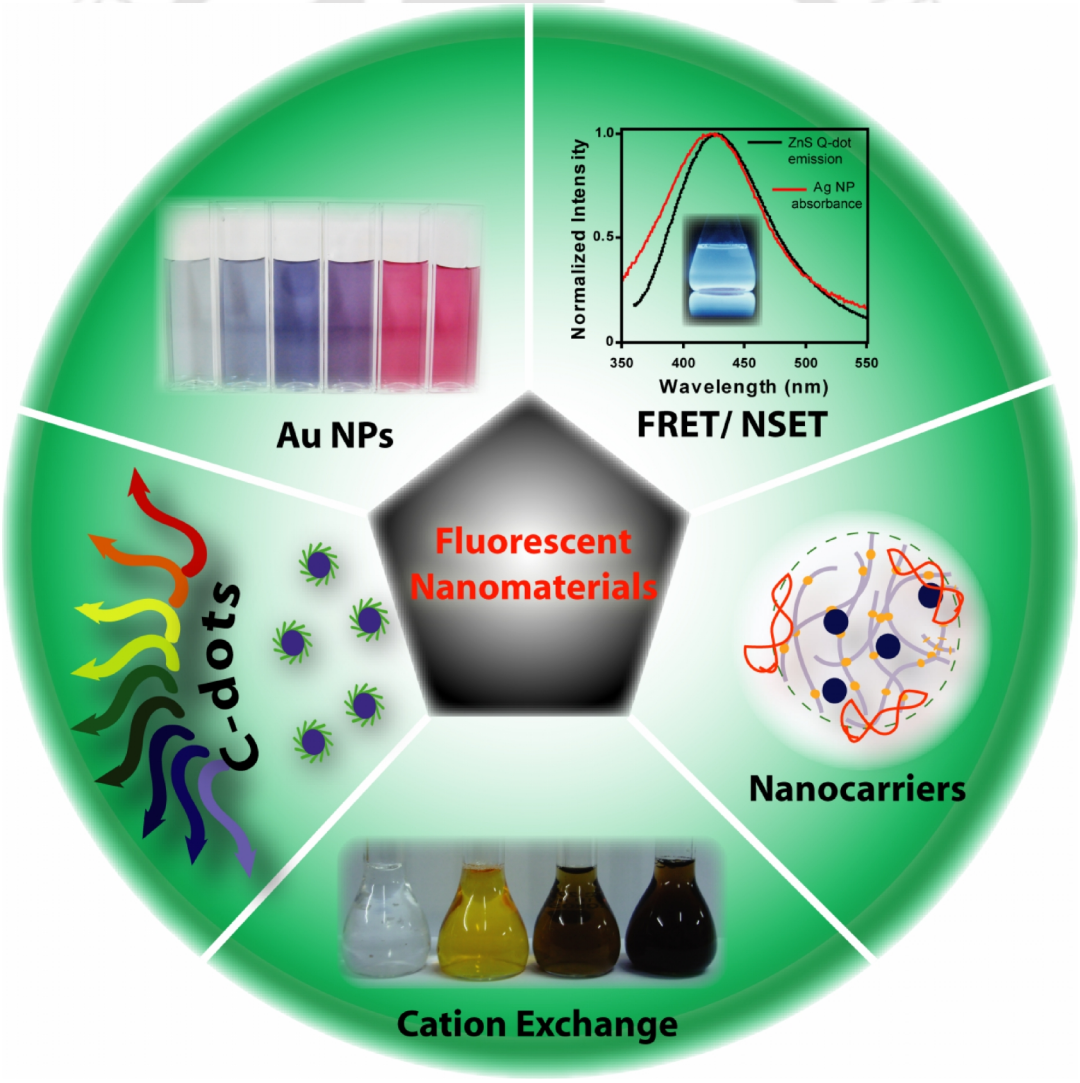

Chapter 7

Conclusion and Future Outlook

7.1. Summary of the present work

Considering the advancement of science and technology in the last few decades, nanotechnology has emerged as one of the most exciting technologies and is expected to continuously provide many benefits for the years to come. One of the most important gifts of nanotechnology to life sciences is the fluorescent nanomaterials, which has revolutionized the bioimaging and bioanlytical applications, due to their unique properties.

In the present thesis, methodology for the synthesis of nontoxic fluorescent nanomaterials and their potential in therapeutics and diagnostics are demonstrated. In this regard, ZnS Q-dots and C-dots were synthesized and were shown to be used for cell labeling applications. Multifunctional chitosan nanocarriers containing Q-dots and folic acid as imaging and targeting agents respectively, were designed and used for the delivery of suicide genes to cancer cells. The effect of silver nanoparticles on the fluorescence property of ZnS Q-dots was studied and its possible application in Förster Resonance Energy Transfer/Nanometal Surface Energy Transfer (FRET/NSET) based techniques was demonstrated. Chitosan film impregnated with Q-dots was fabricated and was used for sensing and removal of heavy metal ions from water. The newer fluorophore C-dots were synthesized using a novel approach and were employed for bioimaging application. The synthesized C-dots were also demonstrated to be used as catalyst in synthesizing Au NPs at ambient temperature.

Initially, water dispersible zinc sulfide quantum dots (ZnS Q-dots) with an average diameter of 2.9 nm was synthesized in an environment friendly method using the biodegradable polymer chitosan as stabilizing agent. These nanocrystals displayed characteristic absorption and emission spectra having an absorbance edge at ~300 nm and emission maxima ($\lambda_{emission}$) at 427 nm. Citrate-capped silver nanoparticles (Ag NPs) of ca. 37 nm diameter were prepared by modified *Turkevich* process. The fluorescence of ZnS Q-dots was significantly quenched in presence of Ag NPs in a concentration dependent manner with K_{sv} value of 9×10^{9} M^{-1}. The quenching mechanism was analyzed using Stern-Volmer plot which indicated mixed nature of quenching. Static mechanism was evident from the formation of electrostatic complex between positively charged ZnS Q-dots and negatively charged Ag NPs as confirmed by absorbance study. Due to excellent overlap between ZnS Q-dots emission and surface plasmon resonance (SPR) band of Ag NPs, the role of energy transfer process as an additional quenching mechanism was investigated by time resolved fluorescence measurements. Time correlated single photon counting (TCSPC) study demonstrated decrease in average lifetime of ZnS Q-dots fluorescence in presence of Ag NPs. The corresponding Förster distance for the present Q-dot – NP pair was calculated to be 18.4 nm. The implication of the present findings may lead to the development of long range FRET – or NSET – based methods for studying biological multicomponent system.

Next, I have designed multifunctional chitosan nanocarriers with targeting and imaging modalities having theranostic applications. Folic acid (FA) was conjugated to chitosan and then it was used to synthesize zinc sulfide quantum dots (ZnS Q-dots). The ZnS Q-dots embedded FA-chitosan was further converted to chitosan nanocarriers using ionic gelation. The integrated FA acts as targeting, and the assembled Q-dots within the nanocarriers as imaging functionalities, respectively. The nanocarriers were almost spherical with sizes of ~75 nm with implanted Q-dots of about 3 nm. Cell viability assay corroborated the nontoxic property of the nanocarriers. Fluorescence of Q-dots enabled imaging of cellular uptake of the nanocarriers. The suicide genes encoding for *E. coli* cytosine deaminase-uracil phosphoribosyltransferase (pCD-UPRT) was able to complex

with the nanocarriers as demonstrated by gel retardation assay. DNAse protection assay proved the stability of the nanocarrier–DNA complex. The synthesized nanocarriers can thus, serve as a potential non-viral vector for gene therapy where the FA can be used to target cancer cells specifically and the Q-dots for tracking the process of delivery.

In addition, ZnS Q-dots impregnated chitosan film was fabricated and its applicability in environmental remediation by sensing and removal of heavy metal ions from contaminated water was demonstrated. The biopolymer chitosan stabilized ZnS Q-dots were synthesized and were converted to HgS, Ag_2S and PbS Q-dots through cation exchange reaction. The transformed Q-dots showed characteristic colour development; Hg^{2+} being exceptionally identified due to the visible bright yellow colour formation in contrast to that of brown colouration for other metal ions. The transformation was driven by the difference in the solubility product of the reactant and the product Q-dots. The cation exchanged Q-dots preserved the morphology of the reactant Q-dots and displayed volume increase based on bulk crystal lattice parameters. Next, we fabricated ZnS Q-dots impregnated chitosan film which showed its capability in the removal of heavy metal ions from contaminated water as demonstrated by atomic absorption spectroscopy (AAS). The present system could suitably be used as a simple dipstick method of elimination of heavy metal contamination in water.

Further, I have demonstrated a rapid, simple and one pot microwave mediated method for synthesizing C-dots using a single biocompatible polymer poly(ethylene glycol) (PEG) for the first time as a precursor and passivating agent. Irradiation of aqueous PEG 200 solution in a domestic microwave oven for 10 min resulted in the formation of C-dots. The synthesized C-dots were well separated with size of ~4.5 nm and were amenable to separation by electrophoresis. The C-dots possess low cytotoxicity as revealed by cell viability assay and were able to enter mammalian cells without any further functionalization. Additionally, C-dots showed excellent photostability in contrast to the organic fluorophore Rhodamine 101 and served as an effective candidate for biolabeling and bioimaging applications overcoming the photobleaching property of organic fluorophore.

Finally, the applicability of C-dots to act as a catalyst for the synthesis of gold nanoparticles (Au NPs) at room temperature was demonstrated. The as-prepared C-dots, in presence of poly (ethylene glycol) displayed its catalytic role in the rapid reduction of Au^{3+} ions. The reaction was carried out in dark to show that C-dots act as a catalyst without any involvement of photoreduction mechanism. The synthesized Au NPs were mostly octahedron and were about 15 nm in size. The usage of varying concentration of the metal precursor led to size tuneable formation of Au NPs. The growth and stability of the Au NPs were demonstrated using absorption spectroscopy and were observed to follow the Finke and Watzky model. Thus, the role of C-dots in synthesis of Au NPs was illustrated.

7.2. Future Outlook

- Different biopolymers, such as alginate and poly(lactic acid) could be used for the easy synthesis of C-dots and can be demonstrated for gene/protein delivery applications.
- The effect of various heavy metal ions on the photophysical properties of C-dots could be investigated.
- The functional groups available on the surface of C-dots could be exploited for conjugation of therapeutic enzymes and the effect of conjugation on the activity of the enzyme could be elucidated.
- The applicability of C-dots in synthesis of other metal nanoparticles of core/shell type or alloy nanoparticles can be performed.
- Method for the reversible cation exchange in ZnS Q-dots could be studied to analyze the reusability of the ZnS Q-dot impregnated chitosan film for heavy metal ion sensing and removal.
- A water filtration system based on the chemical transformation ability of the ZnS Q-dots and the antibacterial and metal ion adsorbing property of chitosan could be designed.

Appendix

A1: Chapter 4

Calculation of band gap of Q-dots

The band gap energies of the different Q dots were derived from the Tauc plot using the following equation 4A.1

$$(\alpha h\nu)^{1/n} = C \times (h\nu - E_g) \quad (4A.1)$$

Where, C is a constant, α is absorption coefficient, E_g is the average band gap of the material, h is the Planck's constant, ν is the frequency and *n* depends on the type of transition. For n = ½, E_g in equation (4A.1) is direct allowed band gap. The absorption coefficient α is calculated using equation 4A.2.

$$\alpha = -\frac{1}{t} \times \ln\left(\frac{I_t}{I_0}\right) = \frac{1}{t} \times A \times \log e \quad (4A.2)$$

Where, t is the path length, which is 1 cm in the present case, I_t and I_0 are transmitted and incident light, A is the absorbance. The average band gap was estimated from the intercept of linear portion of the $(\alpha h\nu)^2$ *vs.* $h\nu$ plots on $h\nu$ axis as shown in Figure 4A.1.

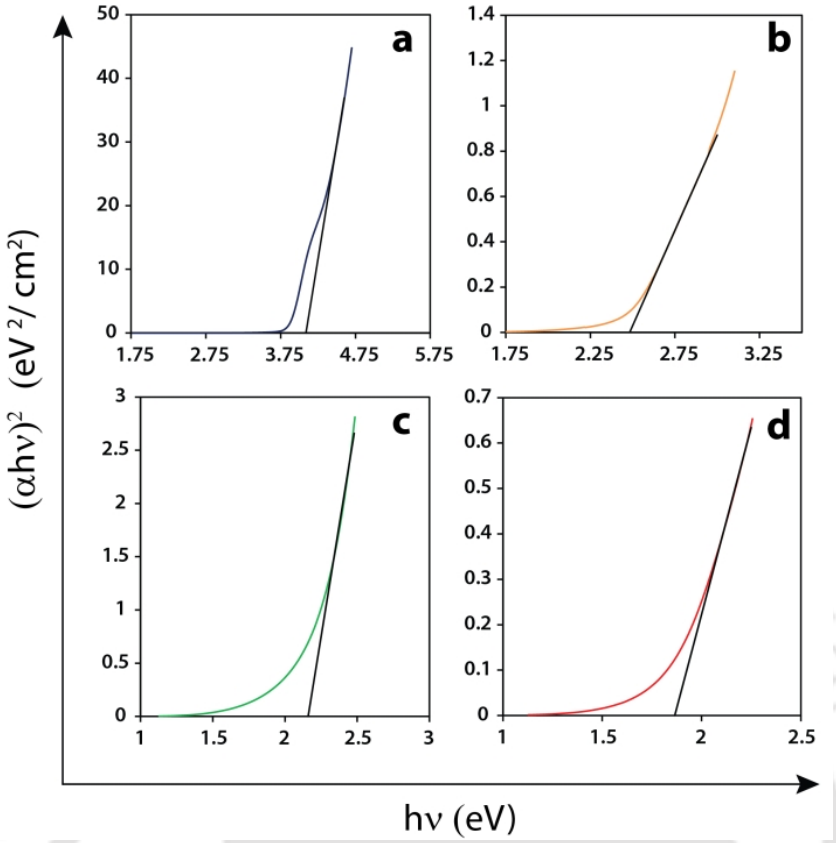

Figure 4A.1. Tauc Plot of (**a**) ZnS Q-dots, (**b**) HgS Q-dots, (**c**) Ag_2S Q-dots and (**d**) PbS Q-dots

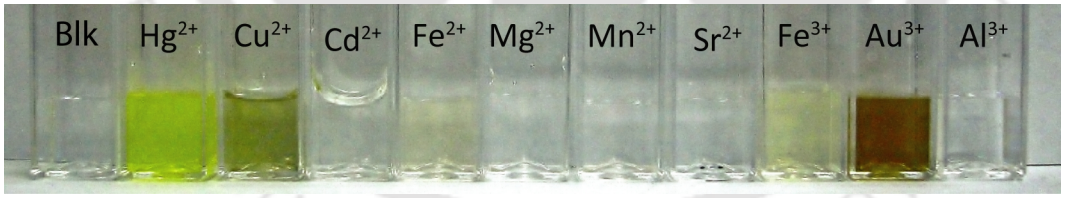

Figure 4A.2. Digital image represents the appearance of the colloidal ZnS Q-dots under visible light illumination, in presence of different metal ions as mentioned.

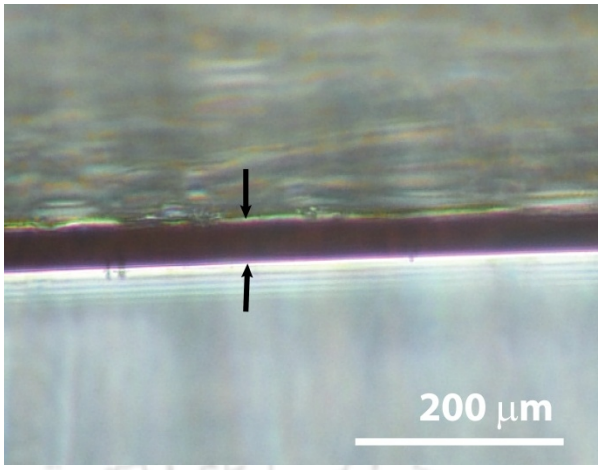

Figure 4A.3. Phase contrast microscopy image of a vertical section of ZnS Q-dots impregnated chitosan film.

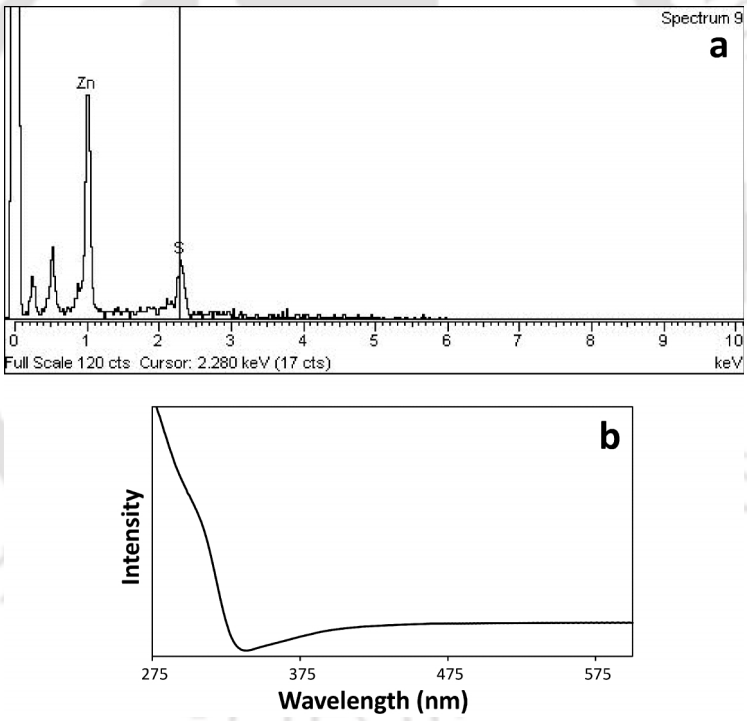

Figure 4A.4. (**a**) EDS spectrum of ZnS Q-dots impregnated chitosan film and (**b**) UV-visible spectrum of ZnS Q-dots impregnated chitosan film.

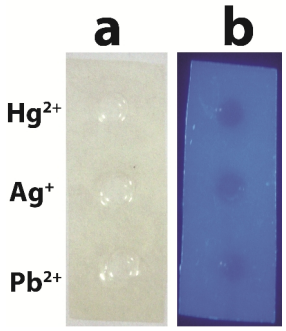

Figure 4A.5. Photographs upon drop cast of different metal ions onto unloaded chitosan film under (a) visible and (b) UV light.

A2: Chapter 5

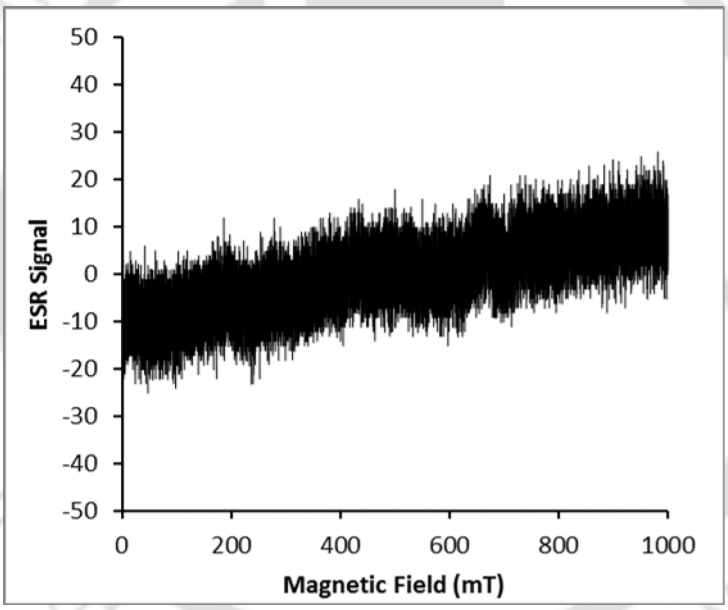

Figure 5A.1. Electron Spin Resonance spectrum of the C-dots

LIST OF PUBLICATIONS

In Peer Reviewed Journals:

1. **Amit Jaiswal**, Pallab Sanpui, Arun Chattopadhyay, Siddhartha Sankar Ghosh; Investigating Fluorescence Quenching of ZnS Quantum Dots by Silver Nanoparticles. *Plasmonics*, **2011**, 6, 1, 125–132.
2. **Amit Jaiswal**, Arun Chattopadhyay, Siddhartha Sankar Ghosh; Functional Chitosan Nanocarriers for Potential Applications in Gene Therapy. *Materials Letters*, **2012**, 68, 261–264.
3. **Amit Jaiswal**, Siddhartha Sankar Ghosh, Arun Chattopadhyay; One Step Synthesis of C-dots by Microwave Mediated Caramelization of Poly(ethylene glycol). *Chemical Communications*, **2012**, 48, 3, 407–409.
4. **Amit Jaiswal**, Siddhartha Sankar Ghosh, Arun. Chattopadhyay; Quantum Dot Impregnated-Chitosan Film for Heavy Metal Ion Sensing and Removal. *Langmuir*, **2012**, 28, 44, 15687–15696.
5. **Amit Jaiswal**, Prateek Kumar Gautam, Siddhartha Sankar Ghosh, Arun Chattopadhyay, Catalytic synthesis of gold nanoparticles using carbon dots. (*In Preparation*)
6. Md Pallashuddin Sk, **Amit Jaiswal**, Anumita Paul, Siddhartha Sankar Ghosh, Arun Chattopadhyay; Presence of Amorphous Carbon Nanoparticles in Food Caramels. *Scientific Reports*, **2012**, 2, 383; DOI:10.1038/srep00383.
7. V. Kohila, **Amit Jaiswal**, Siddhartha Sankar Ghosh; Rationally designed Escherichia coli cytosine deaminase mutants with improved specificity towards the prodrug 5-fluorocytosine for potential gene therapy applications. *Medicinal Chemistry Communications*, **2012**, 3, 1316–1322.
8. Rumi Khandelia**,** **Amit Jaiswal**, Siddhartha Sankar Ghosh, Arun Chattopadhyay; Gold Nanoparticle-protein agglomerates as versatile nanocarriers for drug delivery. (*Small, In Press, DOI: 10.1002/smll.201203095*).
9. V. Kohila, **Amit Jaiswal**, Siddhartha Sankar Ghosh; Cloning, Expression and Purification of the bifunctional Cytosine deaminase-Uracil phosphoribosyltransferase (CD-UPRT) fusion protein. *(Submitted)*.

LIST OF PUBLICATIONS

In Conference Proceedings:

1. **Amit Jaiswal**, Pallab Sanpui, Arun Chattopadhyay, Siddhartha Sankar Ghosh. Effect of Silver Nanoparticles on the Fluorescence Property of ZnS Quantum Dots, *DAE-BRNS 3rd International Symposium on Materials Chemistry (**ISMC-2010**)*, Bhabha Atomic Research Centre, Mumbai, India.
2. **Amit Jaiswal**, Arum Chattopadhyay, Siddhartha Sankar Ghosh; Multifunctional Chitosan Nanocarriers; Synthesis and Application, *Indo-US Bilateral Workshop on Nanoparticle Assembly: From Fundamentals to Applications* (***2011***), IIT Delhi, India.
3. **Amit Jaiswal**, Siddhartha Sankar Ghosh, Arun Chattopadhyay; Cation Exchange Based Chemical Transformation of ZnS Q-dots and its Application in Heavy Metal Ion Sensing and Removal, *National Fluorescence Workshop - **FCS 2012***, Saha Institute of Nuclear Physics and IICB, Kolkata, India.
4. **Amit Jaiswal**, Siddhartha Sankar Ghosh, Arun Chattopadhyay; Facile Synthesis of Carbon Dots using Poly(ethylene glycol) as Precursor and Passivizing Agent, *International Conference On Nanoscience And Technology (**ICONSAT-2012**)*, International Advanced Research Centre for Powder Metallurgy & New Materials (ARCI), Hyderabad, India.
5. **Amit Jaiswal**, Siddhartha Sankar Ghosh, Arun Chattopadhyay; Carbon Dots: Emergence of a Newer 'Nanolight', *Conference on Photochemistry & Luminescence **(CPL-2012)***, IIT Guwahati, India.
6. V. Kohila, **Amit Jaiswal**, Siddhartha Sankar Ghosh; Redesigning of E. coli Cytosine deaminase in the Perspective of Cancer Therapeutics, *3rd International Conference on Stem Cells and Cancer: Proliferation, Differentiation and Apoptosis* (**ICSCC 2012**), PGIMER, New Delhi, India.
7. Rumi Khandelia**,** **Amit Jaiswal**, Siddhartha Sankar Ghosh, Arun Chattopadhyay; Nanoparticle-Protein Aggregates for Diagnostics and Therapeutics, *DAE-BRNS 4th International Symposium on Materials Chemistry (**ISMC-2012**)*, Bhabha Atomic Research Centre, Mumbai, India.

8. Rumi Khandelia**,** **Amit Jaiswal**, Siddhartha Sankar Ghosh, Arun Chattopadhyay; Interaction of Gold Nanoparticles with biomolecules, *21st International Symposium on Processing and Fabrication of Advanced Materials (**PFAM-2012**)*, IIT Guwahati, India.
9. Rumi Khandelia, Jashmini Deka**,** **Amit Jaiswal**, Anumita Paul, Siddhartha Sankar Ghosh, Arun Chattopadhyay; Interaction of Gold Nanoparticles with Proteins and their biomedical applications, *National Conference on Frontiers in Chemical Sciences (**FICS-2012**)*, IIT Guwahati, India.
10. Md. Pallasuddin. Sk, **Amit Jaiswal**, Anumita Paul, Siddhartha Sankar Ghosh, Arun Chattopadhyay; Food Caramel Originated Carbon Dots for Newer and Biofriendly Fluorescence Materials Applications, *National Conference on Frontiers in Chemical Sciences (**FICS-2012**)*, IIT Guwahati, India.

Order Completed

Thank you very much for your order.

This is a License Agreement between Amit Jaiswal ("You") and Springer ("Springer"). The license consists of your order details, the terms and conditions provided by Springer, and the payment terms and conditions.

Get the printable license.

License Number	3105900785566
License date	Mar 11, 2013
Licensed content publisher	Springer
Licensed content publication	Annals of Biomedical Engineering
Licensed content title	Engineering Luminescent Quantum Dots for In Vivo Molecular and Cellular Imaging
Licensed content author	Andrew M. Smith
Licensed content date	Jan 1, 2006
Volume number	34
Issue number	1
Type of Use	Thesis/Dissertation
Portion	Figures
Author of this Springer article	No
Title of your thesis / dissertation	Fluorescent Nanomaterials for Biological Applications
Expected completion date	May 2013
Estimated size(pages)	150
Total	0.00 USD

CLOSE WINDOW

Copyright Clearance Center RightsLink®

Home | Account Info | Help

nature publishing group

Title: Strategies in the design of nanoparticles for therapeutic applications
Author: Robby A. Petros and Joseph M. DeSimone
Publication: Nature Reviews Drug Discovery
Publisher: Nature Publishing Group
Date: Aug 1, 2010

Logged in as:
Amit Jaiswal
Account #:
3000540358

LOGOUT

Order Completed

Thank you very much for your order.

This is a License Agreement between Amit Jaiswal ("You") and Nature Publishing Group ("Nature Publishing Group"). The license consists of your order details, the terms and conditions provided by Nature Publishing Group, and the payment terms and conditions.

Get the printable license.

License Number	3100200270376
License date	Mar 01, 2013
Licensed content publisher	Nature Publishing Group
Licensed content publication	Nature Reviews Drug Discovery
Licensed content title	Strategies in the design of nanoparticles for therapeutic applications
Licensed content author	Robby A. Petros and Joseph M. DeSimone
Licensed content date	Aug 1, 2010
Type of Use	reuse in a thesis/dissertation
Volume number	9
Issue number	8
Requestor type	academic/educational
Format	print and electronic
Portion	figures/tables/illustrations
Number of figures/tables /illustrations	1
High-res required	no
Figures	Figure 2 | Modes of cellular internalization of nanoparticles and respective size limitations.
Author of this NPG article	no
Your reference number	
Title of your thesis / dissertation	Fluorescent Nanomaterials for Biological Applications
Expected completion date	May 2013
Estimated size (number of pages)	150
Total	0.00 USD

ORDER MORE... CLOSE WINDOW

Copyright Clearance Center RightsLink®

Home Account Info Help

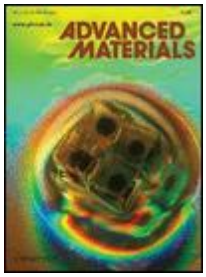

Title: Intracellular Delivery of Quantum Dots for Live Cell Labeling and Organelle Tracking
Author: A. M. Derfus,W. C. W. Chan,S. N. Bhatia
Publication: Advanced Materials
Publisher: John Wiley and Sons
Date: May 19, 2004

Logged in as:
Amit Jaiswal
Account #:
3000540358

LOGOUT

Order Completed

Thank you very much for your order.

This is a License Agreement between Amit Jaiswal ("You") and John Wiley and Sons ("John Wiley and Sons"). The license consists of your order details, the terms and conditions provided by John Wiley and Sons, and the payment terms and conditions.

Get the printable license.

License Number	3106071281980
License date	Mar 11, 2013
Licensed content publisher	John Wiley and Sons
Licensed content publication	Advanced Materials
Licensed content title	Intracellular Delivery of Quantum Dots for Live Cell Labeling and Organelle Tracking
Licensed copyright line	Copyright © 2004 WILEY-VCH Verlag GmbH & Co. KGaA, Weinheim
Licensed content author	A. M. Derfus,W. C. W. Chan,S. N. Bhatia
Licensed content date	May 19, 2004
Start page	961
End page	966
Type of use	Dissertation/Thesis
Requestor type	University/Academic
Format	Print and electronic
Portion	Figure/table
Number of figures/tables	1
Original Wiley figure/table number(s)	Figure 2
Will you be translating?	No
Order reference number	
Total	0.00 USD

ORDER MORE... CLOSE WINDOW

Copyright Clearance Center RightsLink®

Home | Account Info | Help

Title: Multifunctional nanoparticles – properties and prospects for their use in human medicine
Author: Nuria Sanvicens,M. Pilar Marco
Publication: Trends in Biotechnology
Publisher: Elsevier
Date: August 2008

Logged in as:
Amit Jaiswal
Account #:
3000540358

LOGOUT

Order Completed

Thank you very much for your order.

This is a License Agreement between Amit Jaiswal ("You") and Elsevier ("Elsevier"). The license consists of your order details, the terms and conditions provided by Elsevier, and the payment terms and conditions.

Get the printable license.

License Number	3105920247671
License date	Mar 11, 2013
Licensed content publisher	Elsevier
Licensed content publication	Trends in Biotechnology
Licensed content title	Multifunctional nanoparticles – properties and prospects for their use in human medicine
Licensed content author	Nuria Sanvicens,M. Pilar Marco
Licensed content date	August 2008
Licensed content volume number	26
Licensed content issue number	8
Number of pages	9
Type of Use	reuse in a thesis/dissertation
Portion	figures/tables/illustrations
Number of figures/tables /illustrations	1
Format	both print and electronic
Are you the author of this Elsevier article?	No
Will you be translating?	No
Order reference number	
Title of your thesis/dissertation	Fluorescent Nanomaterials for Biological Applications
Expected completion date	May 2013
Estimated size (number of pages)	150
Elsevier VAT number	GB 494 6272 12
Permissions price	0.00 USD
VAT/Local Sales Tax	0.00 USD
Total	0.00 USD

ORDER MORE... CLOSE WINDOW

Title: Luminescent Carbon Nanodots: Emergent Nanolights
Author: Sheila N. Baker,Gary A. Baker
Publication: Angewandte Chemie International Edition
Publisher: John Wiley and Sons
Date: Aug 4, 2010

Order Completed

Thank you very much for your order.

This is a License Agreement between Amit Jaiswal ("You") and John Wiley and Sons ("John Wiley and Sons"). The license consists of your order details, the terms and conditions provided by John Wiley and Sons, and the payment terms and conditions.

Get the printable license.

License Number	3100220241602
License date	Mar 01, 2013
Licensed content publisher	John Wiley and Sons
Licensed content publication	Angewandte Chemie International Edition
Licensed content title	Luminescent Carbon Nanodots: Emergent Nanolights
Licensed copyright line	Copyright © 2010 WILEY-VCH Verlag GmbH & Co. KGaA, Weinheim
Licensed content author	Sheila N. Baker,Gary A. Baker
Licensed content date	Aug 4, 2010
Start page	6726
End page	6744
Type of use	Dissertation/Thesis
Requestor type	University/Academic
Format	Print and electronic
Portion	Figure/table
Number of figures/tables	1
Original Wiley figure/table number(s)	Figure 1
Will you be translating?	No
Order reference number	
Total	0.00 USD

Title: Investigating Fluorescence Quenching of ZnS Quantum Dots by Silver Nanoparticles

Author: Amit Jaiswal

Publication: Plasmonics

Publisher: Springer

Date: Jan 1, 2010

Order Completed

Thank you very much for your order.

This is a License Agreement between Amit Jaiswal ("You") and Springer ("Springer"). The license consists of your order details, the terms and conditions provided by Springer, and the payment terms and conditions.

Get the printable license.

License Number	3100161401737
License date	Mar 01, 2013
Licensed content publisher	Springer
Licensed content publication	Plasmonics
Licensed content title	Investigating Fluorescence Quenching of ZnS Quantum Dots by Silver Nanoparticles
Licensed content author	Amit Jaiswal
Licensed content date	Jan 1, 2010
Volume number	6
Issue number	1
Type of Use	Thesis/Dissertation
Portion	Full text
Number of copies	9
Author of this Springer article	Yes and you are the sole author of the new work
Title of your thesis / dissertation	Fluorescent Nanomaterials for Biological Applications
Expected completion date	May 2013
Estimated size(pages)	150
Total	0.00 USD

CLOSE WINDOW

Copyright Clearance Center RightsLink®

Home | Account Info | Help

Title: Functional chitosan nanocarriers for potential applications in gene therapy

Author: Amit Jaiswal,Arun Chattopadhyay,Siddhartha Sankar Ghosh

Publication: Materials Letters

Publisher: Elsevier

Date: 1 February 2012

Logged in as:
Amit Jaiswal
Account #:
3000540358

LOGOUT

Order Completed

Thank you very much for your order.

This is a License Agreement between Amit Jaiswal ("You") and Elsevier ("Elsevier"). The license consists of your order details, the terms and conditions provided by Elsevier, and the payment terms and conditions.

Get the printable license.

License Number	3100170361488
License date	Mar 01, 2013
Licensed content publisher	Elsevier
Licensed content publication	Materials Letters
Licensed content title	Functional chitosan nanocarriers for potential applications in gene therapy
Licensed content author	Amit Jaiswal,Arun Chattopadhyay,Siddhartha Sankar Ghosh
Licensed content date	1 February 2012
Licensed content volume number	68
Number of pages	4
Type of Use	reuse in a thesis/dissertation
Portion	full article
Format	both print and electronic
Are you the author of this Elsevier article?	Yes
Will you be translating?	No
Order reference number	
Title of your thesis/dissertation	Fluorescent Nanomaterials for Biological Applications
Expected completion date	May 2013
Estimated size (number of pages)	150
Elsevier VAT number	GB 494 6272 12
Permissions price	0.00 USD
VAT/Local Sales Tax	0.00 USD
Total	0.00 USD

ORDER MORE... CLOSE WINDOW

RSC | Advancing the Chemical Sciences

Royal Society of Chemistry
Thomas Graham House
Science Park
Milton Road
Cambridge
CB4 0WF

Tel: +44 (0)1223 420 066
Fax: +44 (0)1223 423 623
Email: contracts-copyright@rsc.org

www.rsc.org

Acknowledgements to be used by RSC authors

Authors of RSC books and journal articles can reproduce material (for example a figure) from the RSC publication in a non-RSC publication, including theses, without formally requesting permission providing that the correct acknowledgement is given to the RSC publication. This permission extends to reproduction of large portions of text or the whole article or book chapter when being reproduced in a thesis.

The acknowledgement to be used depends on the RSC publication in which the material was published and the form of the acknowledgements is as follows:

- For material being reproduced from an article in *New Journal of Chemistry* the acknowledgement should be in the form:
  - [Original citation] - Reproduced by permission of The Royal Society of Chemistry (RSC) on behalf of the Centre National de la Recherche Scientifique (CNRS) and the RSC
- For material being reproduced from an article *Photochemical & Photobiological Sciences* the acknowledgement should be in the form:
  - [Original citation] - Reproduced by permission of The Royal Society of Chemistry (RSC) on behalf of the European Society for Photobiology, the European Photochemistry Association, and RSC
- For material being reproduced from an article in *Physical Chemistry Chemical Physics* the acknowledgement should be in the form:
  - [Original citation] - Reproduced by permission of the PCCP Owner Societies
- For material reproduced from books and any other journal the acknowledgement should be in the form:
  - [Original citation] - Reproduced by permission of The Royal Society of Chemistry

The acknowledgement should also include a hyperlink to the article on the RSC website.

The form of the acknowledgement is also specified in the RSC agreement/licence signed by the corresponding author.

Except in cases of republication in a thesis, this express permission does not cover the reproduction of large portions of text from the RSC publication or reproduction of the whole article or book chapter.

A publisher of a non-RSC publication can use this document as proof that permission is granted to use the material in the non-RSC publication.

BIOGRAPHY

Amit Jaiswal is currently a research scholar at the Centre for Nanotechnology, IIT Guwahati. He was born in Kolkata, West Bengal, in the year 1986. He completed his secondary and senior secondary examination from Indira Gandhi Memorial High School and Hariyana Vidya Mandir respectively. In the year 2004, he qualified AIEEE and was admitted to Heritage Institute of Technology, where he completed his Bachelor of Technology (B. Tech.) Degree in Biotechnology. After the successful qualification of GATE 2008 examination with 98.6 percentile he was awarded the MHRD fellowship and underwent Master of Technology (M. Tech.) Degree in Biotechnology from IIT Guwahati. He was the departmental topper of his batch (2010) and was bestowed with gold medal in a National level biotechnology examination organized during his Master's Degree tenure. In the year 2010, he joined Centre for Nanotechnology as a Ph.D. student under the joint supervision of Prof. Siddhartha Sankar Ghosh and Prof. Arun Chattopadhyay. His main research is focused on the synthesis of nontoxic quantum dots and its bioimaging and analytical applications. He has seven peer reviewed journal and fourteen conference publications. He has also qualified the joint CSIR-UGC NET JRF examination in Life Sciences in the year 2011. He has been serving as an invited reviewer for the International journals such as Chemical Communications, Polymer Chemistry, RSC Advances, Analyst, PCCP, Plasmonics, etc.